REPORT DOCUMENTATION PAGE

Form Approved OMB NO. 0704-0188

1. AGENCY USE ONLY (Leave Blank)	2. REPORT DATE:	3. REPORT TYPE AND DATES COVERED
	31-Jul-2007	Final Report 1-Aug-2006 - 30-Apr-2007

4. TITLE AND SUBTITLE

Time Reversal for Ultra-wideband (UWB) Sensor Networking

5. FUNDING NUMBERS

W911NF-06-1-0349

6. AUTHORS

Martha A. Calderon and Robert C. Qiu

8. PERFORMING ORGANIZATION REPORT NUMBER

7. PERFORMING ORGANIZATION NAMES AND ADDRESSES

Tennessee Technological University
Derrberry Hall, Room 306

Cookeville, TN 38501 -

9. SPONSORING/MONITORING AGENCY NAME(S) AND ADDRESS(ES)

U.S. Army Research Office
P.O. Box 12211
Research Triangle Park, NC 27709-2211

10. SPONSORING / MONITORING AGENCY REPORT NUMBER

51073-CI-II.1

11. SUPPLEMENTARY NOTES

The views, opinions and/or findings contained in this report are those of the author(s) and should not contrued as an official Department of the Army position, policy or decision, unless so designated by other documentation.

12. DISTRIBUTION AVAILIBILITY STATEMENT

Approved for public release; distribution unlimited

12b. DISTRIBUTION CODE

13. ABSTRACT (Maximum 200 words)

The abstract is below since many authors do not follow the 200 word limit

14. SUBJECT TERMS

ultra-wideband, sensor, time reversal, multiple-input multiple output

15. NUMBER OF PAGES

Unknown due to possible attachments

16. PRICE CODE

17. SECURITY CLASSIFICATION OF REPORT	18. SECURITY CLASSIFICATION ON THIS PAGE	19. SECURITY CLASSIFICATION OF ABSTRACT	20. LIMITATION OF ABSTRACT
UNCLASSIFIED	UNCLASSIFIED	UNCLASSIFIED	UL

NSN 7540-01-280-5500

Standard Form 298 (Rev .2-89)
Prescribed by ANSI Std.
239-18 298-102

Report Title

Time Reversal for Ultra-wideband (UWB) Sensor Networking

ABSTRACT

This report is organized into six chapters. It addresses coupling e□ects, an
analysis of the virtual array, single-user and multi-user time reversal UWB-MIMO system performance, and a comparison with time reversal UWB-MISO. The central topic of this report is to experimentally study the multiuser MIMO with time reversal transmission. When transmitting to 10 users simultaneously in the system, it is found that the interference is high and BER performance is poor, thus, MIMO multiple access schemes such as zero-forcing at the transmitter must be considered.

List of papers submitted or published that acknowledge ARO support during this reporting period. List the papers, including journal references, in the following categories:

(a) Papers published in peer-reviewed journals (N/A for none)

1. R.C. Qiu, C. Zhou, N. Guo, and J.Q. Zhang, "Time Reversal with MISO for Ultra-Wideband Communications: Experimental Results," IEEE Antenna and Wireless Propagation Letters, pp. 269-273, Vol. 5, 2006.

2. C. Zhou and R.C. Qiu, "Pulse Distortion Caused by Cylinder Diffraction and Its Impact on UWB Communications," IEEE Trans. Vehicular Technology, to appear.

3. N. Guo and R.C. Qiu, "Improved Autocorrelation Demodulation Receivers Based on Multiple-Symbol Detection for UWB Communications", IEEE Trans. Wireless Communications, Vol. 5, No. 8, pp. 2026-2031, Aug. 2006.

4. R.C. Qiu, J.Q. Zhang, N. Guo, "Detection of physics-based ultra-wideband signals using generalized RAKE and multi-user detection (MUD)," IEEE J. Select. Areas Commun., Vol. 24, No. 4, pp. 724-730, April 2006.

Number of Papers published in peer-reviewed journals: 4.00

(b) Papers published in non-peer-reviewed journals or in conference proceedings (N/A for none)

Number of Papers published in non peer-reviewed journals: 0.00

(c) Presentations

Number of Presentations: 0.00

Non Peer-Reviewed Conference Proceeding publications (other than abstracts):

Number of Non Peer-Reviewed Conference Proceeding publications (other than abstracts): 0

Peer-Reviewed Conference Proceeding publications (other than abstracts):

1. R. C. Qiu, C. Zhou, J. Q. Zhang, and N. Guo, "Channel Reciprocity and Time-Reversed Propagation for Ultra-Wideband Communications," IEEE AP-S International Symposium on Antennas and Propagation, Honolulu, Hawaii, USA, June, 2007.

2. N. Guo, R.C. Qiu, B.M. Sadler, "A UWB Radio Network Using Multiple Delay Capture Enabled by Time Reversal," IEEE MILCOM'06, Washington, DC, Oct. 23-25, 2006.

3. C. Zhou, N. Guo, and R.C. Qiu, "Experimental Results on Multiple-Input Single-Output (MISO) Time Reversal for UWB Systems in an Office Environment," Military Communications Conference (MILCOM06), Washington DC, Oct. 2006.

4. R.C. Qiu, ``A Theory of Time-Reversed Impulse Multiple-Input Multiple-Output (MIMO) for Ultra-Wideband (UWB) Communications (invited paper)," IEEE International Conference on Ultra-Wideband (ICUWB06), Boston, MA, USA, Sept., 2006.

5. N. Guo, J.Q. Zhang and R.C. Qiu, "A UWB Radio Testbed-System Design and Implementation," IEEE 38th Southeastern Symposium on System Theory, Cookeville, TN, USA, 2006.

6. J.Q. Zhang and R.C. Qiu, "Detection of Physics-based Ultra-wideband Signals Using Generalized RAKE in Presence of Inter-Symbol Interference," IEEE 38th Southeastern Symposium on System Theory, Cookeville, TN, USA, 2006.

7. C.Zhou and R. C. Qiu, "Spatial Focusing of Time-Reversed UWB Electromagnetic Waves in a Hallway Environment," IEEE 38th Southeastern Symposium on System Theory, Cookeville, TN, USA, 2006.

10. R.C. Qiu, C. Zhou, N. Guo, J.Q. Zhang, "Time Reversal with MISO for Ultra-Wideband Communications: Experimental Results," Invited Paper, IEEE Radio and Wireless Symposium, San Diego, CA, 2006.

11. R. C. Qiu, C. Zhou, J. Q. Zhang, and N. Guo, “Channel Reciprocity and Time-Reversed Propagation for Ultra-Wideband Communications,” IEEE
AP-S International Symposium on Antennas and Propagation, Honolulu,
Hawaii, USA, June 2007.

12. C. M. Zhou, N. Guo, B. M. Sadler, R. C. Qiu, “Performance Study on Time Reversed Impulse MIMO for UWB Communications Based on
Realistic Channels, IEEE MILCOM 07, Orlando, Florida, Oct. 29-31,
2007.

13. R. C. Qiu, B. M. Sadler, Z. Hu, ``Time Reversed Transmission with Chirp Signaling for UWB Communications and Its Application in
Confined Metal Environments,” IEEE Int'l Conf. UWB, Singapore, Oct. 2007.

Number of Peer-Reviewed Conference Proceeding publications (other than abstracts): 13

(d) Manuscripts

1. N. Guo, R.C. Qiu, and B. M. Sadler, “Reduced-Complexity Time Reversal Enhanced Autocorrelation Receivers Considering Experiment-Based UWB Channels,” IEEE Trans. Wireless Comm., Submitted for publication, March 2006.

Number of Manuscripts: 1.00

Number of Inventions:

Graduate Students

NAME	PERCENT SUPPORTED
FTE Equivalent:	
Total Number:	

Names of Post Doctorates

NAME	PERCENT_SUPPORTED
FTE Equivalent:	
Total Number:	

Names of Faculty Supported

NAME	PERCENT_SUPPORTED	National Academy Member
Robert Qiu	0.50	No
FTE Equivalent:	**0.50**	
Total Number:	**1**	

Names of Under Graduate students supported

NAME	PERCENT_SUPPORTED
FTE Equivalent:	
Total Number:	

Student Metrics

This section only applies to graduating undergraduates supported by this agreement in this reporting period

The number of undergraduates funded by this agreement who graduated during this period:	0.00
The number of undergraduates funded by this agreement who graduated during this period with a degree in science, mathematics, engineering, or technology fields:.....	0.00
The number of undergraduates funded by your agreement who graduated during this period and will continue to pursue a graduate or Ph.D. degree in science, mathematics, engineering, or technology fields:.....	0.00
Number of graduating undergraduates who achieved a 3.5 GPA to 4.0 (4.0 max scale):	0.00
Number of graduating undergraduates funded by a DoD funded Center of Excellence grant for Education, Research and Engineering:	0.00
The number of undergraduates funded by your agreement who graduated during this period and intend to work for the Department of Defense	0.00
The number of undergraduates funded by your agreement who graduated during this period and will receive scholarships or fellowships for further studies in science, mathematics, engineering or technology fields:	0.00

Names of Personnel receiving masters degrees

NAME
Martha Calderon
Total Number: 1

Names of personnel receiving PHDs

NAME
Total Number:

Names of other research staff

NAME	PERCENT_SUPPORTED
FTE Equivalent:	
Total Number:	

Sub Contractors (DD882)

Inventions (DD882)

Time Reversal for Ultra-wideband (UWB) Sensor Networking

Final Report

to

US Army Research Office

4300 South Miami Boulevard

Research Triangle Park, NC 27709-2111

for

Grant # W911NF-06-1-0349

Prepared by

Martha A. Calderon

and

Robert C. Qiu

July 31, 2007

Tennessee Technological University

Cookeville, TN 38501

Acknowledgment

We want to thank B. M. Sadler for his support for this project. This work has been improved by discussions with B. M. Sadler (ARL) and R. Ulman(ARO). We want to thank N. (Terry) Guo, C. M. (Jim) Zhou, and Q. (John) Zhang (at TTU) for their help in experiments and simulations. K. Currie (TTU) has provided a lot of support for this project.

Abstract

This report is organized into six chapters. It addresses coupling effects, an analysis of the virtual array, single-user and multi-user time reversal UWB-MIMO system performance, and a comparison with time reversal UWB-MISO. The central topic of this report is to experimentally study the multiuser MIMO with time reversal transmission. When transmitting to 10 users simultaneously in the system, it is found that the interference is high and BER performance is poor, thus, MIMO multiple access schemes such as zero-forcing at the transmitter must be considered.

TABLE OF CONTENTS

Chapter Page

Chapter Page

Chapter Page

LIST OF TABLES

LIST OF FIGURES

Figure Page

Figure Page

Figure Page

Figure Page

Figure Page

Figure Page

Figure Page

Figure Page

CHAPTER 1
INTRODUCTION

1.1 Motivation and Scope of Research

Wireless communication is one of the fastest growing segments of all communications. Ultra-wideband (UWB) technology has evolved rapidly in the last few years. It allows low-power and low-cost implementation of communications systems which overcomes other existing technologies. The UWB spectrum was recently legalized in the US with a bandwidth of 7.5GHz, and thus, higher data rates compared to narrowband systems. In 2002, the United States Federal Communication Commission (FCC) allocated the 3.1 GHz to 10.6GHz spectrum for UWB devices. The great features of UWB will allow a new range of applications including military, medical, domestic, logistics, and security. The bandwidth of a UWB signal is in the range of several GHz, therefore, the corresponding time resolution of the channel is in the order of fractions of nanoseconds which allows to distinguish surfaces separated by mere centimeters.

Time Reversal (TiR) is a technique in which the channel state information (CSI) is used to pre-code the transmitted symbols with the time reversed version of the channel impulse response (CIR). The receiver (Rx) first sounds the channel by sending a pulse which the transmitter (Tx) will receive and use to calculate channel information. A time-reversed version is used as a pre-coder to transmit the intended data to the receiver. The signal propagates focusing both power and time at receiver. As discussed in [10], the use of TiR for wireless communications over channels with big scattering presents three advantages: (1) spatial focusing (when multiple antennas

are present) which means that the power in the space domain peaks at the intended receiver and decays rapidly away from it, this results in a very low co-channel interference for a multi-user system; (2) temporal focusing which means that the impulse response of the channel at the receiver has a short effective length (in the time domain), reducing the requirement for sophisticated equalization; and (3) hardening of the effective channel which means that the distribution function of the effective channel impulse response is more stable resulting in a high diversity gain.

The use of TiR technique on UWB systems has been studied in many papers, and it has been found that the rich scattering and multipath in UWB communication systems can be used as an advantage with TiR to focus the signal sent at the intended receiver. The use of UWB and TiR results in lower Inter Symbol Interference (ISI) and less complexity at the receiver, which means a low-cost, low-power, high data rate, and spatial-time focused system that looks promising for many applications.

Antenna array systems are used as a *space diversity* method in wireless communications systems. As discussed in [27], *multiple antennas have been used in the reverse link of mobile communication systems to suppress or cancel interference and to achieve transmit or receive diversity.* Antenna array configurations inlude: (1) Single-input single-output (SISO), (2) Multiple-input single-output (MISO), (3) Single-input multiple-output (SIMO), and (4) Multiple-input multiple-output (MIMO). MIMO has been shown to improve system performance and increase processing gain. The use of MIMO in UWB wireless communications is known as UWB-MIMO and has been recently addressed in the literature. Results show improvements over other systems like UWB-SISO and UWB-MISO [27, 35].

The objective of this work is to study Time-Reversed UWB-MIMO for sensor networking. The robustness of TiR for UWB-MIMO will be evaluated by performing

measurement experiments and simulations. The advantages of UWB-MIMO over UWB-MISO will be discussed as well. In UWB-MIMO, two antenna effects arise when receive antennas are close to each other: Antenna mutual coupling and channel spatial correlation. Mutual coupling between two close antennas degrades the performance of a communication system and has been studied before for wireless communications. Channel spatial correlation has been experienced in communication systems with space diversity. These coupling effects for a TiR UWB-MIMO system have not been well addressed yet and are the scope of this research. Therefore, the performance of the system when the distance between two receive antennas is small (i.e. when receive antennas experience mutual coupling and channel spatial correlation) will be evaluated and discussed.

1.2 Basic Idea

Consider a total of K users. Each user has M transmit antennas[1] and only one receive antenna. There are P users simultaneously operating $M \times 1$ MISO systems, each one targeting a different user. For a SISO link with time reversal, it follows for the target user that $s(t) * [h_{ij}(-t)^* * h_{ij}(t)]$, where $h_{ij}(t)$ is the CIR between i-th transmit antenna and j-th receive antenna, and $s(t)$ is the transmitted symbol. For the off-target user, the received signal has the incoherent form $s(t) * [h_{ij}(-t)^* * h_{ik}(t)]$, where $h_{ik}(t)$ denotes the CIR from the i-th transmit point to the k-th off-target point. Note that the cross-correlation of the two CIRs,rather than the coherent auto-correlation of the CIR for the target user, is involved. For the j-th user, $j = 1, 2, .., K$,

[1]Even only one antenna is available, i.e.,$M = 1$, the phenomenon in the following will still be true.

the received signal becomes

$$y_j(t) = \underbrace{s_j(t) * \left[\sum_{i=1}^{M} h_{ij}(-t)^* * h_{ij}(t)\right]}_{Signal(j)=s_j(t)*h_j^{eq}(t)} + \underbrace{\sum_{i=1}^{M}\sum_{k=1;k\neq j}^{K} s_j(t) * [h_{ij}(-t)^* * h_{ik}(t)]}_{Interference(j)} + \underbrace{n_j(t)}_{Noise(j)} \tag{1.1}$$

Link capacity and performance are expressed as a function of signal-to-interference-plus-noise ratio (SINR) defined at the same time lag that reaches the peak of the Signal(j)

$$SINR_j = \frac{|Signal(j)_{peak}|^2}{|Interference(j)_{peak} + Noise(j)_{peak}|^2} \tag{1.2}$$

In (1.1), the received signal are not only coherently added up in the time domain but also in the spatial domain (multiple antennas). Spatial focusing/selectivity and temporal compression are achieved *at the same time* by time-reversal. The rich scattering environment, which makes the propagation channel of each link independent and unique, can provide the natural, quasi-orthogonal codes, $h_{ij}(t)$ and $h_{ik}(t)$. These codes are useful in further separating the signals intended for different users, thus minimizing the cross-correlation term in (1.1). Consequentially, the data throughput can be further improved by taking advantage of the spatial diversity focusing properties of the time-reversal array, using MISO and MIMO discussed above.

Robustness to narrowband interference is essential to military communications. Time reversal serves as another level of protection from this problem. When

narrowband interference is present, (1.1) is modified as

$$y_j(t) = \underbrace{s_j(t) * \left[\sum_{i=1}^{M} h_{ij}(-t)^* * h_{ij}(t)\right]}_{Signal(j)=s_j(t)*h_j^{eq}(t)} + \underbrace{\sum_{i=1}^{M}\sum_{k=1;k\neq j}^{K} s_j(t) * [h_{ij}(-t)^* * h_{ik}(t)]}_{Interference(j)} + \underbrace{I_j(t)}_{NB\ Interference(j)} \tag{1.3}$$

Three mechanisms are exploited to achieve robustness in (1.1). First, short pulse or spread spectrum can be used in $s_j(t)$. Precoding each transmit antenna by its $CIR h_{ij}$ serves for two functions: a generalization of time-domain, broadband beam forming and spatio-temporal focusing. It appears that no research has been done from this view. Analysis is necessary to establish the additional performance gain offered by spatio-temporal focusing. The beauty is that the spatial separation from narrowband interference is obtained without bandwidth spreading. From LPD/LPI point of view, there is an incentive to use impulsive signals to maximize this spatial separation.

1.3 Literature Survey

UWB wireless communication has many advantages which include a low-cost design, a large processing gain, and a fine time resolution. An overview of UWB technology as well as transceiver design and challenges are presented in [43, 54]. The UWB channel is investigated in [39], and in [63] the robustness of the UWB signal in an indoor environment is evaluated. Pulse distortion and degradation of the signal-to-noise ratio in a UWB correlator receiver is addressed in [49, 41]. UWB receiver design is of great interest due to the many challenges it faces, including capturing multipath energy, supressing intersymbol interference, and the need of high-sampling-rate analog-to-digital (ADC) converters. Rake receivers are studied in [19, 26] and autocorrelation demodulation (ACD) is addressed in [16]. A comparison of

the transmit reference (TR) receiver and a math filter (MF) receiver is performed in [21], and a study of non-coherent receivers can be found in [8]. A UWB testbed system is discussed in [18] where challenges and considerations for UWB transceiver design are presented.

Time-reversal (TiR) was first addressed in underwater acoustics [9, 22]. The basic principles for TiR are presented in [11] and it is experimentally demonstrated for a wireless communication system in [25]. The extension of TiR to broadband wireless systems presents some advantages over channels with large delay spreads (i.e. when large bandwith signals are used) [37]. A study of TiR on UWB communication systems is presented in [10] and in [67] the feature of spatial focusing is demonstrated. In [58], it is found that the number of taps in an MMSE equalizer can be reduced and an improvement of performance can be obtained when using TiR. Some improvements to TiR technique can be found in [65, 32].

Antenna diversity is being widely investigated for its potential improvement of processing gain [29]. A study of capacity in underwater acoustics using MIMO systems is presented in [66]. Furthermore, the use of MIMO in wireless communications improves capacity as presented in [33, 31]. Transmit diversity for wireless communications is addressed in [3]. An analysis of correlation, based on measurements of a MIMO wireless system, is presented in [23], and the impact of correlation in the performance of a MIMO system is discussed in [28]. The use of TiR and MIMO for underwater acoustics is investigated in [20], where is demonstrated that the use of antenna diversity improves the spatial focusing property of TiR, and a TiR-MISO system can transmit with low probability of intercept(LPI). The extension of TiR and antenna diversity to wireless communications allows high data rates as investigated in [7] and improves bit-error-rate (BER) as discussed in [36].

The use of antenna diversity in UWB communications improves the performance of the system [62] even in the prescence of multi-user interference (MUI) [59]. An analysis of the error performance for a UWB-MIMO system is presented in [27] where an analytical expression was derived for the error rate which can be used to predict the performance of most pulse-based UWB-MIMO systems. A TiR UWB-MISO and a UWB-MIMO system are discussed in [35]. It is shown that the use of a multiple element antenna (MEA) system improves performance and is promising for multi-user systems. Finally, power allocation when using TiR and transmit diversity is addressed in [24].

1.4 Research Approach

Measurement and simulation experiments are the key approach of this work. The UWB channel is measured using a time domain technique and the recorded signals are used for simulation experiments. The measurement equipment is integrated with two channel modules that allows to measure two channel simultaneously. For the MIMO system, two receive antennas are considered in which the distance ,D, between them is varied. Thus, the measurement approach is to record the signal of two receive antennas simultaneously when D is decreased and coupling effects are experienced. Data is obtained for several distances D and is used for simulations.

From the data obtained, three research approaches are considered. The first approach takes a closer look at both coupling effects when Tx and Rx are close (1m) and the channel has a low influence on the received data. The signal at the targeted receive antenna is analized when there is no other antenna present (i.e. without coupling effects) and when another antenna is placed near by (i.e. with coupling effects). The second approach investigates the validity of measuring a virtual array

when the distance between two receive antennas is small. To achieve this, a real array and a virtual array are measured. For both, the recorded data is compared and used to evaluate the performance of a TiR UWB-SIMO system. The third approach investigates TiR UWB-MIMO for a single-user system and a multi-user system. The performance of both systems is evaluated when each user has two receive antennas and the distance between these antennas is small. The data is obtained from measurement experiments. The performance is evaluated using two metrics: bit-error-probability (BER) and signal-to-interference-and-noise ratio (SINR). Furthermore, TiR UWB-MISO is also evaluated and compared with TiR UWB-MIMO.

1.5 Organization of the Report

This report is organized into six chapters. Chapter 1 states the motivation and scope of this research, presents a literature survey, and introduces the research approach. Chapter 2 presents the concept and features of UWB wireless communications. It gives several applications for UWB technology and challenges that faces. Chapter 3 introduces UWB channel measurements and channel modeling. Results for measurement experiments are presented as well. Time-Reversal and antenna array systems are presented in Chapter 4. It gives the background and theory behind the simulations. Chapter 5 shows the results obtained from simulation experiments. It addresses coupling effects, an analysis of the virtual array, single-user and multi-user TiR UWB-MIMO system performance, and a comparison with TiR UWB-MISO. Finally, the main conclusions of this report and recommendations for future work are presented in Chapter 6.

1.6 Related to Other Work

This report is prepared at the same time as another final report [42].

Time reversal have been studied systematically for single users, e.g. [68]. This report that is mainly based on the thesis of Martha Calderon (2007) [5], however, deals with spatial focusing for multiple users. It will be found that, by exploiting multipath [68] [48], time reversal, indeed, increases the anti-jamming capability of the network by around 10 dB in a typical indoor environment. This is insufficient for some applications. Several directions can be pursued. First, the non-coherent detection is simple, but performs poorly for anti-jamming. Matched-filter based chirp UWB can be combined with time reversal [46] to achieve better anti-jamming. Second, spatial filtering is needed by using beam-forming using multiple antennas. Third, impulsive waveforms need to be dynamically adapted to the spectrum, according to the sensed environments. This is especially true to RF harsh environments such as confined metal environment [46] and intra-vehicle [48].

CHAPTER 2
ULTRA-WIDEBAND COMMUNICATIONS

Ultra-wideband (UWB) communication is classified as a type of wireless communication with very large fractional bandwidth. Its first applications were as UWB radar systems for military purposes due to its penetration capabilities. Recently, other applications like communications and consumer electronics have been considered for UWB technology. UWB promises low power, low cost, high data rates, precise positioning capability and low interference. This chapter presents a brief history of UWB communications. It then discusses the definition and features of UWB. Modulation and demodulation techniques, as well as some UWB applications, are also stated. It concludes with a brief description of the challenges ahead.

2.1 Historical Development of UWB

UWB communication is not a new technology, though only in 1989 the Department of Defense created the nomenclature *ultra-wideband* to describe communications via the transmission and recepcion of impulses. Marconi used it in 1901 to transmit Morse Code sequences using spark gap radio transmitters [34]. The modern era for UWB began in the early 1960s with the work done in time domain electromagnetics. The development of the sampling oscilloscope, by both Tektronix and Hewelet-Packard, and the work on techniques to generate sub-nanosecond baseband pulses contributed to the development of UWB technology.

From the 1960s to the 1990s, the applications of UWB communications were mainly military (radar and highly secure communications). With the development

of fast switching in semiconductors and the advancement in microprocessing, new commercial applications have recently been proposed.

Robert Scholtz at the University of Southern California presented a multiple access technique for UWB communication systems in 1993 [52]. This technique made UWB capable of supporting wireless networks besides radar and point-to-point communications.

In the late 1990s and early 2000s, a series of investigations were performed on UWB propagation. Channel models were developed from measurements and a variety of publications began to appear. The DARPA-funded Networking in Extreme Environments (NETEX) project carried out experiments on indoor and outdoor UWB propagation modeling, characterization of the response of building materials to UWB impulses, and characterization of antenna response to UWB signals [52].

New applications like UWB wireless and personal area networks have been proposed in which data rates range between Mbps and Gbps at distances of 1 to 10 meters [38]. In 2002, the Federal Communications Commission (FCC) approved the use of UWB communications for commercial use, and in april 2003 the first FCC-compliant UWB chipsets were announced by the Time Domain Corporation.

2.2 Concept and Features of UWB

As stated before, UWB communiations are categorized as communication systems with large fractional bandwidth which is defined as the ratio of the bandwidth occupied by the signal to the center frequency of the signal and it is expressed by

$$B_f = \frac{f_H - f_L}{f_C} \tag{2.1}$$

where

f_H is the -10dB point upper frequency

f_L is the -10dB point lower frequency

f_C is the center frequency

The fractional bandwidth for traditional communication systems is in the order of 0.01. The FCC defined UWB signals as those which have a fractional bandwidth greater than 0.2 or a bandwidth greater than 500MHz. Figure 2.1 shows the comparison of fractional bandwidths between Narrowband and UWB communications systems. UWB communication is based on impulse radio. Unlike classic communication systems in which a modulated sinusoidal carrier conveys the information, in impulse radio, a series of baseband pulses are transmitted. The duration of the pulses is in the order of nanoseconds, and thus, the transmit signal bandwidth is in the order of Gigahertz. Also, due to the large bandwidth associated with UWB signals, the power spectral density can be quite small. The FCC has imposed strict limitations on UWB power spectral density in order to co-exist with current wireless technologies

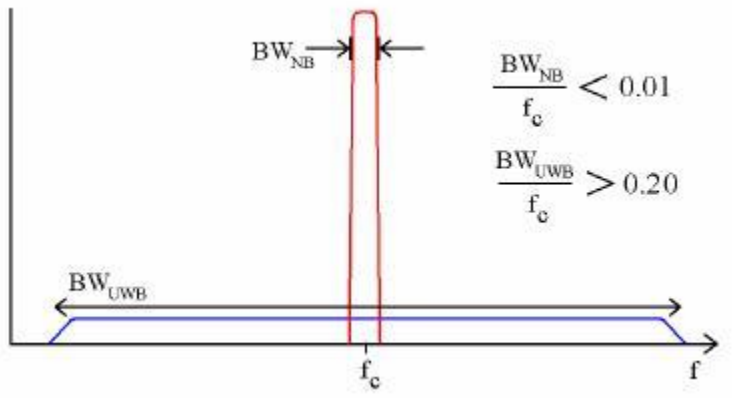

Figure 2.1 Fractional bandwidth comparison

like spread spectrum and narrowband. Figure 2.2 shows the spectral mask for indoor and outdoor operations.

The features of UWB include:

1. Large instantaneous bandwidth enables fine time resolution (and thus location capabilities) and higher data rates compared with Narrowband systems.
2. Short duration pulses help to resolve the various paths of propagation and hence provide robust performance in dense multipath environments.
3. Low power spectral density results in Low Probability of Intercept (LPI) and hence allows coexistence with other users.
4. Power spectral density and multipath performance can be traded for data rate.
5. Simple implementation results in low-cost digital design.

Figure 2.3 shows the allocation of spectrum for wireless communication technologies. UWB communication is allowed between 3.1GHz and 10.6GHz with a maximum power spectral density of -41dBm/MHz.

2.3 UWB Signals

The signal for UWB communication consists of a series of pulses of short duration that carry the information. These sub-nanosecond pulses travel through the channel and can be represented at the receiver as

$$s(t) = \sum_{i=-\infty}^{\infty} A_i(t)p(t - iT_f) \tag{2.2}$$

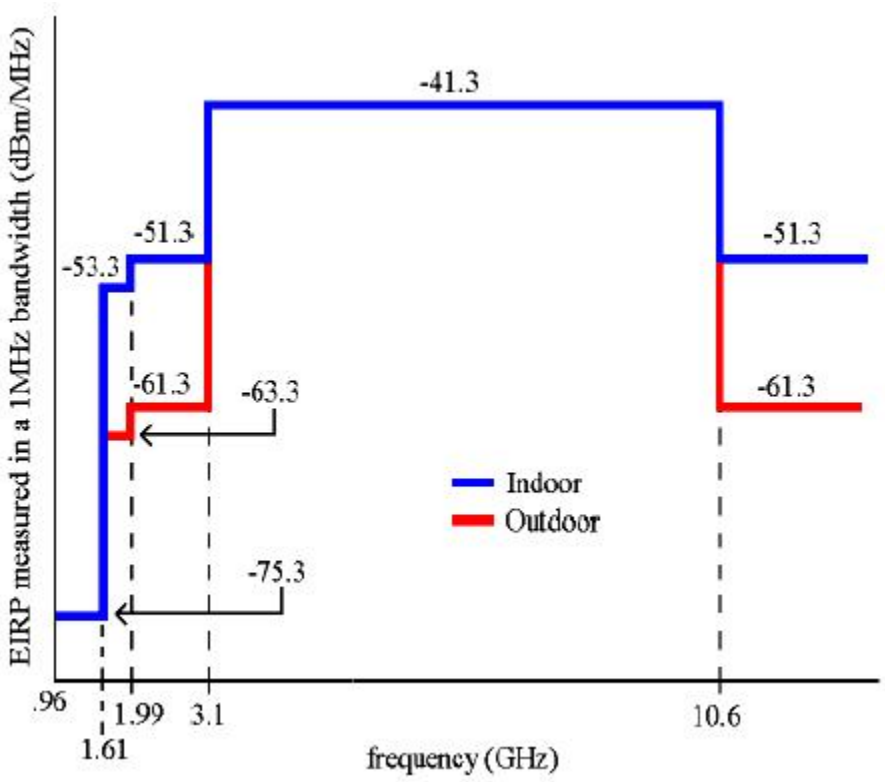

Figure 2.2 Power spectral mask for indoor and outdoor UWB operation

where $A_i(t)$ is the amplitude of the pulse equal to $\pm\sqrt{E_p}$, and E_p is the energy per pulse. $p(t)$ is the received pulse shape (with the same shape as the sent pulse) having normalized energy, and T_f is the frame repetition time. Equation 2.2 assumes that the pulse is not distorted by the channel and that the Signal-to-Noise Ratio (SNR) is infinite (i.e. a noiseless channel). In reality, this is not the case since the pulse shape is distorted by transmit and receive antennas, as well as by the channel which will also introduce noise to the received signal.

The popular pulse shapes used for UWB communication include the Gaussian pulse and its derivatives. Analytically, the Gaussian pulse can be expressed as

$$p(t) = \frac{1}{\sqrt{2\pi\sigma^2}} e^{-(t-\mu)^2/2\sigma^2} \tag{2.3}$$

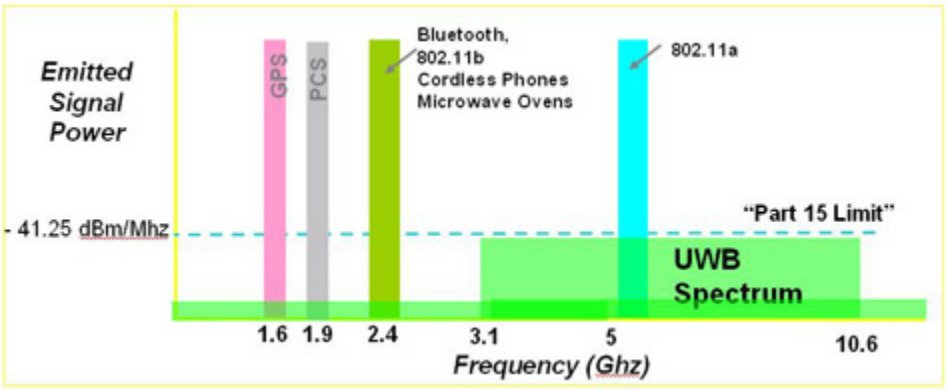

Figure 2.3 FCC ruling for wireless communications

where σ is the standard deviation of the Gaussian pulse in seconds, and μ is the location in time for the midpoint of the Gaussian pulse in seconds. The pulse width is related to the standard deviation as $\tau_p = 2\pi\sigma$ [52]. Figure 2.4 shows a Gaussian pulse for different σ, and their spectral components.

The first and second derivatives of the Gaussian pulse, also called the Gaussian monocycle and Gaussian Doublet respectively, can be used as pulse shapes for UWB systems. Figure 2.5 shows several gaussian monocycles and gaussian doublets for different pulse widths. An important characteristic of the gaussian, monocycle and doublet waveforms is that they are almost uniformily distributed over their frequency spectrum, therefore, are noise-like. A noise-like signal results in LPI which is desired for secure applications.

For commercial systems, the Gaussian modulated sinusoidal pulse is a more practical approach since the frequency band (3.1-10.6GHz) allocated by the FCC for UWB communications suggests a bandpass signal. Also, this pulse shape allows multi-band modulation, in which multiple frequency bands are used to efficiently occupy the UWB spectrum. Multiple UWB signals can be transmitted at the same

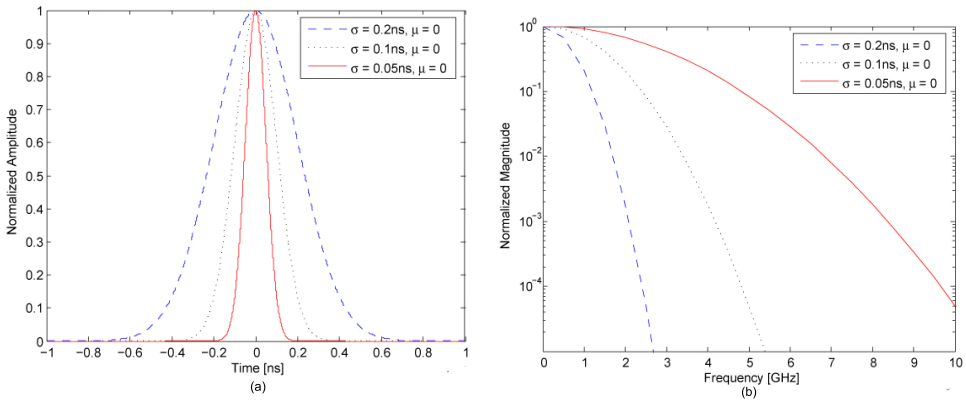

Figure 2.4 Gaussian pulse: (a) in time domain and (b) in frequency domain

time and will not interfere with each other since their frequencies are different. The Gaussian modulated sinusoidal pulse is plotted in Figure 2.6 and can be expressed by

$$p(t) = \left(\frac{8k}{\pi}\right)^{\frac{1}{4}} \frac{1}{\sqrt{1 + e^{\frac{2\pi^2 f_c^2}{k}}}} e^{-(kt)^2} \cos 2\pi f_c t \tag{2.4}$$

where f_c is the desired center frequency of the pulse and k is a constant that determines the pulse width.

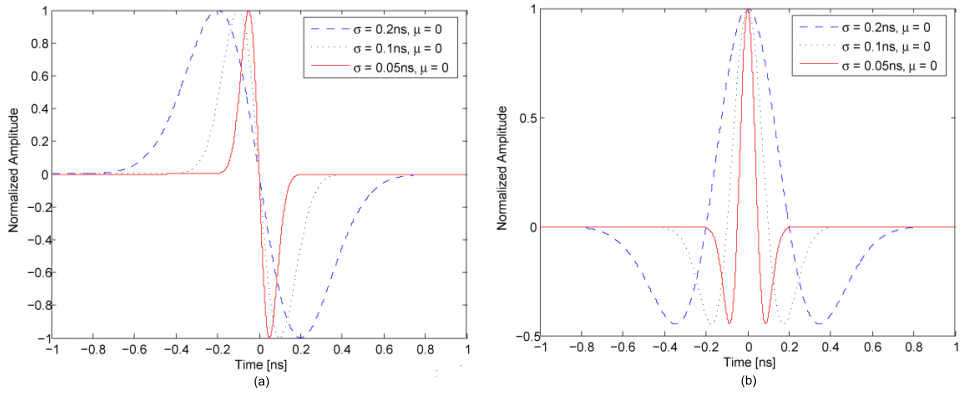

Figure 2.5 Other pulses: (a) Gaussian monocycle, and (b) Gaussian doublet

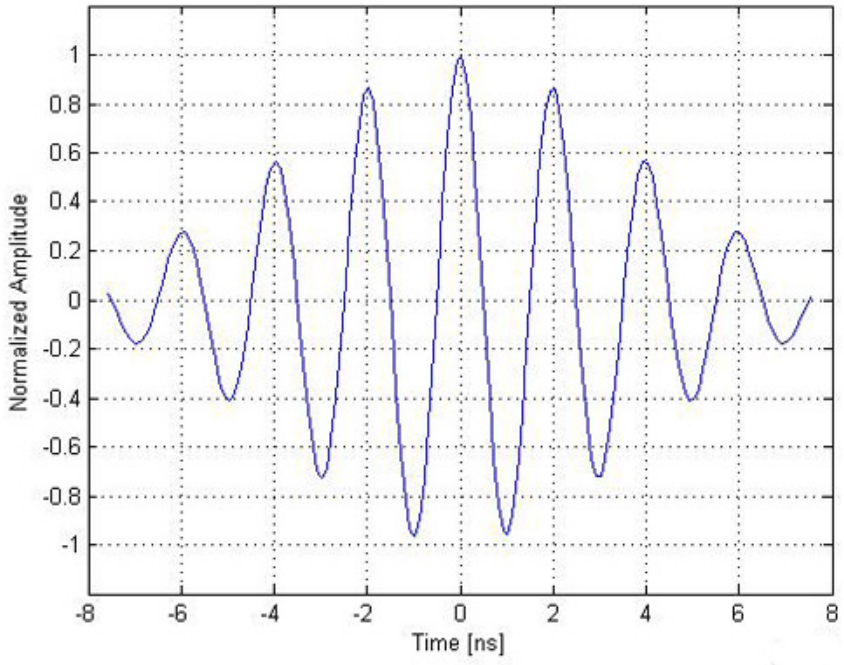

Figure 2.6 Gaussian sinusoid for UWB commercial use

2.4 UWB Modulation Techniques

Time-modulated ultra-wideband (TM-UWB) communication is based on discontinuous emission of very short pulses which corresponds to a baseband signal approach [38]. Processing gain could be achieved by sending N monocycles per symbol. A generalized transmitter structure is shown in Figure 2.7. Types of data modulation considered for UWB include Pulse Position Modulation (PPM), Pulse Amplitude Modulation (PAM), and On-Off Keying (OOK).

The *delay spread* is a metric of how much a signal is diluted in time. For a UWB multipath channel, the *delay spread* is usually described by its root mean square (rms) value. The *rms delay spread* is the standard deviation value of the delay of reflections, weighted proportional to the energy in the reflected waves [14]. No

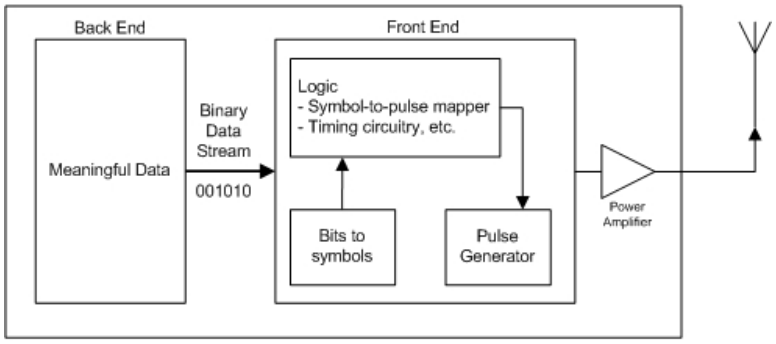

Figure 2.7 A general UWB transmitter block diagram [14]

inter symbol interference (ISI) is present if the time between pulses is greater than the rms delay spread (i.e. ten times greater).

2.4.1 Pulse Amplitude Modulation (PAM)

In pulse amplitude modulation the information is conveyed in the amplitude of the pulses. A typical binary PAM modulation can be achieved using two antipodal Gaussian pulses as shown in Figure 2.8. The expression for the modulated information is given by

$$x(t) = d_j \cdot w_{tr}(t) \tag{2.5}$$

where $w_{tr}(t)$ is the UWB pulse waveform, j represents the bit to be transmitted (i.e. for binary '0' or '1'), and

$$d_j = \begin{cases} -1, & \text{j} = 0 \\ 1, & \text{j} = 1 \end{cases} \tag{2.6}$$

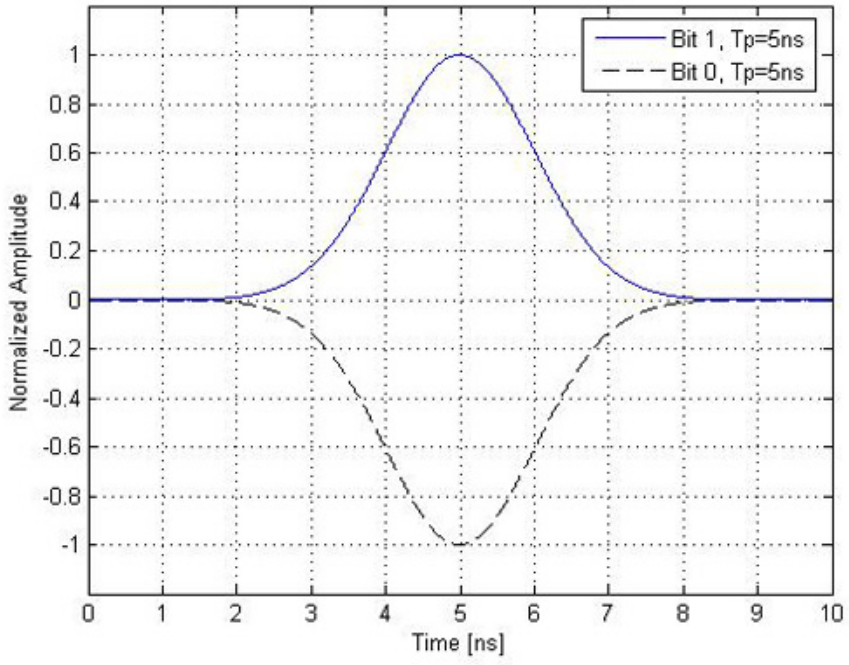

Figure 2.8 Binary PAM modulation

2.4.2 On-Off Keying (OOK)

As the name states, binary OOK modulation is achieved by sending or not sending a signal. Its signal can be represented as a PAM modulation signal in Equation 2.5, but now d_j has values

$$d_j = \begin{cases} 0, & \text{j} = 0 \\ 1, & \text{j} = 1 \end{cases} \tag{2.7}$$

where j is the bit to be transmitted.

2.4.3 Pulse Position Modulation (PPM)

Pulse position modulation is widely use in UWB communications. As the name implies, the information is conveyed in the position of the pulse. In binary PPM, a pulse originated at time instant 0 is used to represent a binary '0', while a pulse shifted in time by δ would represent a binary '1'. The drawback for PPM is that a longer bit period is required. The expression for a PPM modulated signal is given by:

$$x(t) = w_{tr}(t - \delta d_j) \tag{2.8}$$

where d_j can be defined as

$$d_j = \begin{cases} 0, & \text{j} = 0 \\ 1, & \text{j} = 1 \end{cases} \tag{2.9}$$

and the value of δ can be chossen according to the autocorrelation characteristics of the pulse [38]. Figure 2.9 shows the PPM pulses for binary modulation.

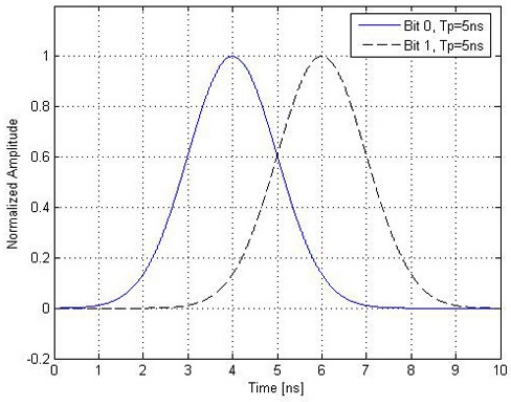

Figure 2.9 Binary PPM modulation

2.4.4 Transmitted-Reference (TR) Modulation

Transmitted-reference modulation is being introduced to UWB communications because of its robust performance in multipath environments, its simplicity, and not requiring a stringent synchronization for conventional pulse-detection techniques [34]. In this type of modulation a set of two pulses separated by a distance D are sent. The first pulse is a reference pulse which does not carry any information. The second pulse is the data pulse known as the 'transmit pulse'. The data is modulated based on the relative polarity of the reference and the transmit pulse. Figure 2.10 shows a TR modulation of data bit '1' and '0'.

2.5 UWB Demodulation and Detection

The UWB signal experiences shadowing effects caused by obstacles between the transmitter and receiver which attenuate the signal power through absorption, reflection, scattering , and diffraction [15]. A good receiver is that in which the information conveyed in the received signal is demodulated and detected with a minimum

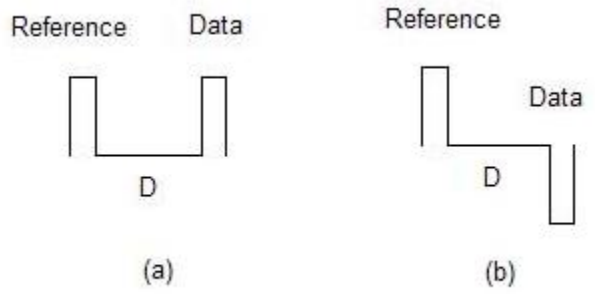

Figure 2.10 Transmitted-reference pulse modulation: (a) Symbol for data bit '1'. (b) Symbol for data bit '0'.

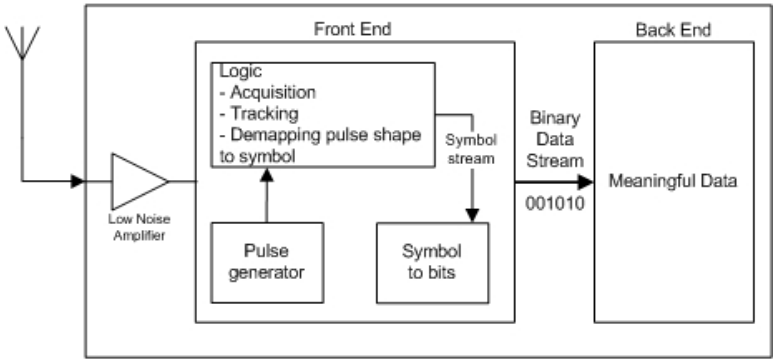

Figure 2.11 A general UWB receiver block diagram [14]

number of errors. Thus, a performance metric for designating a UWB receiver is the Bit Error Probability (BER).

There are two main parts in a receiver: detection and decision. UWB detectors are different from those used for narrowband signals since they operate in a carrier-less fashion [2]. There are a variety of UWB receiver designs including the correlator (match filter) receiver and the RAKE receiver. Other non-coherent detection schemes are becoming attractive for the simplicity in their implementation and low cost. New techniques like Time-Reversal (TiR) at the transmitter result in receiver design which are less complex without the cost of high performance degradation. A general diagram for a UWB receiver is presented in Figure 2.11.

2.5.1 Correlation Detection (CD) Receiver

The correlator receiver, also called matched filter receiver, is a simple and optimal method for detecting a signal in random noise and it is based on the correlation process [34]. It has been used for narrowband communication systems for many years and it can provide optimum detection. A block diagram of a correlation receiver is shown in Figure 2.12.

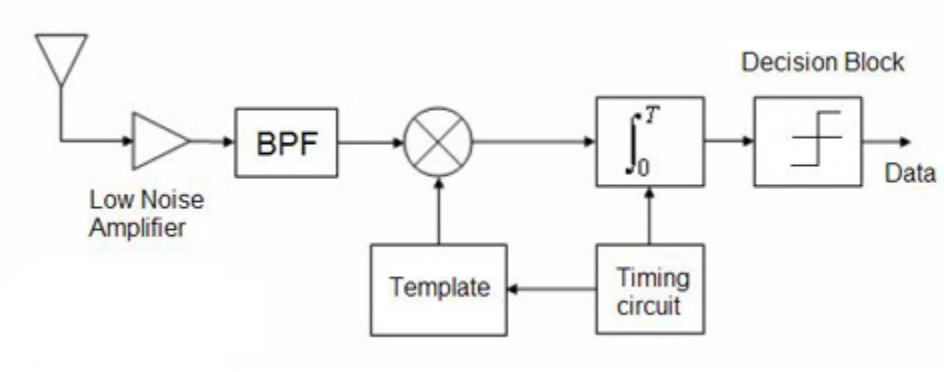

Figure 2.12 Correlator receiver diagram

The input signal is multiplied by a template waveform which identifies how well the template waveform matches the input waveform in time and space [52]. Optimum detection is achieved when the template waveform exactly matches the input waveform.

For an Additive White Gaussian Noise (AWGN) channel, the received signal can be modeled by

$$r(t) = s(t) + n(t) \tag{2.10}$$

where $r(t)$ is the received waveform, $s(t)$ corresponds to the transmitted waveform and $n(t)$ is white Gaussian noise with mean of zero and power spectral density of $N_o/2$. The optimum BER curve as a function of the signal to noise ratio can be calculated for antipodal PAM (A-PAM), OOK, and PPM modulation using the Euclidean distance d_{min} between the two symbols in the signal space [15].

$$P_b = Q\left\{\sqrt{\frac{d_{min}^2}{2N_o}}\right\} \tag{2.11}$$

Equation 2.11, presents the analytical formula to calculate the probability of bit error for binary detection in an AWGN channel. The distance d_{min} depends on the modulation scheme and is given by:

$$d_{min} = \sqrt{2E_s} \text{ for orthogonal signaling}$$

$$d_{min} = 2\sqrt{E_s} \text{ for antipodal signaling}$$

where E_s is the average Energy per symbol and $Q()$ is the Q function which is defined as the probability that a Gaussian random variable x with mean 0 and variance 1 is bigger than z:

$$Q(x) = p(x > z) = \int_z^\infty \frac{1}{\sqrt{2\pi}} e^{-x^2/2} dx \tag{2.12}$$

Figure 2.13 shows the BER curves for antipodal and orthogonal signaling. It may be noted that PPM and OOK are orthogonal modulation schemes and A-PAM is antipodal modulation with a 3dB improvement over OOK and PPM.

2.5.2 RAKE receiver

The RAKE receiver is used in any kind of spread spectrum communication system to accumulate the energy in the significant multipath components [52]. It consists of a bank of correlators located in different fingers. Each finger is synchronized to a multipath component of the received signal and the output of each finger is coherently combined using maximum ratio combining (MRC).

There are two drawbacks for UWB RAKE receivers. First, the number of multipath components in a UWB signal in a non-line-of-sight (NLOS) scenario is approximately 70 and thus a great number of fingers would be needed for a RAKE receiver to capture as much energy as possible. Second, each multipath travels through

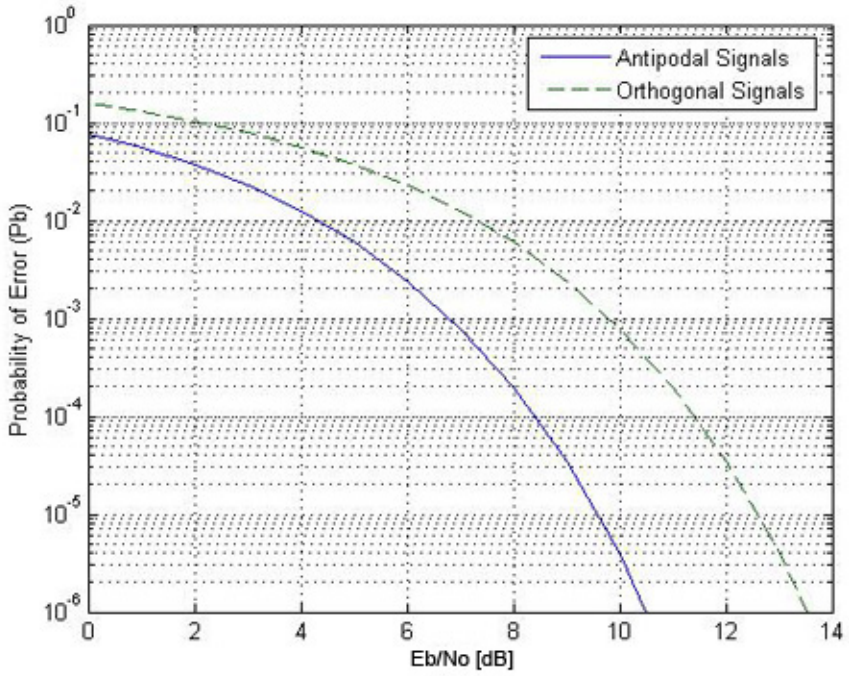

Figure 2.13 Performance of optimum correlator receiver for antipodal and orthogonal signaling

a different channel and experiments different pulse distortion which makes the use of a single line-of-sight (LOS) pulse, a sub-optimal template [52]. Synchronization and channel estimation are critical for RAKE receivers. Sub-nanosecond pulses make synchronization a major problem and performance degradation is observed due to imperfect channel estimates.

2.5.3 Non-coherent (Sub-optimal) Receivers

The complexity of receivers presented in previous sections and the advances in modulation schemes have given the opportunity to design sub-optimal receivers also known as non-coherent receivers. Research on non-coherent detection can be found in [6] and [8]. In this section two threshold detection receivers are presented.

Threshold detectors are also known as leading edge detection (LED) receivers and are a simple type of UWB receivers [52]. As the name states, this type of receivers are based on a threshold value. Any incoming pulse that passes the threshold value is detected and demodulated. A mayor drawback for this kind of receivers is that noise spikes which happen to cross the threshold value are erroneously detected. These pulses are called *false alarm* or *false detection*. To minimize false detections, an adaptive receiver can be implemented in which the threshold value changes depending on the input noise signal.

2.5.3.1 Amplitude Detection. Amplitude Detectors are based on the amplitude of the incoming signal. A block diagram of a simple amplitude detector is shown in Figure 2.14. The receiver consists of an integration block and a decision block. This receiver is capable of acquiring a single pulse, but cannot take advantage of collecting energy from multipath components, as well as being very sensitive to noise and interference.

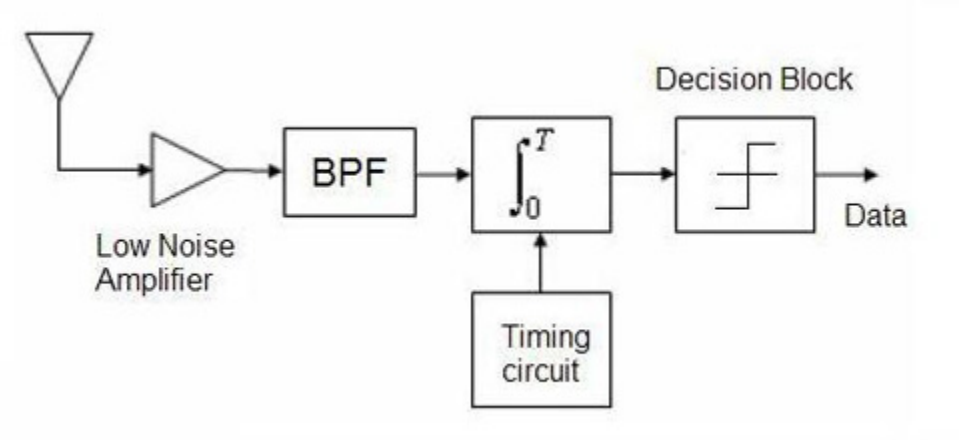

Figure 2.14 Amplitude threshold receiver block diagram

2.5.3.2 Energy Detection. Energy detectors are another type of non-coherent receivers. Figure 2.15 presents the block diagram for an energy detector. The first part consists of the energy calculation which is performed by squaring the input signal. The second part consists of an integration block. The ouput of the integrator goes to the decision block in which the value is compared to a threshold value and the output is the demodulated data bit.

2.6 Multiple Access Techniques for UWB

UWB communication is attractive for short-range and high data rate applications. Multiple users in a particular UWB covered area should be able to coexist. To achieve this, the need for multiple access techniques is essential to perform chanalization between users.

In a multiple access communication system, several users transmit information simultaneously over a shared channel [34]. The received signal at one user is the superposition of the intended signal, multiple access interference (MAI) and channel noise. MAI is given by the cross-correlation of unwanted user's signals on the intended

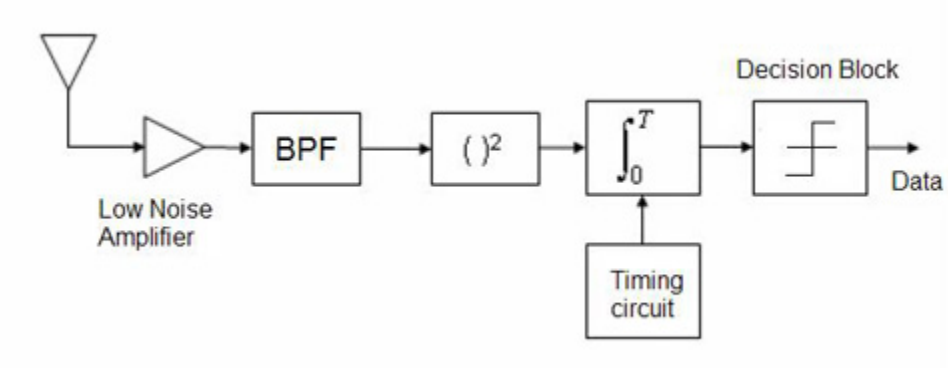

Figure 2.15 Energy threshold receiver block diagram

signal caused by partial overlap. A multi-user receiver must be capable of extracting the desired user signal from the received signal using proper demodulation techniques.

As stated by Nekoogar [34], the deteriorating effect of MAI is more severe in UWB systems due to their strict transmit power limitation. Thus, multiple access techniques must be used to obtain better system performance in multi-user scenarios. The two techniques for mulitple access in UWB systems are Time Hopping (TH-UWB) and Direct Sequence (DS-UWB). Both TH-UWB and DS-UWB are based on spreading in which a randomizing technique is applied to modulate the signal intended for each user.

2.6.1 Time Hopping UWB

In TH-UWB, unique time hopping codes are used to position each of the UWB pulses within a given time frame of a particular bit. Using PPM as the modulation technique, a time frame, T_f, is divided into chips of duration T_c. Each data bit is represented by a shifted pulse using a pseudorandom (PR) code in each time frame. A general signal model for PPM TH-UWB in a multiple access channel can be given by

$$s(t) = \sum_{n=1}^{N} \sum_{m=1}^{M} P\left(t - mT_f - c_m^{(n)} T_c - b_m^{(n)} \delta\right) \tag{2.13}$$

where

$c_m^{(n)}$ is the code word of the time hopping sequence for the data of an intended user

T_c is the chip duration

δ is the modulation index providing unique time shift to represent digital bits

N is the maximum number of users

M is the maximum number of transmitted bits

$P(t)$ is the UWB pulse

$b_m \in [0, 1]$ is the m^{th} data bit

and T is the pulse repetition period.

2.6.2 Direct Sequence UWB

DS-UWB is similar to CDMA in which a different spreading code is assigned to each user. In this case, the pulse waveform is the chip in DS. For PAM and OOK, the information signal $s(t)$ for the m^{th} user can be presented as

$$s(t) = \sum_{k=-\infty}^{\infty} \sum_{j=0}^{N-1} w\left(t - kT_d - jT_c\right) \left(c_p\right)_j^{(m)} d_k^{(m)} \tag{2.14}$$

where

d_k is the k^{th} data bit

$(c_p)_j$ is the j^{th} chip of the pseudo random code

$w(t)$ is the pulse waveform

N is the number of pulses to be used per data bit

T_c is the chip length

and the pseudo random code is bipolar assuming values [-1,+1], and the bit lenght is $T_d = NT_c = NT_p$.

2.7 Applications for UWB

UWB has become very popular for its penetration capabilities, low cost design, low probability of intercept, precise time resolution and high data rates. Some applications include UWB radar, positioning, logistics, sensor networks, search-and-rescue, medical imaging and consumer electronics. Table 2.1 show various applications for UWB signals.

Table 2.1 Some UWB applications in military and commercial sectors [34]

Application	**Military/Govmnt**	**Commercial**
Data Communications	Secure LPI/D Communications Covert wireless sensor networks (battlefield operations)	Local and personal area networks Wireless streaming video distribution (home networking) Wireless sensor networks (health and habitat monitoring, home automation)
Radar	Through-wall imaging (law enforcement, firefighters) Ground-penetrating radar (rescue operations) Surveillance and monitoring	Medical imaging (remote heart monitoring) Ground penetrating (detection of wires, studs, etc.) Automotive industry (collision avoidance, roadside assistance) Home security (proximity detectors)
Localization	Personnel identification Lost children Prisoner tracking	Inventory tracking Tagging and identification Asset management

2.7.1 Positioning

UWB is an ideal candidate for positioning an object in space due to its very short time-domain pulses. Using the time of arrival of a pulse traveling from the source to a receiver, an estimate of the traveled distance can be obtained [13]. Combining several receivers, a simple triangulation technique can solve the position of the source [38]. The bandwidth of UWB is in the order of GHz, which represents a resolution in the order of 133 picoseconds. This small resolution can achieve centimeter accuracy in positioning compared to resolutions of nanoseconds provided by narrower bandwidth signals. Positioning location with UWB is very attractive for many indoor situations (i.e. fire fighters in search-and-rescue applications).

2.7.2 Sensor Networks

Sensors are being used today in many applications like homes, automobiles, industry, medical situations, etc. Using wires to configure sensor networks is costly and tedious. UWB signals as sensors can reduce the cost of installation and maintenance of a sensor network. For its noise-like type of signal, UWB can achieve security improvements and low interference as well.

2.7.3 UWB Radar

UWB signals enables inexpensive high definition radar [57] since UWB systems have a low cost and time resolution for UWB communications achieves detection of objects separated by mere centimeters. Radar applications range from military and government to commercial situations (i.e. medical imaging or home security). The

advantage of through-wall motion detection makes UWB a great candidate for Radar. The capability of ground penetration is also an attractive feature of UWB Radars used for geophysical location and civil engineering applications.

2.8 Challenges ahead

There are many challenges for UWB communications due to the use of sub-nanosecond pulses for data transmission. Some challenges ahead are pulse-shape distortion, channel estimation, synchronization and multiple-access interference.

The transmission channel distorts UWB pulses significantly. This limits the performance of UWB receivers since the predefined template does not match the received pulse shape. Distortion on the pulse shape is also suffered if antennas are close to each other in systems with more than one receive antenna (multiple antenna arrays). Channel estimation is another important challenge of UWB communications and it is related to pulse distortion since the channel distorts the transmitted pulse. It is critical for a receiver design since training sequences are needed to estimate the channel and obtain a predefined template signal.

Synchronization, a key element on UWB receiver design, is a major challenge. Difficulty in sampling and synchronizing nano-second pulses limits the performance of UWB systems. The need for very fast analog-to-digital converters (ADC's) to sample these short duration pulses is critical. Timing errors such as jitter and drift also arise due to power limitations and short pulses which become a major problem for PPM modulation receivers [34]. A chirp UWB system—accepted into IEEE 802.15.4a in December 2006—uses a pair matched-filtering of SAW (surface acoustic wave) devices to greatly reduce the requirement for synchronization [46].

A multiple access system is formed of several users or devices that send and receive information over the same transmission medium. Receivers should be able to detect the information intended for each user in a medium where multiple access interference (MAI) is present. MAI limits channel capacity and performance of UWB receivers. Compared to narrowband systems, UWB's low power makes detection of the received information more challenging.

Narrowband interference is a big issue for co-existence of UWB systems with narrowband systems. Chirp UWB, again, is a good solution [56].

Range extension needs consideration for a class of sensor network applications.

2.9 Summary

In this chapter the fundamentals and advantages of UWB communication were presented. It was shown that UWB communication is based on impulse radio (IR) and the typical pulse shapes used were presented along with their spectra. At the transmitter, modulation schemes were discussed; and at the receiver, detection and demodulation of the received information was presented. It was shown that the optimum receiver consists of a correlator receiver with a template that matches the received waveform (match filter receiver). For this optimum receiver, the BER curve shows that antipodal PAM has a 3dB performance improvement over orthogonal PPM and OOK signaling. Typical multiple access techniques to overcome MAI (TH-UWB and DS-UWB) were discussed. Finally, applications and challenges for UWB were presented.

CHAPTER 3
UWB CHANNEL MEASUREMENTS AND MODELING

A channel is the propagation environment (or medium) in which a signal travels from transmitter to receiver. A feature of the UWB channel is its rich multipath profile which has a significant time resolution and very low power per multipath component. Also, the UWB channel is quasi-static which means that the coherent time of the channel is very large. This is a relevant feature since the transmitter can take full advantage of the CIR or channel state information (CSI), and thus, perfect channel estimation is realistic. UWB channel modeling has been an area of research in recent years due to the promising applications for UWB. To characterize and model the UWB channel, measurements are needed. Various measurement campaigns have been performed in the literature and several channel models for the UWB propagation have been proposed.

In this chapter, two techniques used to measure a UWB channel are presented. The simulation experiments in this thesis are based on measurements performed at indoor and outdoor environments during which the channel information is obtained. The creation of a control system for efficiency and reliability of the measurement process is also explained. It concludes with a brief description of UWB channel modeling and examples of common UWB channel models in the literature.

3.1 Measurement Techniques

UWB channel measurements are performed by sounding the channel. There are two approaches to sound the UWB channel: frequency domain (FD) technique and time domain (TD) technique. In the first, a frequency sweeping techinque is used.

While the second technique uses channel sounders based on impulse transmission or direct sequence spread spectrum (DSSS) signaling. Theoretically, the same result will be obtained from both techniques if there is a static environment and an unlimited bandwidth [38].

3.1.1 Frequency Domain Measurement

The FD channel sounding is performed by sweeping a set of narrowband sinusoid signals through a wide frequency band. The channel frequency response is then recorded using a Vector Network Analyzer (VNA). Figure 3.1 shows a VNA displaying a typical channel measurement. The advantage of the FD measurement technique is its larger dynamic range which improves the measurement precision. The channel impulse response (CIR), which yields the required information to characterize the UWB channel, is obtained by using the inverse Fourier transform (IFT) of the recorded signal. Therefore, a disadvantage of the FD approach is the need of extra signal processing.

The diagram for the measurement setup of an UWB channel using a VNA is shown in Figure 3.2. Both magnitude and phase are measured directly. To measure the complex frequency domain transfer function, a S_{21}-parameter measurement is performed where the device under test (DUT) is the UWB channel. A limitation of the frequency domain channel sounding is the need of a static environment through out the measurement.

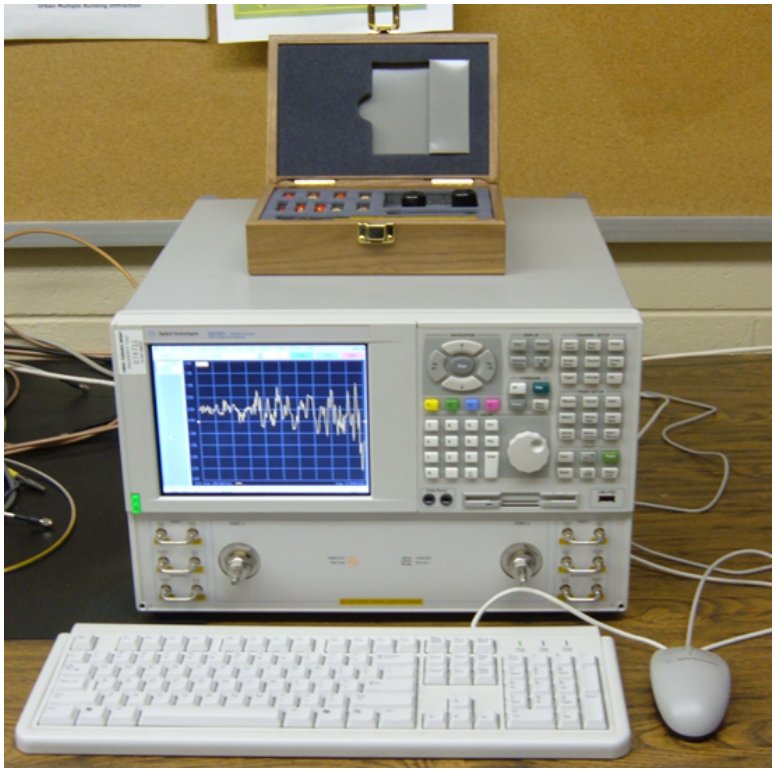

Figure 3.1 Vector Network Analyzer for FD channel sounding

3.1.2 Time Domain Measurement

For the TD approach, the channel is sounded by sending a series of narrow pulses and measuring the received waveform using a Digital Sampling Oscilloscope (DSO). The channel impulse response (CIR) can then be obtained from the recorded signal using a deconvolution method. Unlike the FD approach, the TD technique can support non-stationary channels. The bandwidth of the sounder will depend on the shape and width of the transmitted pulse.

A diagram of the time domain measurement setup for UWB channel characterization is presented in Figure 3.3. The setup consists of a pulse generator, transmit and receive antennas, a triggering signal generator, and the DSO. Figure 3.4 shows a Digital Sampling Oscilloscope for UWB channel sounding. Measurements using the

TD approach are susceptible to wideband noise. By averaging multiple acquisitions this type of noise can be reduced significantly [52].

UWB channel measurements were carried out in this work to conduct simulation experiments. All measurements are performed using the TD approach since all signal processing is performed in the time domain. Aditionally, two channel modules in the DSO allow to measure the channel on two close coupled antennas simultaneously.

3.2 Deconvolution Techniques

Deconvolution is the inverse operation of convolution. It is used to separate two signals that have been combined by convolution [2]. In a measurement, the recorded signal is the result of the convolution of the transmitted pulse with the impulse response of the channel

$$y(t) = p(t) \otimes h(t) \tag{3.1}$$

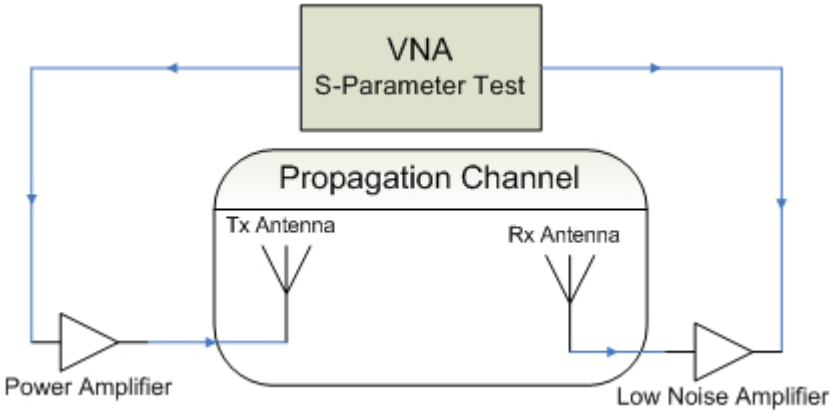

Figure 3.2 FD measurement setup block diagram

where $y(t)$ is the recorded signal, $p(t)$ is the transmitted pulse, and $h(t)$ is the CIR. Since the pulse is not an impulse ($p(t) \neq \delta(t)$), a deconvolution technique must be applied to extract the CIR. Deconvolution can be performed in frequency domain or in time domain. A number of deconvolution techniques have been proposed in the literature [53].

Inverse filtering is a typical method used in frequency domain. Convolution in the time domain is mapped as multiplication in the frequency domain and then from Equation 3.1 it follows that

$$Y(f) = P(f)H(f) \tag{3.2}$$

where $Y(f)$, $P(f)$, and $H(f)$ are the Fourier transform of $y(t)$, $p(t)$, and $h(t)$ respectively. Then to obtain the channel impulse response a simple division followed by inverse Fourier transform can be performed.

Other deconvolution techniques can be performed in the time domain. Examples include the Van-Cittert deconvolution and the CLEAN algorithm [30]. The CLEAN algorithm is a common method for obtaining the CIR of UWB TD channel measurements. The CLEAN algorithm uses match filtering to find the strength and

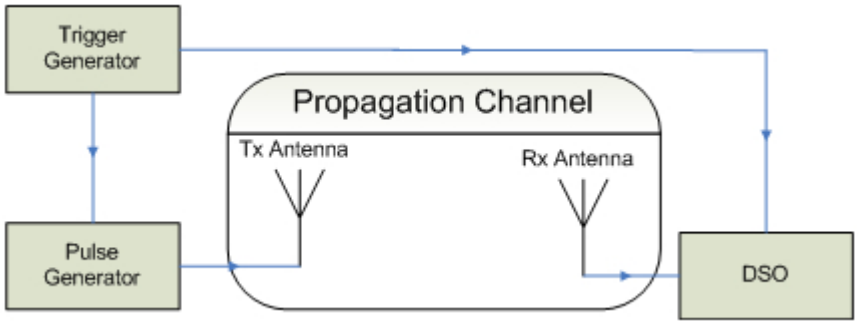

Figure 3.3 TD measurement setup block diagram

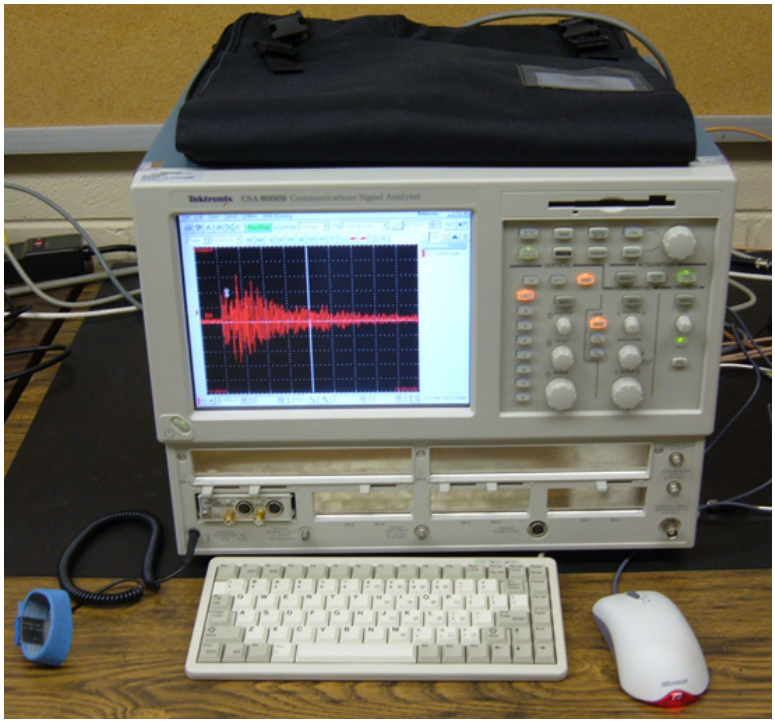

Figure 3.4 Digital Sampling Oscilloscope for TD channel sounding

delay of individual multipath components [52]. In this work time domain measurements and simulations make the CLEAN algorithm more suitable for obtaining the CIR.

3.2.1 CLEAN Algorithm

The CLEAN algorithm is often preferred as a deconvolution method because of its ability to produce a discrete CIR in the time domain. It is consistent with the channel models that consider the UWB channel as a series of impulses. A waveform template is needed for this deconvolution technique which is obtained by performing a line-of-sight (LOS) measurement where the distance between the transmitter and

receiver is 1m. Figure 3.5 shows the waveform template used in this thesis to obtain the CIR from measurement results.

If $s(t)$ is the waveform template, $y(t)$ is the received waveform, and $h(t) = 0$ as an initial value; the steps involved in the CLEAN algorithm to find the CIR $h(t)$ are [52, 61]

1. The autocorrelation of the template $r_{ss}(t)$ and the cross-correlation of the template and the received waveform $r_{sy}(t)$ are calculated as follows

$$r_{ss}(t) = \int_{-\infty}^{\infty} s(\tau)x(t-\tau)d\tau \tag{3.3}$$

$$r_{sy}(t) = \int_{-\infty}^{\infty} s(\tau)y(t-\tau)d\tau \tag{3.4}$$

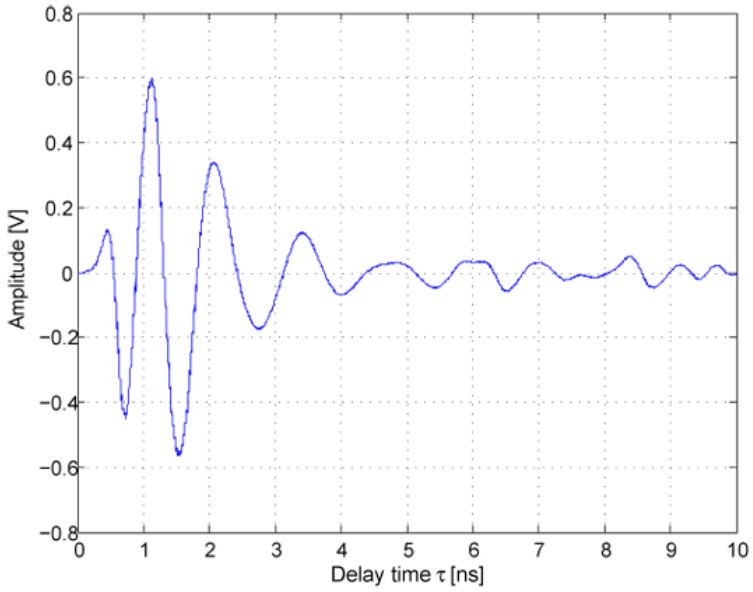

Figure 3.5 Template waveform required for deconvolution using CLEAN algorithm

2. The largest correlation peak in $r_{sy}(t)$ is found and the normalized amplitudes α_k and the relative time delay τ_k of the correlation peak are recorded

$$|\alpha_k(\tau_k)| = \max |r_{sy}(t)| \tag{3.5}$$

3. The CIR is constructed as follows

$$h(t) = h(t) + \alpha_k \delta(t - \tau_k) \tag{3.6}$$

4. Then, $r_{ss}(t)$ scaled by α_k is subtracted from $r_{sy}(t)$ at the time delay τ_k

$$r_{sy}(\tau) = r_{sy}(\tau) - \alpha_k r_{ss}(\tau_k) \tag{3.7}$$

5. If the peak correlation in $r_{sy}(t)$ is less than a set minimum threshold value (-15dB in this thesis) the algorithm stops, if not the algorithm continues at step 2.

3.2.1.1 Limitations of the CLEAN Algorithm. Since the CLEAN algorithm uses a match filtered signal to evaluate the strength and arrival time of the multipath components, unresolvable paths affect the match filter output and thus the output will not give the true CIR. Also, if the pulses at the receiver side are significantly distorted, the CLEAN algorithm may generate spurious taps that are not physically linked to multipath components, but rather represent distortions. When different paths are associated with different pulse shapes the use of one LOS template would not yield a good estimate of the CIR [30].

To evaluate how accurate the output generated by the CLEAN algorithm is compared to the true CIR, the energy capture ratio and relative error can be calculated [30]. The calculated CIR is convolved with the LOS template to create an estimate of the received signal r_{est}. The energy of this estimate is divided by the energy in the measured signal r_{meas} as follows

$$Energy\ Capture\ Ratio = \frac{\|r_{est}\|^2}{\|r_{meas}\|^2} \tag{3.8}$$

and the difference between the estimate and the measured signal is defined by

$$Relative\ Error = \frac{\|r_{meas} - r_{est}\|^2}{\|r_{meas}\|^2} \tag{3.9}$$

3.3 Measurement Results

Antenna coupling and channel spatial correlation are two effects of antennas located close to each other that interact and distort the received signal. These two effects cannot be separated from each other, and therefore, must be measured together. Antenna coupling refers to the near-field effect an antenna has on the performance of another nearby antenna. Channel spatial correlation deals with the correlation of the received signals for two closely located antennas. The objective of the experimental measurements in this work is to evaluate these effects on UWB wireless systems with two receiver antennas that are located near each other. Therefore, the experiments performed deal with measuring two channels simultaneously as the distance between two receive antennas decreases. Since this work focuses on antenna coupling and channel spatial correlation, the term *coupling effects* will refer to these two mechanisms from now on.

The UWB channel is measured using the TD technique. The equipment setup used is similar to the one explained in Section 3.1.2, but now two receive antennas are considered. In this work, the two channels are measured simultaneously as shown in the system's block diagram presented in Figure 3.6.

The equipment at the transmitter side consists of a UWB pulser which generates a Gaussian pulse with a width of 250ps, a function generator (Agilent 33220A) which is used for triggering the pulser and as a synchronization signal, and the transmit antenna as presented in Figure 3.7. Other type of pulses (gaussian monocycle or doublet) can be obtained by using a differentiator at the pulser output.

At the receiver side, the equipment consists of a DSO (TDS8000E3) from Tektronix with a bandwidth of up to 20GHz which is set to record two channels and is triggered by the synchronization signal coming from the function generator. The Notebook PC serves as the control system for the DSO and communicates using a GPIB-USB cable. Two receiver antennas are used for each receiver location as presented in Figure 3.8.

To ensure safety on the DSO, attenuation pads are placed on several parts of the system. All antennas are omni-directional, linear in polarization, and span

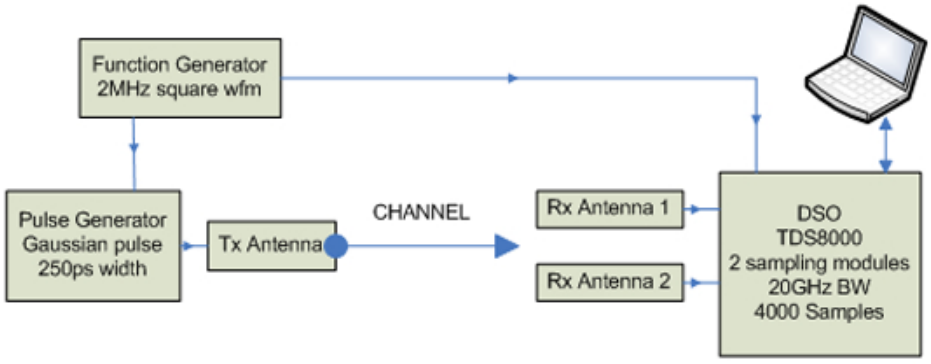

Figure 3.6 Block diagram for TD measurement of two channels simultaneously

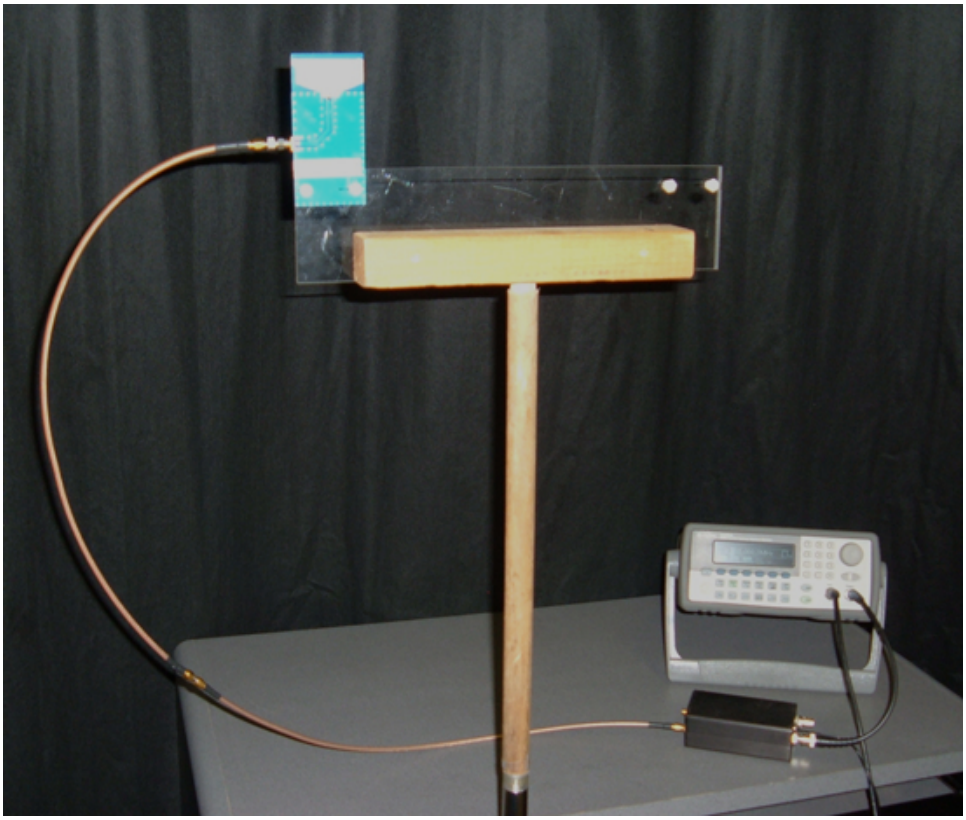

Figure 3.7 Transmitter equipment setup for TD measurements

a bandwidth of 0.824-2.4GHz with a feed impedance of 50 ohms. To obtain the best received signal energy [2], each antenna is set with an angle of 0 degrees with the vertical and the distance of all antennas from the ground is 1.35m for all experiments.

To record the signal in each channel, a series of files are manually saved in the DSO. This process is tedious and inacurate when two channels have to be measured at the same time. A control system was implemented to overcome this problem and is explained in Section 3.3.1.

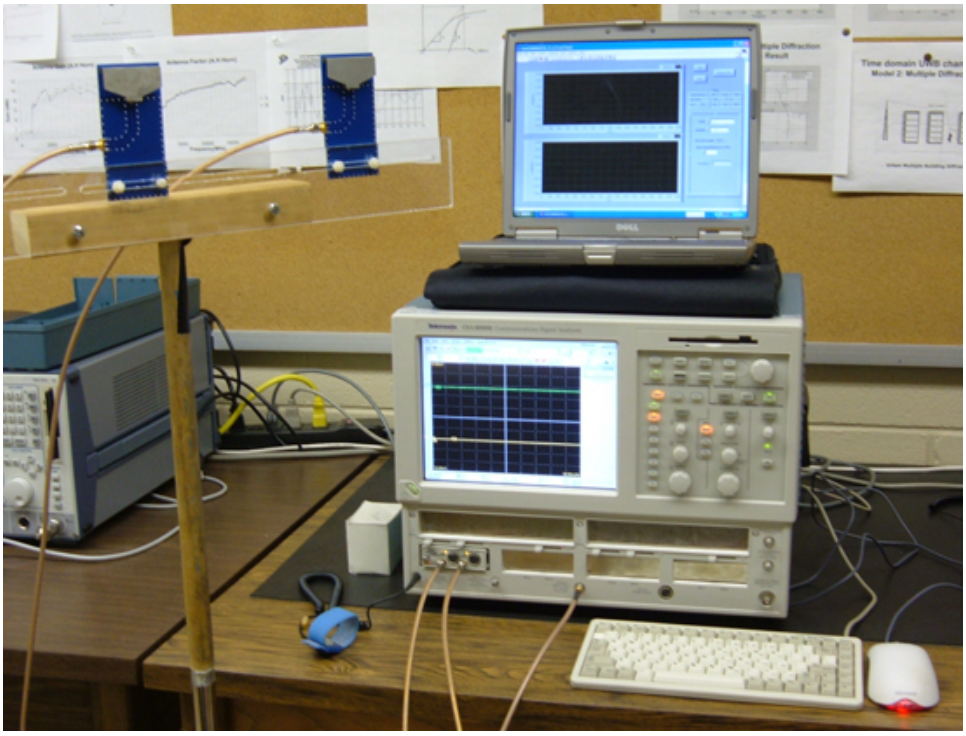

Figure 3.8 Receiver equipment setup for TD measurements

3.3.1 Measurement Control System

The control system was developed by the author using a communication link between the DSO and a Notebook PC. The communication is achieved using National Instrument's Labview Software. A user interface was created at the Notebook PC to control many features of the DSO and obtain measurements on two channels with more accuracy. Some features and capabilities of this control system are:

1. Save all required files in the shortest amount of time
2. Backing up files at the Notebook PC
3. Post-process the signal inmideately after acquisition
4. Record several channels simultaneously
5. Record a signal for a long period of time

6. Precise measurement by stepping farther away from the equipment (to not disturb the channel measurement) using long cables.

Figure 3.9 shows the Labview user interface on the Notebook PC and a typical UWB channel measurement. The communication between the two devices is performed using the GPIB protocol in the DSO and USB protocol at the Notebook PC.

3.3.2 Antenna Coupling and Channel Spatial Correlation

To understand the effects of antenna coupling and channel spatial correlation, outdoor and indoor measurements are performed. In an outdoor environment scatterers are not present, therefore, the channel is multipath free and the recorded signal contains only the waveform distortion caused by the *coupling effects*. In an indoor

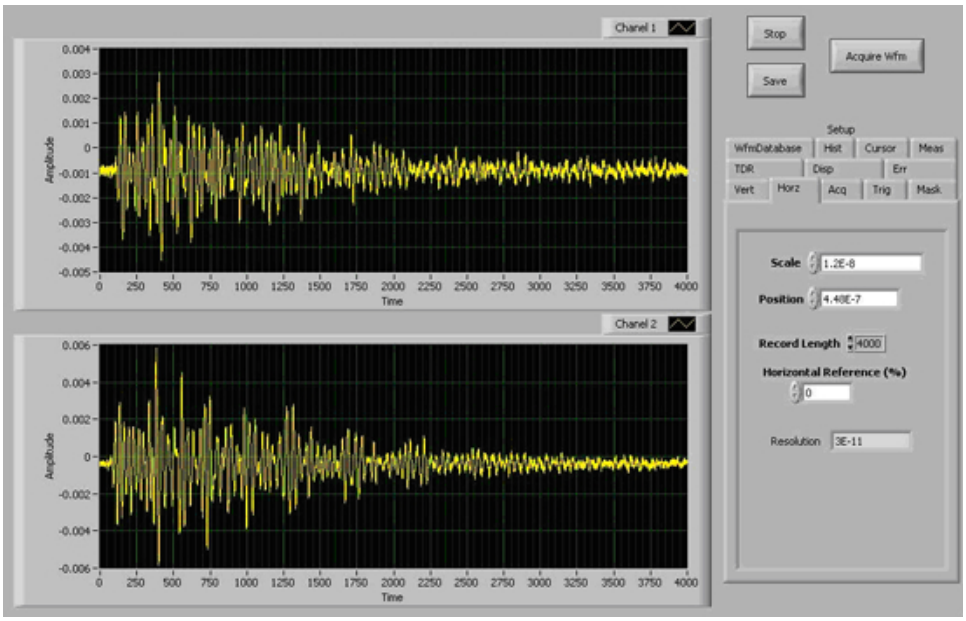

Figure 3.9 Typical measurement at Notebook PC using Labview Interface to control DSO

environment, the channel profile contains multipath components and the received signal experiences distortion.

3.3.2.1 Outdoor measurement. The purpose of this experiment is to obtain the antenna impulse response and visualize the distortion of the received pulse having two antennas near each other. Figure 3.10 shows the measurement setup for this experiment. Transmitter and receiver antennas are omni-direccional and are 1.35m above the ground. The goal is to record the signal at different distances, D, between two receiver antennas and compare the obtained waveform with the case where only one receiver antenna is present.

This experiment consists of a UWB LOS link where the distance between the transmitter and the receiver is 1m. The first measurement consists of recording the signal at receiver antenna 1 (Rx1) without the presence of receiver antenna 2 (Rx2) and it is presented in Figure 3.11.

The following measurements are carried out with Rx2 present. The distance D is varied from 3cm to 15cm in 3cm steps. For comparison, a measurement at $D = 30cm$ is also performed where the distance is big and antenna effects are small. The waveforms obtained for $D = 3cm$ and $D = 30cm$ at Rx1 are shown in Figure 3.12 and 3.13 respectively. Figure 3.14 and 3.15 display the recorded signals at Rx2 for $D = 3cm$ and $D = 30cm$ where the signal is stronger in amplitude due to antenna gain. Measurement results are processed to obtain the antenna impulse response and evaluate pulse distortion. These results are presented in Chapter 5.

3.3.2.2 Indoor measurement. The purpose of this experiment is to visualize pulse distortion and coupling effects on the multipath components of the recorded signal in an indoor environment. Figure 3.16 shows the office environment in which the experiment is performed.

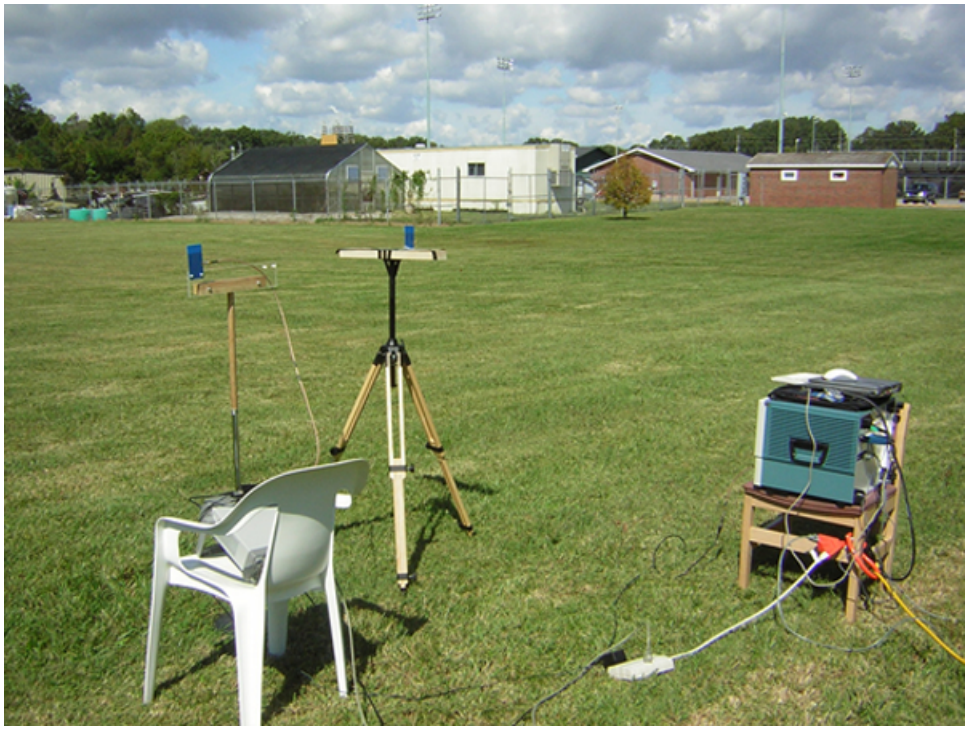

Figure 3.10 Outdoor measurement setup and location

In this experiment, one transmit antenna (Tx1) and two receive antennas (Rx1 and Rx2) are present and the distance between transmitter and receiver is 1m in a LOS link. Figure 3.17 show the recorded signal when only Rx1 is present, thus, no distortion due to coupling effects is observed and this waveform can be used for comparison. Figure 3.18 shows the recorded signal at Rx1 when Rx2 is present and the distance D, between them is 3cm ($D = 3cm$). Figure 3.19 shows the recorded signal at Rx1 when $D = 30cm$. It is observed how the received signal is distorted and the signal is smaller in amplitude when the distance between Rx1 and Rx2 decreases.

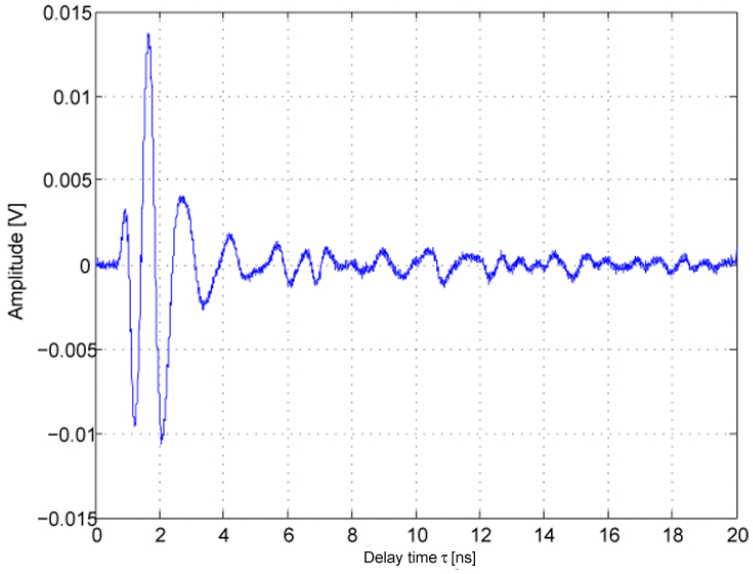

Figure 3.11 Recorded signal for Rx1 alone

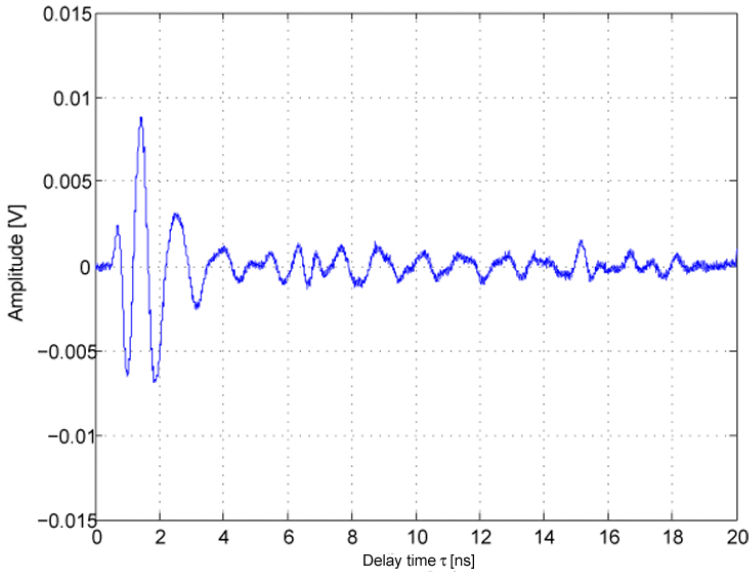

Figure 3.12 Recorded signal at Rx1 for $D = 3cm$

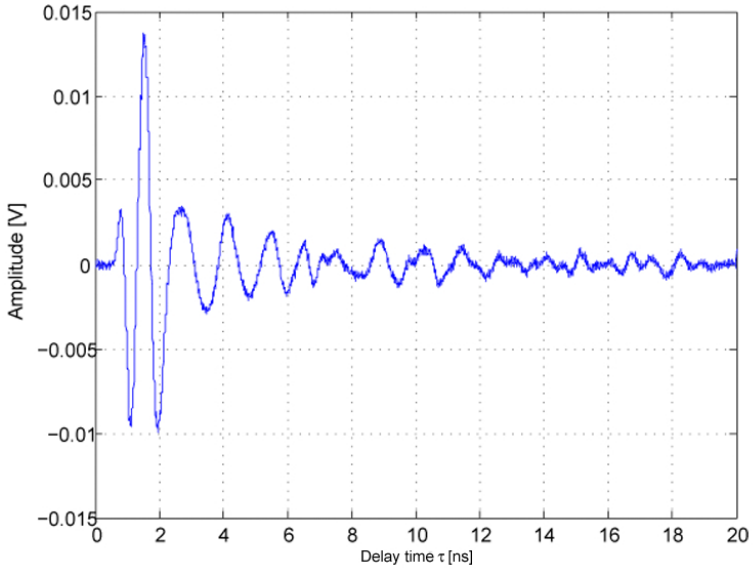

Figure 3.13 Recorded signal at Rx1 for $D = 30cm$

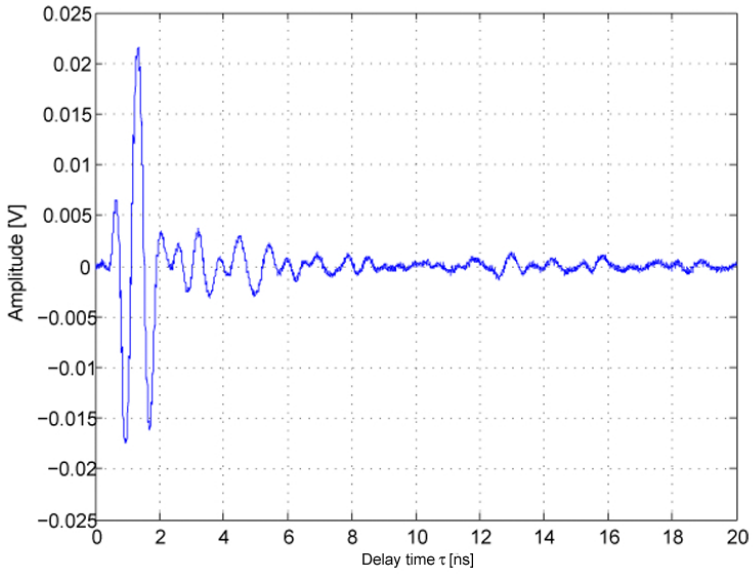

Figure 3.14 Recorded signal at Rx2 for $D = 3cm$

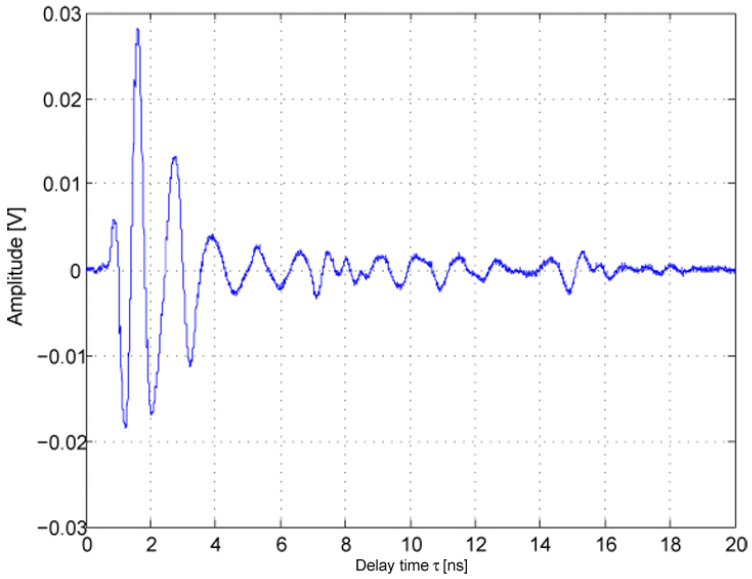

Figure 3.15 Recorded signal at Rx2 for $D = 30cm$

Figure 3.16 Office environment in CH-403

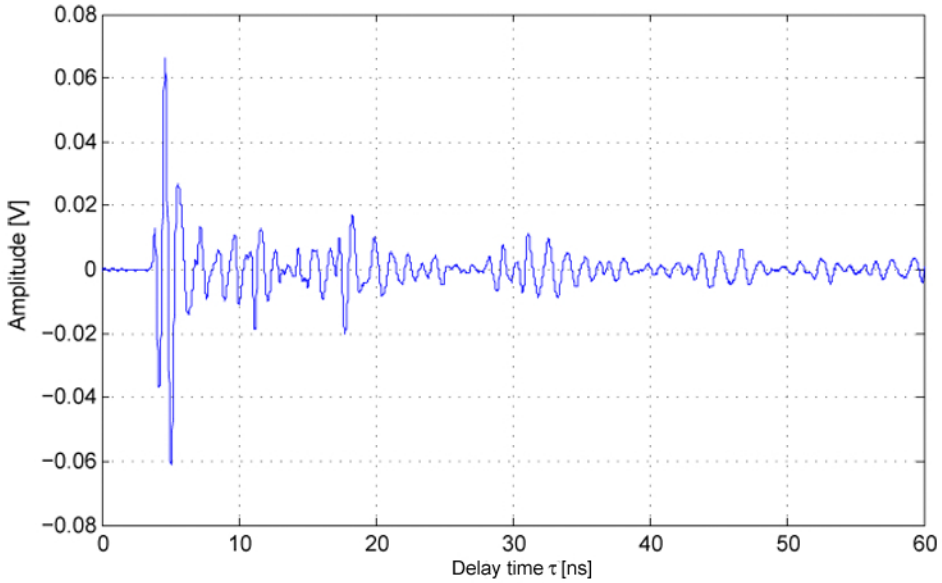

Figure 3.17 Recorded signal for Rx1 alone

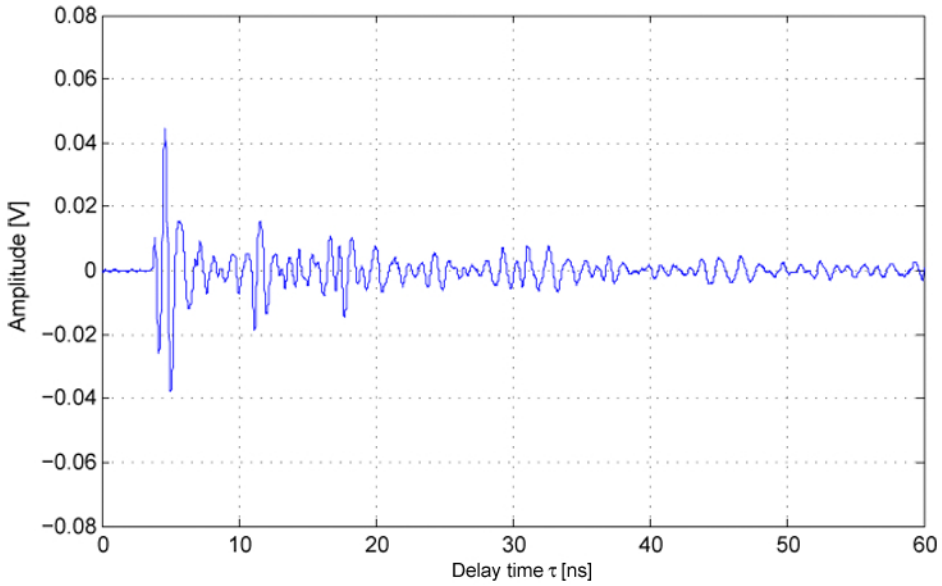

Figure 3.18 Recorded signal for Rx1 with Rx2 present and $D = 3cm$

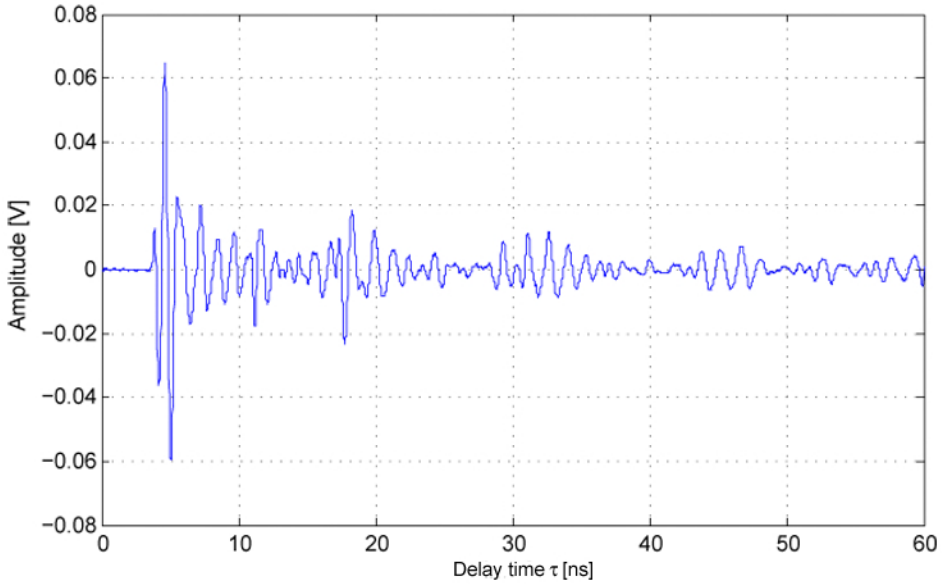

Figure 3.19 Recorded signal for Rx1 with Rx2 present and $D = 30cm$

3.3.3 Virtual Array and Real Array Measurements

A virtual array can be measured by recording the received signal at different points independently and using the recorded waveforms to construct the array. When a system with multiple antennas is considered and the distance between the antennas is small, coupling effects arise and the virtual array is no longer valid. In this case, a model for the coupling effects must be added to the received data or a real array must be measured. A real array is one in which the received signal at different points is measured simultaneously. The objective of this measurement is to identify the distance between the receive antennas at which the coupling effects become recognizable and a virtual array is invalid.

The experiment is performed at the Wireless Networking Systems Lab located at Room CH-400. This site is an indoor environment and is shown in Figure 3.20.

Figure 3.20 Wireless Networking Systems Lab environment in CH-400

In this experiment, one transmit antenna is located 6m away from two receive antennas whose distance between them D, is varied from 5cm to 40cm in 5cm increments. Two different aproaches for this measurement are considered: (1) a virtual array approach in which only one antenna is present and (2) a real array approach in which both antennas are present and channels are measured simultaneously. Results for the real array and virtual array for the recorded signal from Tx1 to Rx1 at $D = 5cm$ and $D = 40cm$ are shown in Figure 3.21 and Figure 3.22 respectively. Clearly, the received waveform for the virtual array is distorted compared to the received waveform for the real array at small distances D. A system simulation experiment is also performed using the recorded waveforms in this experiment. These results are discussed in Chapter 5.

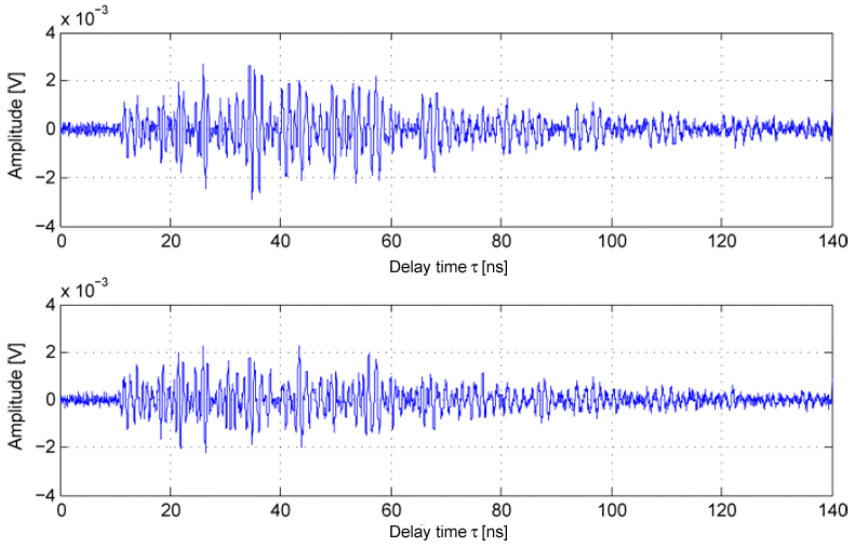

Figure 3.21 Recorded signal from Tx1 to Rx1 for $D = 6cm$. (a) Virtual Array and (b) Real Array

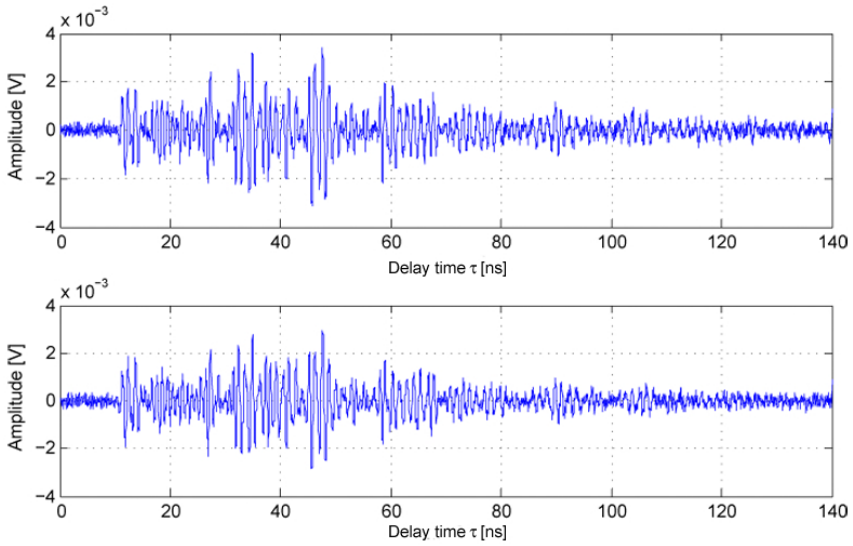

Figure 3.22 Recorded signal from Tx1 to Rx1 for $D = 40cm$. (a) Virtual Array and (b) Real Array

3.3.4 Single-user and Multi-user Measurements

Single-user and multi-user measurements are carried out on both indoor environments presented before: the Wireless Networking Systems Lab and the Office environment. In both environments, measurements are performed at off-peak hours to decrease noise from other sources. The distance between each transmitter and receiver pair ranges between 2m and 10m. Since the best results for TiR are obtained for a non-line-of-sight (NLOS) link and in this work UWB systems using TiR are investigated, all experiments carried out use NLOS links.

The Wireless Networking System Lab is an L-shape room enclosed in a brick wall and divided in two spaces as shown in Figure 3.23. The first space (left side) measures 2.8m by 11.3m and transmitter antennas are positioned in this area in 4 locations (Tx1-Tx4) as shown in Figure 3.23. The second space (right side) measures 5.8m by 3.1m and receiver antennas are positioned at locations shown in Figure 3.23. There are four locations (i.e. four users), each having two receiver antennas (Rx1 and Rx2). The distance between the Rx1 and Rx2, D, is varied from 5cm to 40cm in 5cm increments.

The Office environment is a space enclosed in a brick wall as shown in Figure 3.24. The room measures 9.3m by 11.3m and transmit and receive antennas are positioned in this area as shown in Figure 3.24. The objective of this experiment is to record and measure the channel for 2 locations at the transmitter (Tx1 and Tx2) and 25 locations for the receiver (25 users), in which each location consists of two receiver antennas (Rx1 and Rx2). The distance between the Rx1 and Rx2, D, is varied from 3cm to 15cm in 3cm increments.

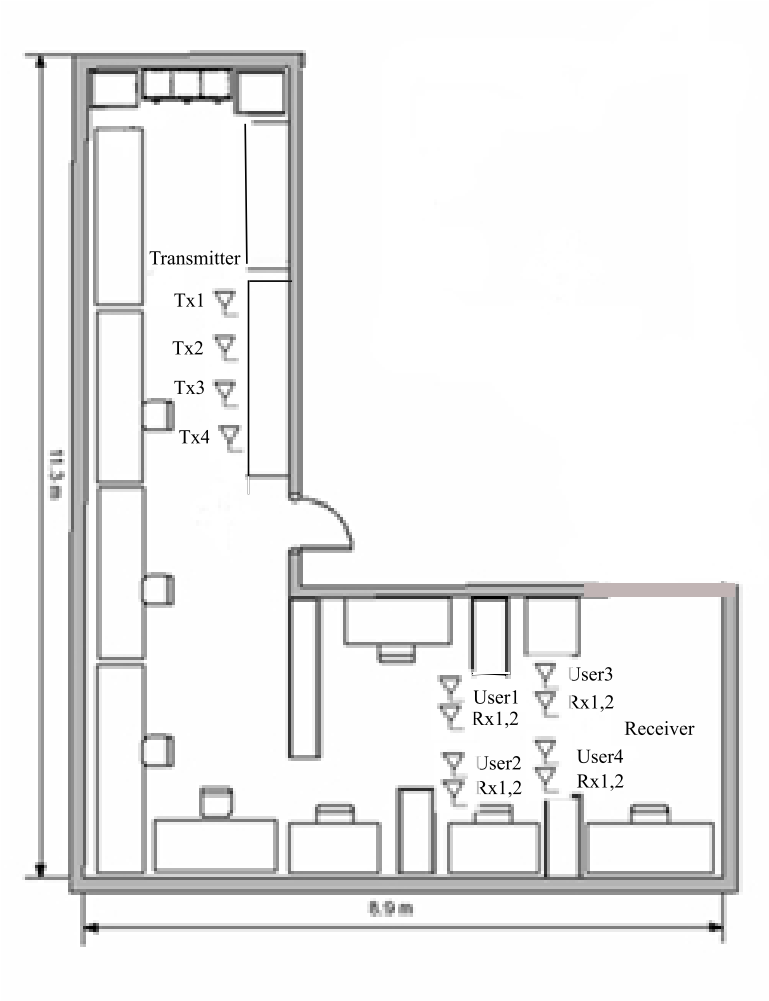

Figure 3.23 Wireless Networking Systems Lab layout with antenna locations

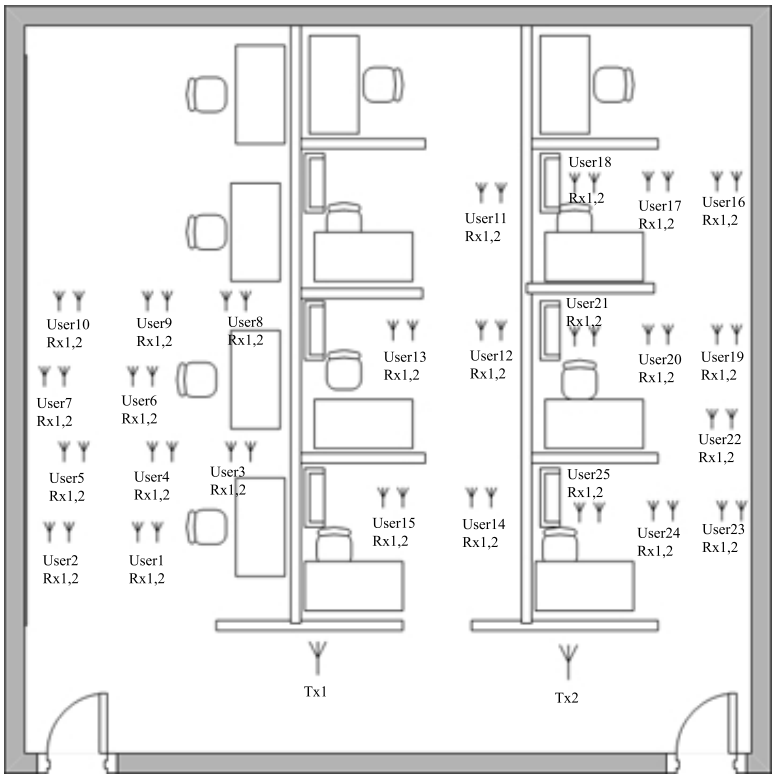

Figure 3.24 Office layout with antenna locations

3.3.4.1 Lab measurement results. In this experiment there are four locations for the transmitter (Tx1 to Tx4) and four locations (i.e. four users) for receiver antennas Rx1 and Rx2. Transmit antennas are spaced 50cm apart and the power delivered is the same for all measurements. Measurement results for signal from Tx1 to Rx1 ($h_{11}(\tau)$) at receiver location 1 for $D = 5cm$ and $D = 40cm$ are presented in Figure 3.25 and Figure 3.26 respectively. Figure 3.27 and Figure 3.28 show the recorded signals from Tx1 to Rx2 ($h_{12}(\tau)$) at receiver location 1 for $D = 5cm$ and $D = 40cm$ respectively. The CLEAN algorithm was used to obtain the CIR and results are presented in Figure 3.29 for $h_{11}(\tau)$ at $D = 5cm$, in Figure 3.30 for $h_{11}(\tau)$ at $D = 40cm$, in Figure 3.31 for $h_{12}(\tau)$ at $D = 5cm$, and in Figure 3.32 for $h_{12}(\tau)$ at $D = 40cm$.

3.3.4.2 Office measurement results. In this experiment there are two locations for the transmitter (Tx1 and Tx2) and 25 locations for receive antennas Rx1 and Rx2 as shown in Figure 3.24. Transmitters are 2m away from each other and the power transmitted is the same for both Tx1 and Tx2 in all measurements. The results for the recorded signal from Tx1 to Rx1 ($h_{11}(\tau)$) at user 1 for $D = 3cm$ is presented in Figure 3.33 and for $D = 15cm$ in Figure 3.34. The measured waveform from Tx1 to Rx2 ($h_{12}(\tau)$) at user 1 for for $D = 3cm$ is presented in Figure 3.35 and for $D = 15cm$ in Figure 3.36. Furthermore, Figure 3.37 shows $h_{21}(\tau)$ for $D = 3cm$ and Figure 3.38 shows $h_{21}(\tau)$ for $D = 15cm$. Figure 3.39 shows $h_{22}(\tau)$ for $D = 3cm$ and Figure 3.40 shows $h_{22}(\tau)$ for $D = 15cm$. The recorded signals in all experiments are used for simulations and to evaluate performance of an UWB communication system using TiR. These simulation results are discussed in Chapter 5.

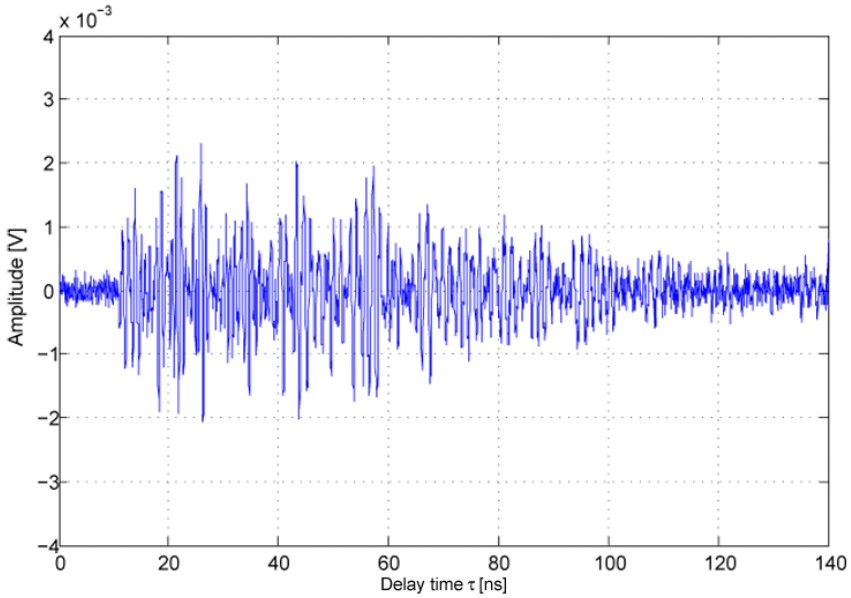

Figure 3.25 Recorded signal from Tx1 to Rx1 at location 1 for $D = 5cm$

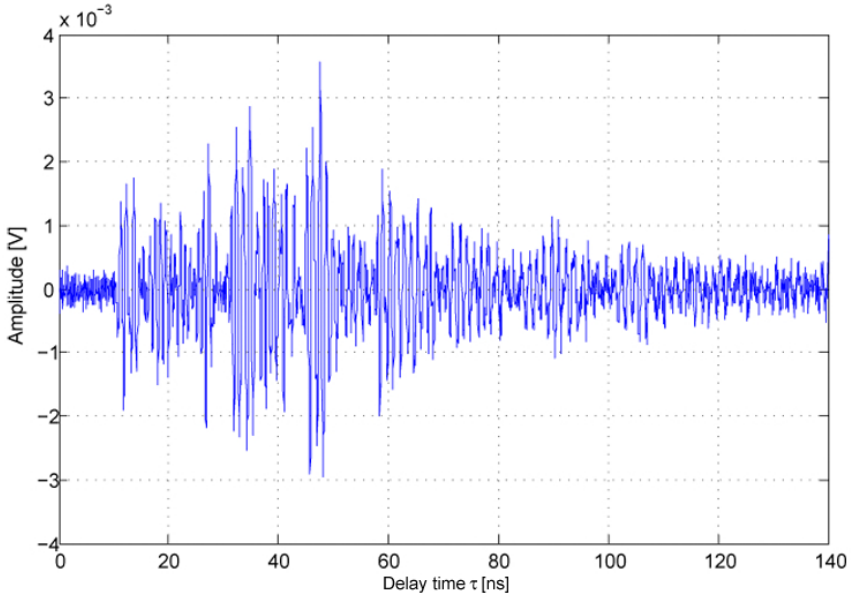

Figure 3.26 Recorded signal from Tx1 to Rx1 at location 1 for $D = 40cm$

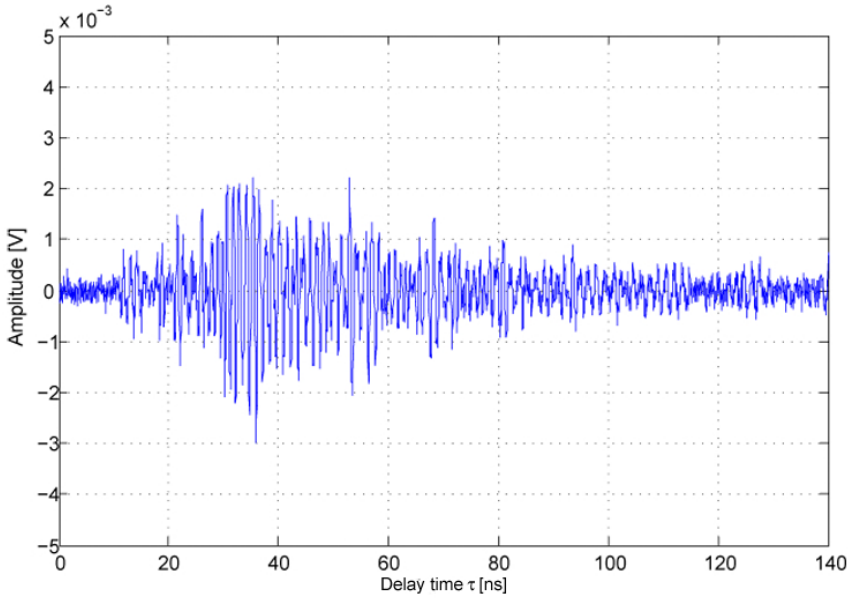

Figure 3.27 Recorded signal from Tx1 to Rx2 at location 1 for $D = 5cm$

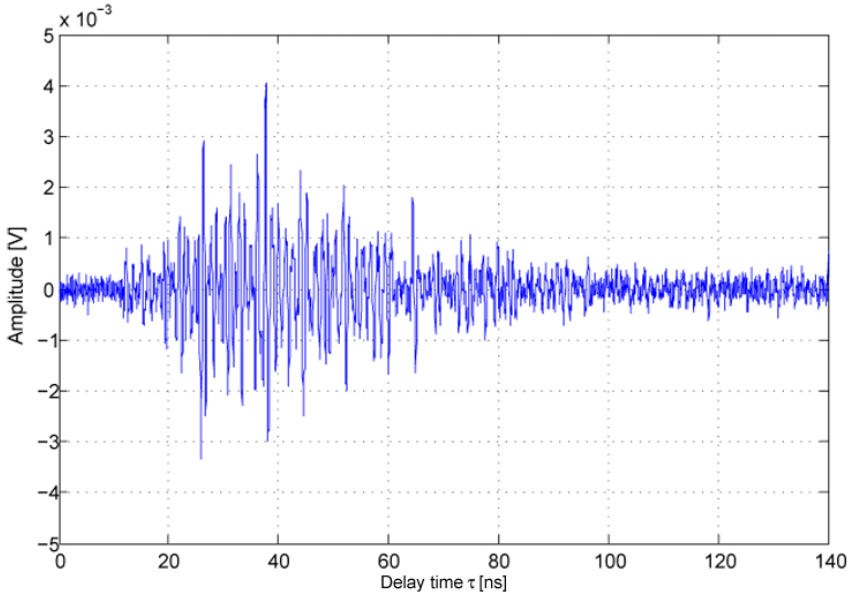

Figure 3.28 Recorded signal from Tx1 to Rx2 at location 1 for $D = 40cm$

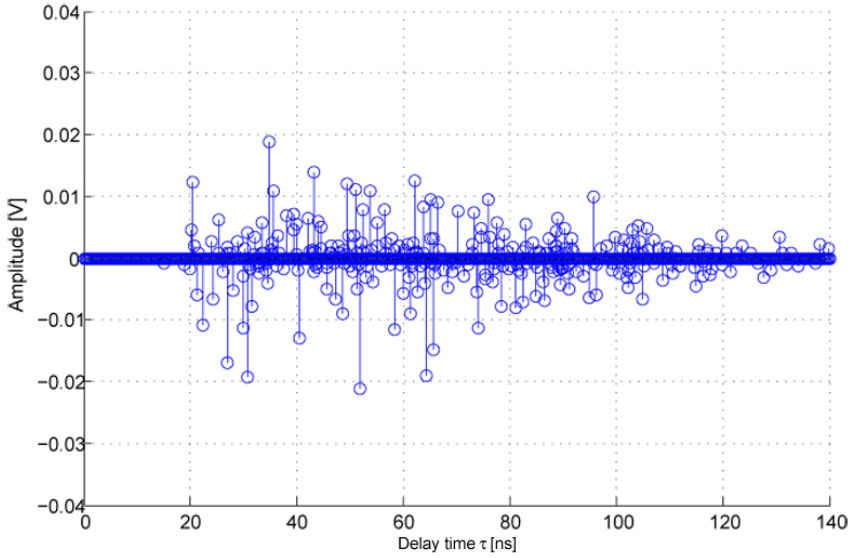

Figure 3.29 CIR for recorded signal from Tx1 to Rx1 at location 1 for $D = 5cm$

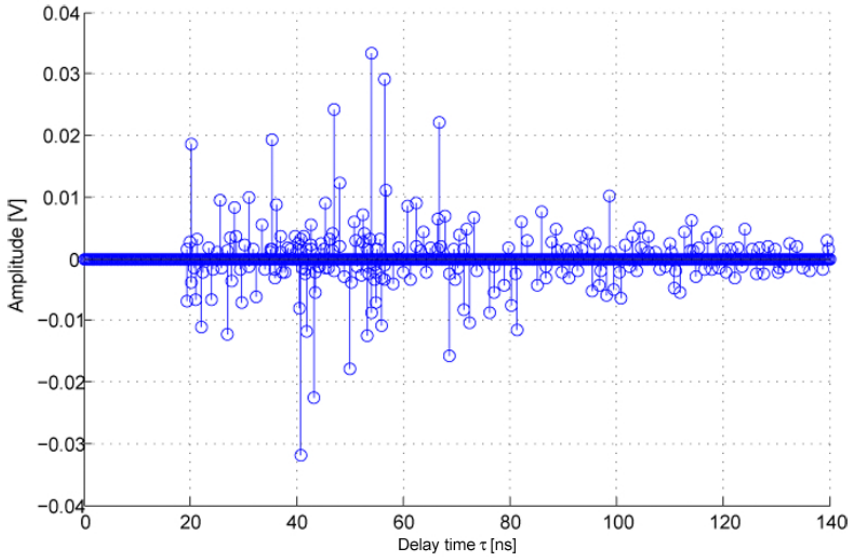

Figure 3.30 CIR for recoded signal from Tx1 to Rx1 at location 1 for $D = 40cm$

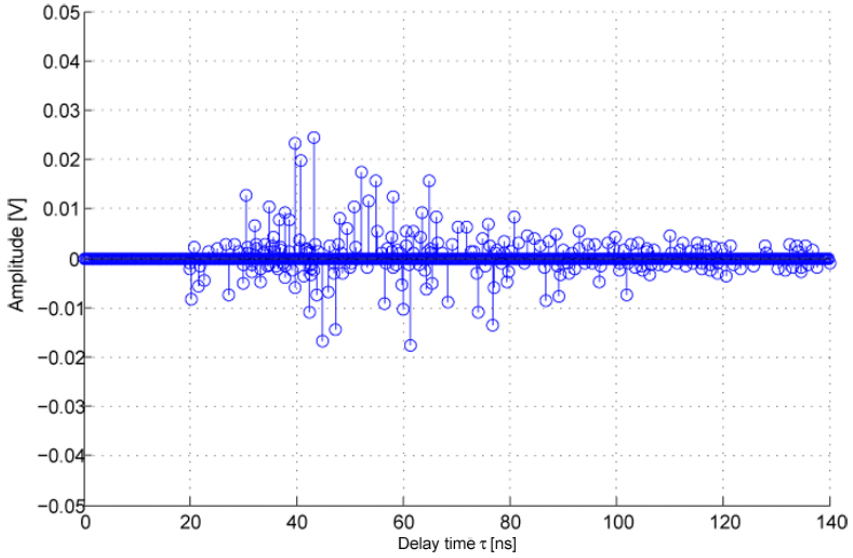

Figure 3.31 CIR for recorded signal from Tx1 to Rx2 at location 1 for $D = 5cm$

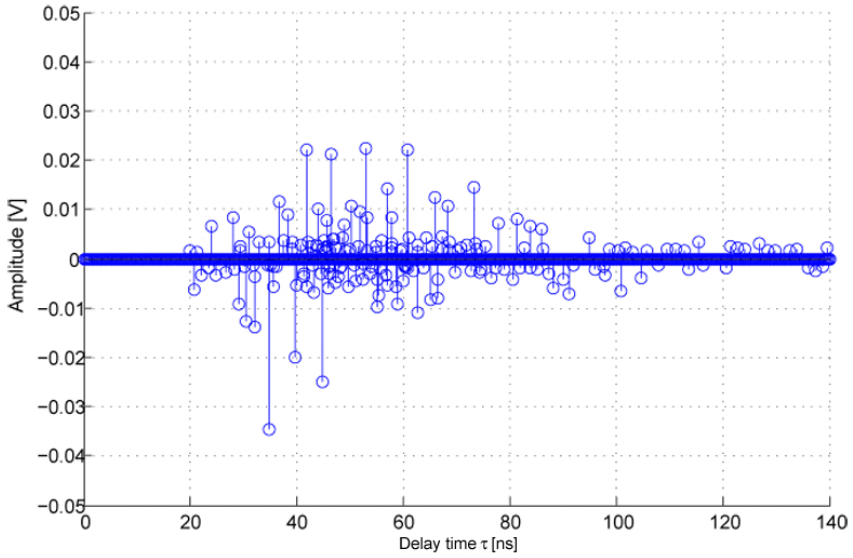

Figure 3.32 CIR for recorded signal from Tx1 to Rx2 at location 1 for $D = 40cm$

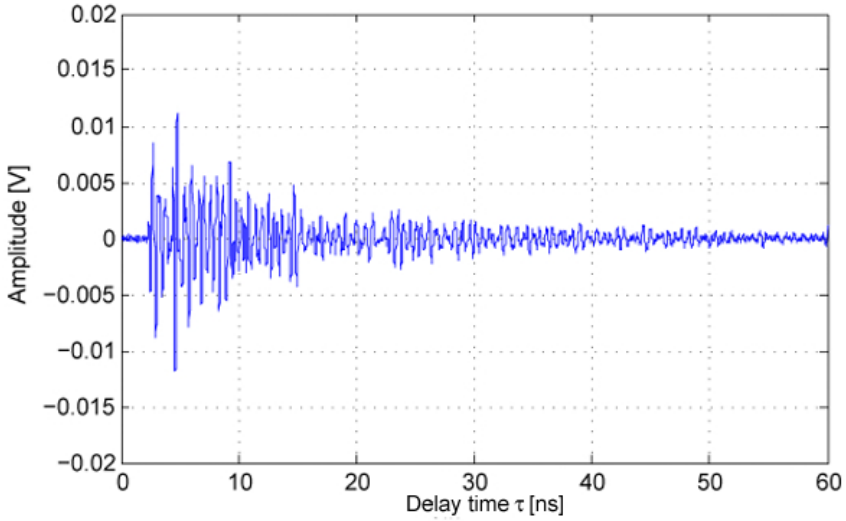

Figure 3.33 Measured signal from Tx1 to Rx1 (h_{11}) at user 1 for $D = 3cm$

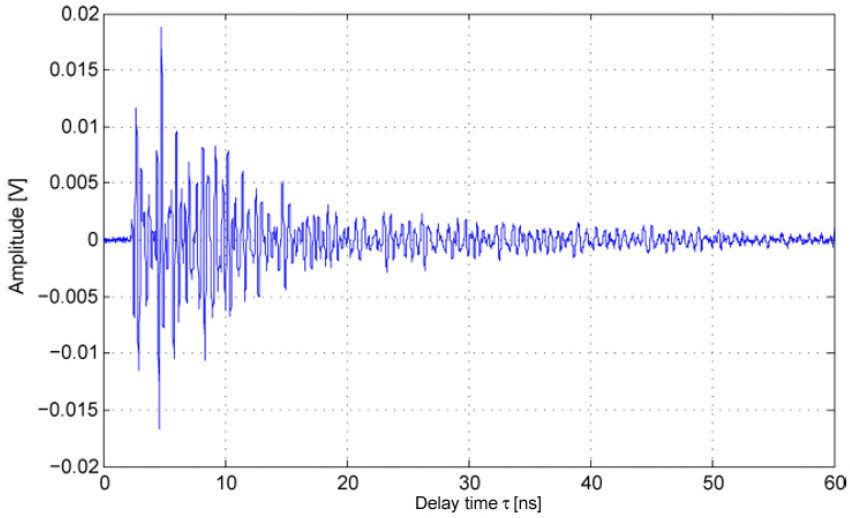

Figure 3.34 Measured signal from Tx1 to Rx1 (h_{11}) at user 1 for $D = 15cm$

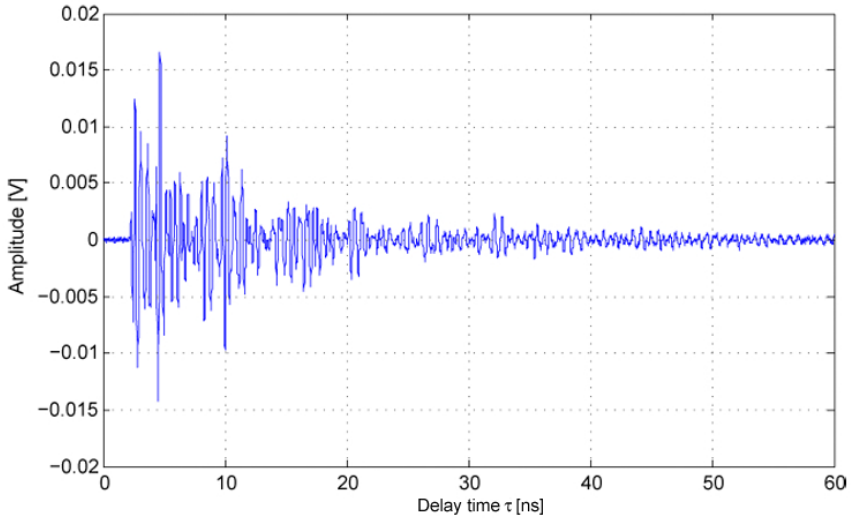

Figure 3.35 Measured signal from Tx1 to Rx2 (h_{12}) at user 1 for $D = 3cm$

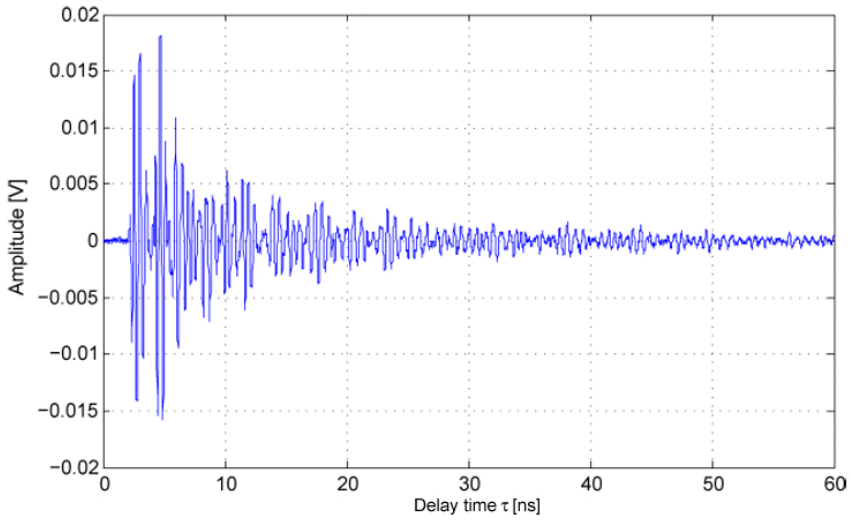

Figure 3.36 Measured signal from Tx1 to Rx2 (h_{12}) at user 1 for $D = 15cm$

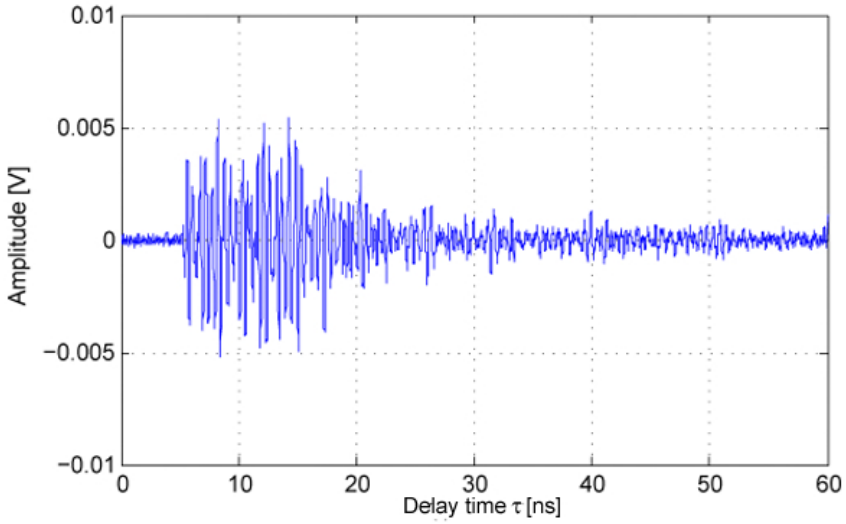

Figure 3.37 Measured signal from Tx2 to Rx1 (h_{21}) at user 1 for $D = 3cm$

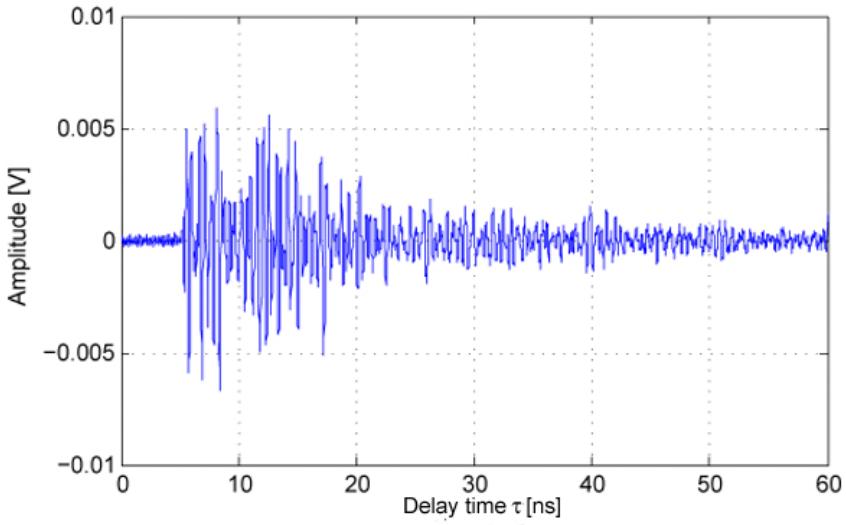

Figure 3.38 Measured signal from Tx2 to Rx1 (h_{21}) at user 1 for $D = 15cm$

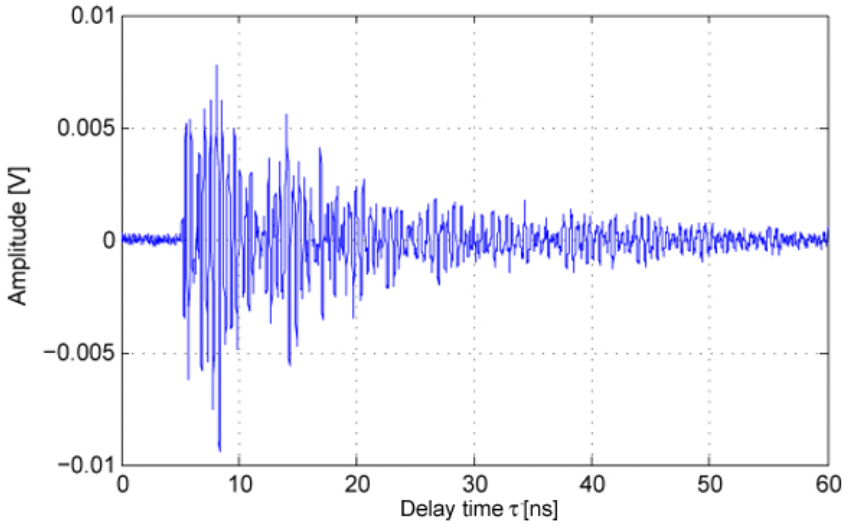

Figure 3.39 Measured signal from Tx2 to Rx2 (h_{22}) at user 1 for $D = 3cm$

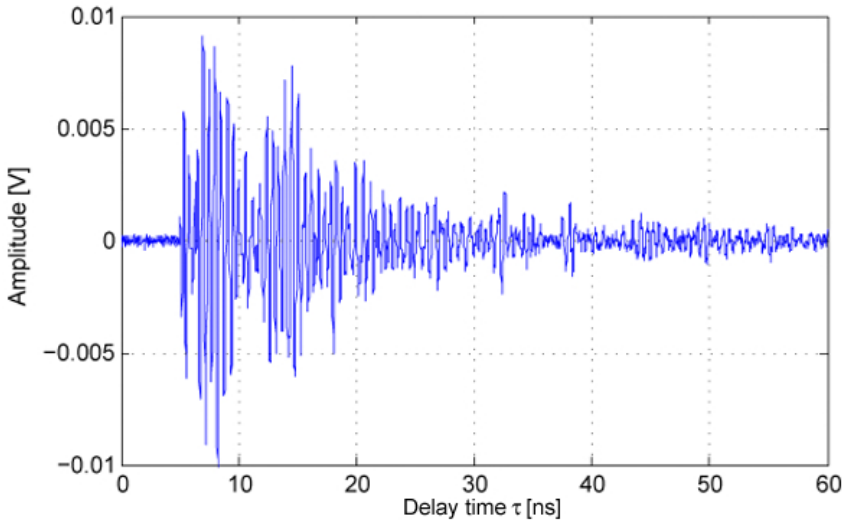

Figure 3.40 Measured signal from Tx2 to Rx2 (h_{22}) at user 1 for $D = 15cm$

3.4 UWB Channel Modeling

Channel models are important for evaluating and designing wireless systems. A detailed characterization of the UWB channel will permit the successful design of UWB transceivers. There are two types of modeling for electromagnetic wave propagation: deterministic modeling and statistical modeling. Deterministic modeling is often used to predict coverage patterns in wireless systems when there is detailed information about the environment [52]. Statistical modeling is useful when designing communication systems that must work in a wide variety of environments and it focuses on the relevant statistics of the received signal [52].

UWB channel modeling is different from narrowband channel modeling due to the large bandwidth associated with UWB signals. A study of UWB channel modeling based on frequency dependence and waveform distortion is presented in [51]. Work performed on UWB channel modeling and its impact on receiver design can be found in [39], [40], [45], and [44].

In [52], the effects of the UWB channel are divided into three categories: (1) large-scale effects, (2) small-scale effects, and (3) undesired signals. Large-scale effects refer to the impact of the channel over large distances which include attenuation effects. Small-scale effects refers to attenuation caused by small distances and distortion of the waveform at the receiver. Undesired signals include noise sources and interference signals.

3.4.1 Statistical Model

The small-scale channel is typically modeled as a time-varying linear filter. The received signal is given by

$$r(t) = \int_{-\infty}^{\infty} s(\tau)h(t,\tau)d\tau + n(t) \tag{3.10}$$

where $s(t)$ is the transmitted signal, $h(t,\tau)$ is the time-varying channel impulse response, and $n(t)$ is additive white Gaussian noise. A channel model using a tap-delay line approach was first proposed in [60], and is given by

$$h(t,\tau) = \sum_{k=0}^{N(t)-1} \beta_k(t)p_k(t)\delta(\tau - \tau_k(t)) \tag{3.11}$$

where $\beta_k(t)$, $p_k(t)$, $\tau_k(t)$ are the time-varying amplitude, polarity and delay of the k^{th} path respectively, and $N(t)$ is the number of multipath components. If the channel is assumed to be static over an interval of interest, the time-invariant model can be used and is given by

$$h(\tau) = \sum_{k=0}^{N-1} \beta_k p_k \delta(\tau - \tau_k) \tag{3.12}$$

The amplitudes, delays, and polarities of the multipath components are also referred to as multipath parameters and are statistically characterized. Other metrics for channel characterization are the mean excess delay, the rms delay spread, and the maximum excess delay, which describe the time dispersive properties of the channel [52].

3.4.2 Saleh-Valenzuela Model

The Saleh-Valenzuela Model is introduced in [55], and is the most common statistical model for the discrete indoor CIR. It was developed for NLOS channels and is mathematically expressed by

$$h(t,\tau) = \sum_{l=0}^{L} \sum_{k=0}^{K} \beta_{k,l} \delta(t - T_l - \tau - \tau_{k,l}) \tag{3.13}$$

where K is the number of clusters and L is the number of paths per cluster. The cluster arrivals, as well as the path arrivals within a cluster, are described by a Poisson process. The cluster and path inter-arrival times are described by exponential random variables.

The amplitude of each path is assumed to have a Rayleigh distribution and the polarity is assumed to be a binary random variable with equal probability. Research has found that for UWB channels a log-normal of Nakagaim distribution is a better assumption for the polarity and amplitude of the paths [52]. The model proposed by IEEE 802.15 is derived from the Saleh-Valenzuela model using a log-normal distribution for the amplitude of each path.

3.5 Summary

In this chapter UWB channel measurements and channel modeling were presented. It was shown that UWB channel measurements can be performed using a TD or a FD approach. For this work, the TD measurement approach was chosen for all experiments since in this work post-processing is done in the time domain. The CLEAN algorithm was discussed as a time domain technique for obtaining the CIR

from the recorded signals. A control system was developed and presented to obtain efficient and reliable measurements of two channels simultaneously. Measurement results for two different indoor environments and one outdoor environment are shown and explained. Finally, UWB channel modeling was presented.

CHAPTER 4
TIME-REVERSED UWB-MIMO

Effects like shadowing, fading, and multipath induce a high penalty on the performance of modulation over wireless channels [15]. To overcome these effects, diversity techniques can be used. Diversity can be divided in to two categories: (1) microdiversity which are techniques that mitigate the effect of multipath fading, and (2) macrodiversity which are techniques to mitigate the effects of shadowing from buildings and objects. Antenna arrays are a type of diversity, also known as *space diversity*, that result in an improvement of system performance.

Time-Reversal (TiR) is an adaptive modulation technique that uses a pre-coder at the transmitter before sending the modulated data information intended for a specific receiver. Recently, a great amount of work has been done on TiR since it shows to be a promising technique. TiR is a transmitter-centric technology which shifts the complexity of the system from the receiver to the transmitter. This technology exploits the two features of the UWB channel (quasi static channel with rich multipath) and uses the time-duplexing division (TDD) nature of the UWB spectrum. Work on TiR for UWB can be found in [10], [27], and [25]. Dirty-paper-coding can be used to further improve the performance of TiR [4].

This chapter introduces antenna arrays as a technique for space diversity in UWB systems and TiR as a modulation technique to focus energy at the intended receiver. It explains the theory behind this two concepts and is the basis to understand the simulation results. It explains antenna array systems and discusses single-user and multi-user TiR UWB-MIMO systems. It concludes with an explanation of power allocation and simulations carried out in this work.

4.1 Antenna Array Systems

The use of multiple transmit or receive antennas, also called *antenna array*, is a method of diversity also known as *space diversity*. One of the major benefits of *space diversity* is the achievement of independent paths in a wireless system that will experience independent fading, multipath and shadowing [15].

There are several antenna array configurations:

1. Single-input single-output (SISO)
2. Single-input multiple-output (SIMO)
3. Multiple-input single-output (MISO)
4. Multiple-input multiple-output (MIMO)

For each configuration, single-input refers to one transmit antenna while multiple-input refers to multiple transmit antennas (transmit diversity). In the same way, single-output means one receive antenna and multiple-output means multiple receive antennas (receive diversity). Figure 4.1 presents the four possible antenna array configurations.

With receiver diversity, independent paths are obtained without the need to increase the transmit power. Array gain and diversity gain are two types of performance gain achieved by using this type of space diversity. Array gain results from coherently combining the signals from multiple receive antennas. In the absence of fading, the increase in SNR at the receiver is proportional to the number of receive antennas. For example, if a wireless system consists of M receive antennas, the average combined SNR is given by M times the SNR with a single receive antenna. For UWB signals, fading is weak as opposed to narrowband signals. Therefore, the advantage of using receive diversity is attractive. Diversity gain refers to the gain achieved by a

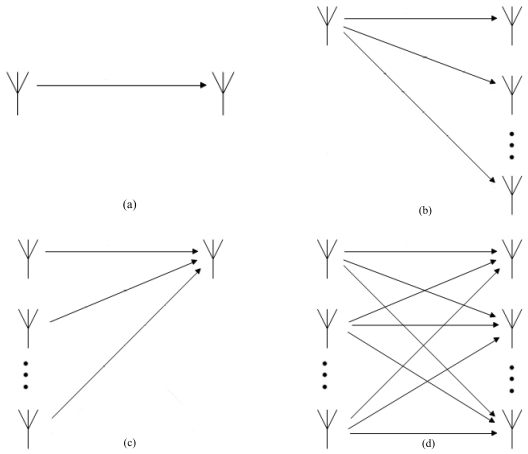

Figure 4.1 Antenna array configurations: (a) SISO, (b) SIMO, (c) MISO, and (d) MIMO configurations

better distribution of the average SNR which results in improvement of performance. For MIMO systems, diversity gain is also referred to as *beamforming* [15].

In transmit diversity, the transmit signal power must be divided among the multiple antennas. The use of TiR and transmit diversity increases the SNR at the receiver which grows linearly with the number of transmit antennas, M. Transmit diversity is desirable in systems where space, power and processing capabilities are more available at the transmitter side than at the receiver side [15]. Thus, knowledge of the channel gain at the transmitter is important to achieve transmit diversity.

For narrowband wireless systems, the separation between each antenna element in the array has to be such that the fading amplitudes corresponding to each antenna are approximately independent [15]. Moreover, when two antennas are two close to each other, antenna coupling and channel spatial correlation effects degrade the performance of the wireless system. For UWB signals, this problem has not yet been adequately addressed. The purpose of this work is to investigate these coupling

effects and performance degradation for UWB-MIMO wireless systems when receive antennas are close to each other.

4.2 UWB-MIMO

Multiple-input multiple-output (MIMO) is being extensively investigated for acoustics and wireless systems. Work on MIMO for acoustic systems can be found in [66]. For wireless systems, it has been shown that MIMO is a good technique to achieve high capacities [23] and is a good method to reduce the effect of multipath fading [3]. Also, receive diversity has been used in mobile communications systems to suppress or cancel interference as stated by Liu in [28].

MIMO uses transmit and receive diversity to increase the performance of the system and can achieve high data rates through multiplexing. In multiplexing, the structure of all the channel paths can be exploited to obtain independent signaling paths for sending different data [15]. In narrowband systems, MIMO promises an efficient way of using the spectrum. The cost and limitations of MIMO systems include space and power requirements for extra antennas and complexity due to multi-dimensional signal processing.

4.2.1 MIMO for a Single User System

A UWB-MIMO communication system with M transmit antennas and N receive antennas is shown in Figure 4.2. $h_{mn}(t)$ denotes the CIR relating the m^{th} element at the transmitter to the n^{th} element at the receiver. If the pulse signal $a_m(t), m = 1, .., M$ is sent from the transmit antenna array, the signal $b_n(t)$ at the

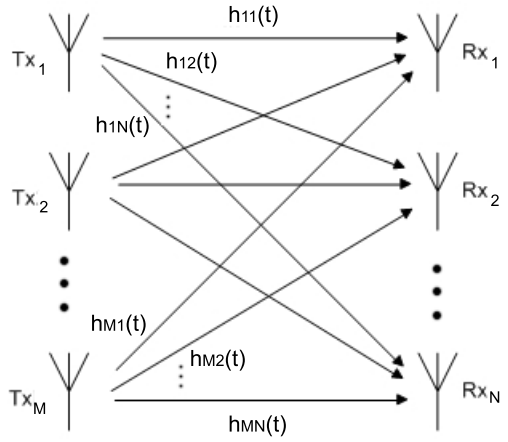

Figure 4.2 MIMO system with M transmit antennas and N recieve antennas

receive antenna array can be expressed by [50]

$$b_n(t) = \sum_{m=1}^{M} h_{mn}(t) \otimes a_m(t), n = 1, .., N \tag{4.1}$$

or in matrix form by

$$\mathbf{b}(t) = \mathbf{H}(t) \otimes \mathbf{a}(t) \tag{4.2}$$

where[1] $\mathbf{b}(t) = [b_1(t), b_2(t), .., b_N(t)]^t$, $\mathbf{a}(t) = [a_1(t), a_2(t), .., a_M(t)]^t$, and $\mathbf{H}(t)$ is a MxN matrix with elements $h_{mn}(t)$ given by

$$\mathbf{H(t)} = \begin{pmatrix} h_{11}(t) & h_{21}(t) & \dots & h_{M1}(t) \\ h_{12}(t) & h_{22}(t) & \dots & h_{M2}(t) \\ \vdots & \vdots & \ddots & \vdots \\ h_{1N}(t) & h_{2N}(t) & \dots & h_{MN}(t) \end{pmatrix} \tag{4.3}$$

[1]The notation $\otimes$ represents element-by-element convolution and the superscript ^{t} is the transpose of a vector or a matrix

The UWB channel has the characteristic of spatial reciprocity [47]. If a signal $c_m(t), m = 1, .., M$ is sent from the receive array the signal $d_n(t), n = 1, .., N$ obtained at the transmit array is given by[2]

$$\mathbf{d}(t) = \mathbf{H}^{\dagger}(t) \otimes \mathbf{c}(t) \tag{4.4}$$

Thus, the forward propagation of impulses from the transmit array to the receive array can be calculated by using $\mathbf{H}(t)$, while the backward propagation from the receive array to the transmit array can be computed using $\mathbf{H}^{\dagger}(t)$. The normalized correlation between the CIRs of the forward and backward links is as high as 0.98 as experimentally confirmed in [47].

4.2.2 MIMO for Multi-users

A multi-user system with multiple antennas at both the transmitter and the receiver result in diversity gain that improves the system performance. The bit-error-probability (BER) is a good metric to evaluate performance of a communication system [15]. Also, multiple antennas can provide directivity gain which spatially separates users and reduces interference. Multiplexing gain can also be exploited and results in an increase of capacity as explained in Section 4.2.

UWB-MIMO capacity is being studied due to the many promising applications of UWB-MIMO systems. Moreover, multi-user diversity can be achieved by allocating resources to users with the best channels. A major challenge for UWB-MIMO multi-user systems is the development of signaling techniques that can exploit performance

[2]Where † is the Hermitian (conjugate transpose)

gains in practical operating environments without high complexity on transceiver design.

4.3 Time-Reversal

Time Reversal (TiR) has been widely researched in acoustics and has lead to interesting applications in underwater communications and ultra-sound. Investigations on TiR in acoustics can be found in [12] and the use of multiple array elements in TiR acoustics is addressed in [20].

The idea of extending TiR to wireless communications has been considered due to the simplicity and performance advantages of applying TiR to a communication link. Investigations of TiR in wireless communications can be found in [67, 1, 58, 25, 36]. It has been found that TiR can reduce ISI significantly without the need of a complex equalizer at the receiver since it achieves temporal compression of the effective channel as will be explained later on. Spatial focusing is also exploited in TiR with antenna diversity, which suggest the advantages to use a UWB-MIMO system. TiR performance has been evaluated in [35, 27]. In this work is extended to UWB-MIMO multi-users.

In a TiR communication system, the intended receiver sounds the channel by transmitting a pilot pulse to the transmitter. The transmitter records, time-reverses, and uses the signal to pre-coder the data to be transmitted. The pre-coder at the transmitter can be specified as the time-reversed replica of the recorded signal or the time-reversed replica of the CIR extracted from the recorded signal. The CIR replica requires extra signal processing and, as explained in the results shown in Chapter 5, does not perform as well as when the time-reversed replica of the received signal is used as the pre-coder. In either case, the energy will be focused on the intended

receiver in time and space, and therefore, the effective delay spread of the channel is greatly reduced. To characterize the amount of temporal focusing, the *temporal peak to total energy ratio* can be evaluated and is defined as [2]

$$g^{TR} = \frac{E_P^{hh}}{E_T^{hh}} \tag{4.5}$$

where E_P^{hh} is the energy in the main peak of the received signal and E_T^{hh} is the total energy in the received signal. Good temporal compression would result in a high *temporal peak to total energy ratio*. TiR can be viewed as a match filter process which allows the design of less complex receivers without a big penalty in performance degradation.

TiR is strong when there is a rich scattering medium as in the UWB channel. Temporal and spatial focusing hardens the effective channel at the point of interest which makes TiR a robust technique to achieve performance improvement. TiR can be further exploited by adding transmit diversity (beamforming). The received signal contains the waveforms from each transmit antenna which are coherently combined at the receiver and result in a select spatial focused signal. Furthermore, MIMO requires knowledge of the channel at the transmitter and receiver which makes TiR an advantage for delivering diversity gain.

Figure 4.3 presents a block diagram of a TiR system when the pre-coder consists of the time-reversed replica of the CIR. The mathematical formulation of the received signal at the intended receiver in a SISO link can be described by

$$r(t) = s(t) \otimes h_{mn}(-t) \otimes h_{mn}(t) = s(t) \otimes R_{mn}^{auto}(t) \tag{4.6}$$

where $r(t)$ is the received signal at the intended receiver, $h_{mn}(t)$ is the CIR of the

UWB channel between the m^{th} transmit antenna and the n^{th} receive antenna, $s(t)$ is the transmitted symbol, and $R_{mn}^{auto}(t)$ represents the autocorrelation of the CIR. The received signal at another point (off-target) can be expressed by

$$r(t) = s(t) \otimes h_{mn}(-t) \otimes h_{mk}(t) = s(t) \otimes R_{mnk}^{cross}(t) \tag{4.7}$$

where $h_{mk}(t)$ is the CIR of the UWB channel between the m^{th} transmit antenna and the k^{th} off-target point, and $R_{mnk}^{cross}(t)$ is the cross-correlation of $h_{mn}(t)$ and $h_{mk}(t)$.

Figure 4.4 shows the signal at the intended receiver if no TiR is used, while Figure 4.5 presents the received signal when the TiR pre-coder is used for the transmitted signal. It can be observed that TiR achieves time compression at the intended receiver. The received signal at an off-target point located 40cm away is also presented in Figure 4.5 which shows spatial focusing of the signal at the intended receiver.

4.3.1 TiR based UWB-MISO

In MISO, the received signal at the intended receiver will be the sum of the received signals from all multiple transmit antennas. The signal, under ideal conditions, is then the sum of all autocorrelations which are coherently added in the time and space domains resulting in a time-focused and space-focused signal at the

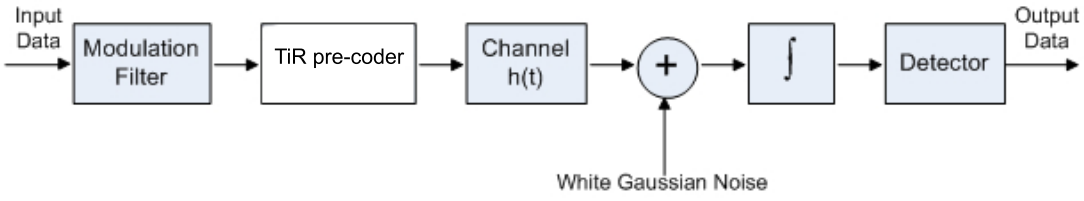

Figure 4.3 Block diagram for a TiR communication system

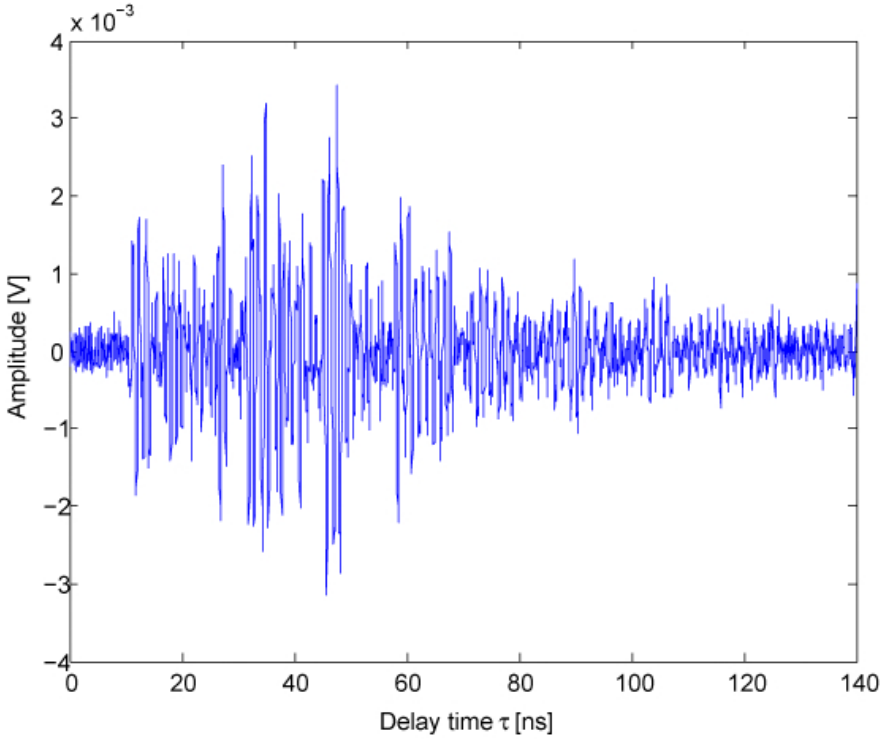

Figure 4.4 Received signal without TiR pre-coder

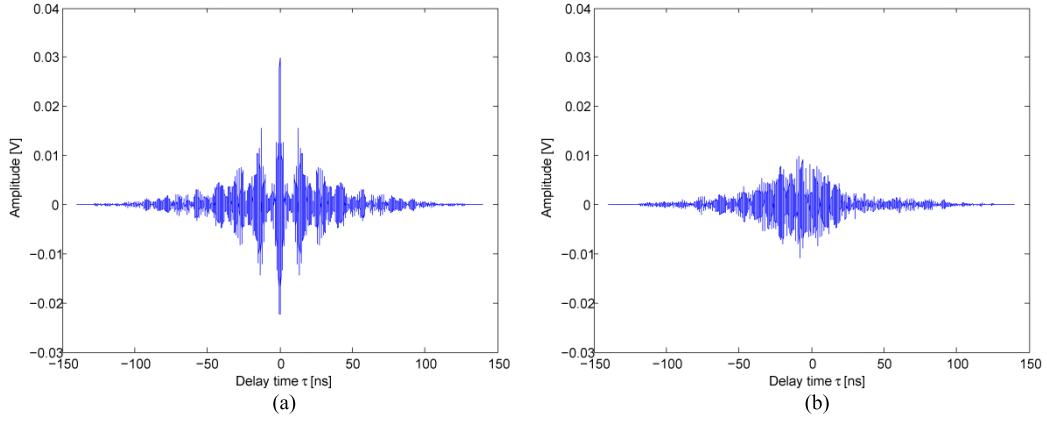

Figure 4.5 Received waveform when TiR pre-coder is used: (a) signal at the intended receiver, and (b) signal at an off-target point

intended receiver. Spatial focusing reduces interference from other users and time compression alleviates ISI. These two mechanisms are achieved simultaneously at the intended receiver location.

In a UWB-MISO multi-user system with M transmit antennas, the received signal at the n^{th} user can be expressed as

$$r_n(t) = s_n(t) \otimes \sum_{m=1}^{M} R_{mn}^{auto}(t) + \sum_{m=1}^{M} \sum_{k=1,k\neq n}^{N_u} s_k(t) \otimes R_{mnk}^{cross}(t) + n_n(t) \tag{4.8}$$

where N_u is the number of users (or receivers). Figure 4.6 shows the received waveforms in a UWB-MISO system with four transmit antennas. At the receiver, the signals are coherently combined and the resulted waveform is presented in Figure 4.7. To evaluate time compression, the *temporal peak to total energy ratio* was evaluated. A ratio of 0.3 was obtained for a MISO system compared to 0.1 in a SISO system.

4.3.2 TiR based UWB-MIMO for a Single User

TiR can be further exploited with the use of UWB-MIMO. The received signal represents an extension of TiR UWB-MISO where now each user has N receive antennas. The mathematical expression for the received signal at the intended user can then be expressed as [50]

$$\begin{aligned} r(t) = {} & s(t) \otimes \sum_{m=1}^{M} \sum_{n=1}^{N} h_{mn}(-t) \otimes h_{mn}(t) \\ & + s(t) \otimes \sum_{m=1}^{M} \left\{ \left[\sum_{n=1,k\neq n}^{N} h_{mn}(-t) \right] \otimes \left[\sum_{k=1,k\neq n}^{N} h_{mk}(t) \right] \right\} + n(t) \end{aligned} \tag{4.9}$$

where the first term represents the signal given by the convolution of the sent data and the autocorrelation of the CIR, the second term represents the inter-channel

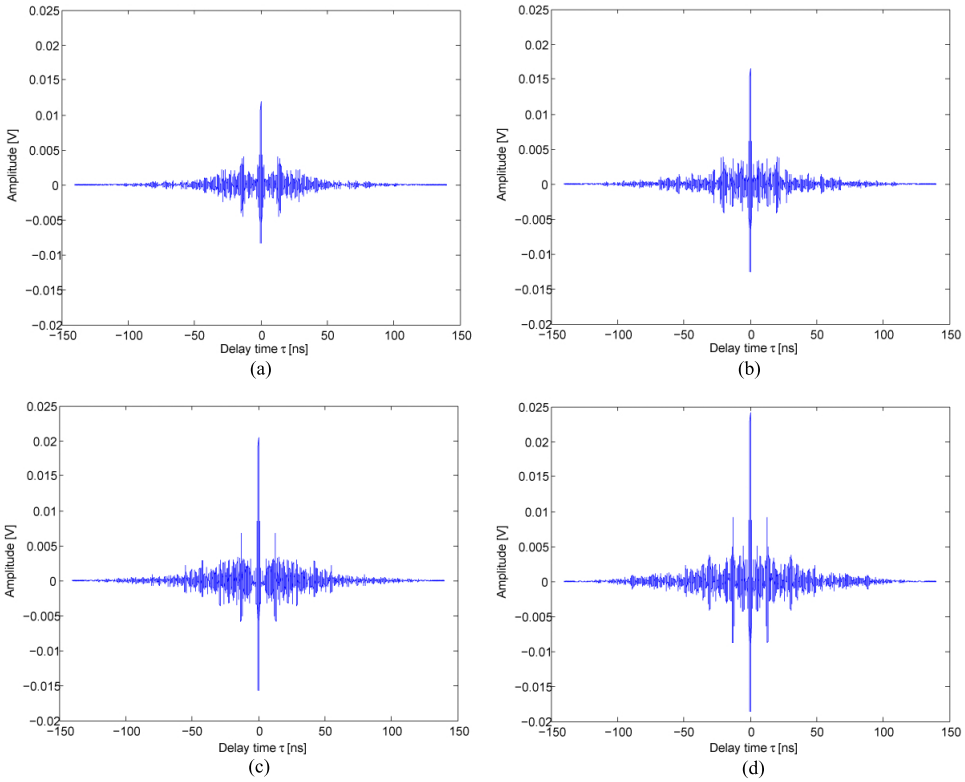

Figure 4.6 Waveforms from each transmit antenna at the intended receiver in a time-reversed UWB-MISO system: (a) from Tx1, (b) from Tx2, (c) from Tx3, and (d) from Tx4

interference, and $n_n(t)$ is white gaussian noise. In matrix form, it follows that [50]

$$\mathbf{r}(t) = \mathbf{s}(t) \otimes \left[\mathbf{H}(-t) \otimes \mathbf{H}^t(t)\right]_{MxM} + \mathbf{n}(t) \tag{4.10}$$

where ^{t} represents the transpose of a matrix, $\otimes$ is element-to-element convolution, and the channel matrix $\mathbf{H}(t)$ of MxN contains real elements $h_{mn}(t)$, $m = 1, 2, .., M$ and $n = 1, 2, .., N$ as shown in Equation 4.3. The vector $\mathbf{s}(t) = [s_1(t), s_2(t), .., s_M(t)]^t$ contains the transmitted data, the received signals correspond to the vector $\mathbf{r}(t) = [r_1(t), r_2(t), .., r_N(t)]^t$, and $\mathbf{n}(t) = [n_1(t), n_2(t), .., n_N(t)]^t$ is the white gaussian noise vector. The rank of the channel matrix in Equation 4.10 determines the number

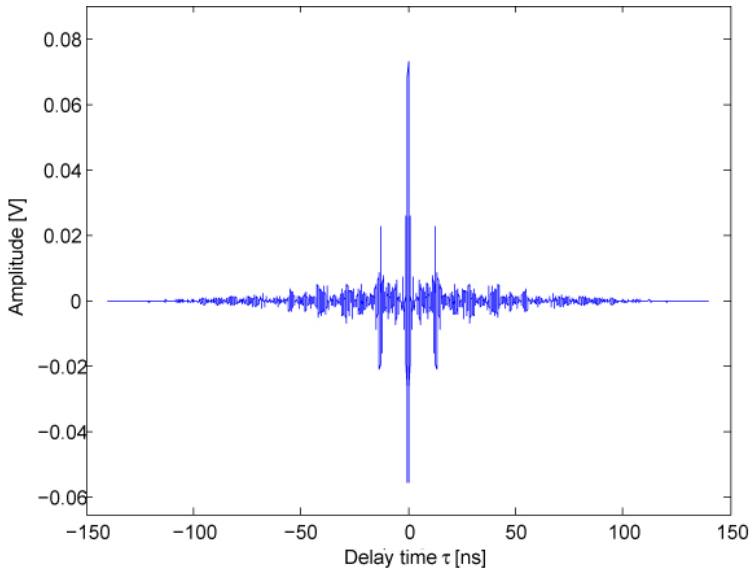

Figure 4.7 Total received signal after adding all waveforms from transmitters at the intended receiver in a time-reversed UWB-MISO system

of parallel channels (the number of spatial degrees of freedom). Figure 4.8 presents the received signal in a single-user TiR UWB-MIMO with two receive antennas after coherently combinging the signals from each antenna. The received signal has a 3dB gain compared with the received signal for a TiR UWB-MISO system.

4.3.3 TiR based UWB-MIMO for Multi-users

In a UWB-MIMO multi-user system, the received signal does not only experience inter-channel interference, but co-channel interference as well. Co-channel interference arises from data that is intended for other users and degrades the performance of the system. The evaluation of BER and the signal-to-interference-plus-noise power ratio (SINR) in a communication system reflects the co-channel interference which can be stronger and more destructive than inter-channel interference.

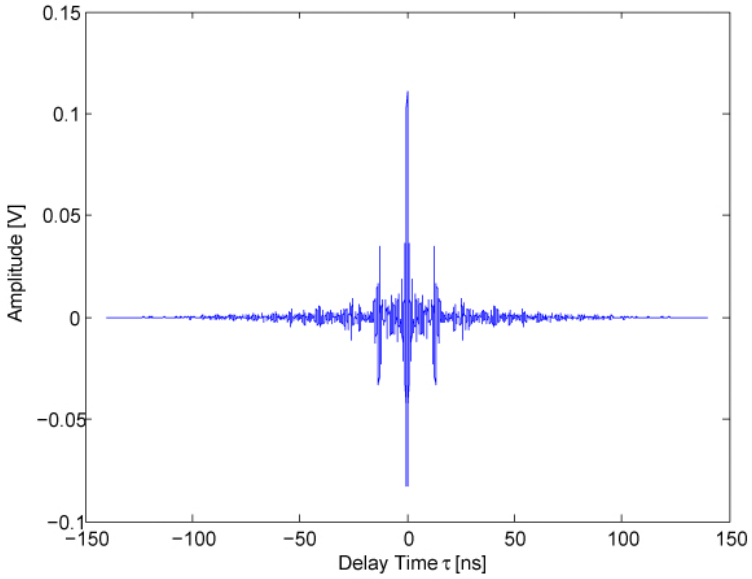

Figure 4.8 Received signal in a single-user TiR UWB-MIMO with two receive antennas after coherently combinging the signals from each antenna

The mathematical expression for the received waveform in a UWB-MIMO multi-user system is an extension of the UWB-MIMO single-user given in Equation 4.9. If a communication system with M transmit antennas, N_i receive antennas for user i, and N_u total number of users is considered, the received waveform at the intended user i can be expressed as

$$\begin{aligned} r_i(t) = s_i(t) \otimes \sum_{m=1}^{M} \sum_{n=1}^{N_i} h_{mn}(-t) \otimes h_{mn}(t) \\ + s_i(t) \otimes \sum_{m=1}^{M} \left\{ \left[\sum_{n=1,k\neq n}^{N_i} h_{mn}(-t) \right] \otimes \left[\sum_{k=1,k\neq n}^{N_i} h_{mk}(t) \right] \right\} \\ + \sum_{j=1,j\neq i}^{N_u} s_j(t) \otimes \sum_{m=1}^{M} \left[\sum_{k_j=1}^{N_j} \sum_{n_i=1}^{N_i} h_{mk_j}(-t) \otimes h_{mn_i}(t) \right] + n_i(t) \end{aligned} \tag{4.11}$$

where the first term represents the intended signal for user $i = 1, 2, .., N_u$, the second term represents the inter-channel interference, the third term represents the

co-channel interference, and $n_i(t)$ is white gaussian noise at user i. For the co-channel interference, k_j is the k^{th} antenna of the j^{th} user and n_i is the n^{th} antenna of the i^{th} user. In matrix form, it follows from Equation 4.10 that

$$\mathbf{r}_i(t) = \mathbf{s}_i(t) \otimes \left[\mathbf{H}_i(-t) \otimes \mathbf{H}_i^t(t)\right]_{MxM} + \mathbf{n}_i(t),\ i = 1, 2, .., N_u \tag{4.12}$$

Time-reversed UWB-MIMO increases the performance of a system compared to other antenna array configurations like MISO as discussed in Chapter 5. Figure 4.9 presents a diagram of a multi-user UWB-MIMO system. It can also be noted that TiR can fully exploit the rich scattering of the UWB channel in a NLOS link. Figure 4.10 shows the effect of the received signal when there is 4 users in a TiR UWB-MIMO system.

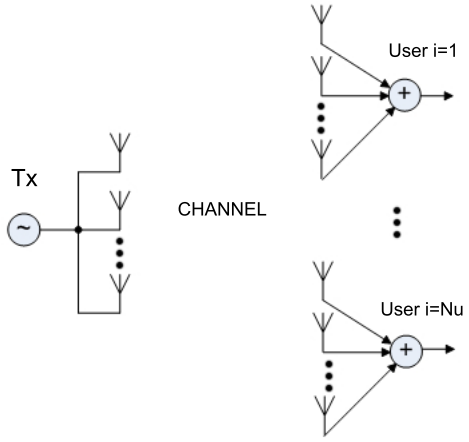

Figure 4.9 A multi-user UWB-MIMO communication system

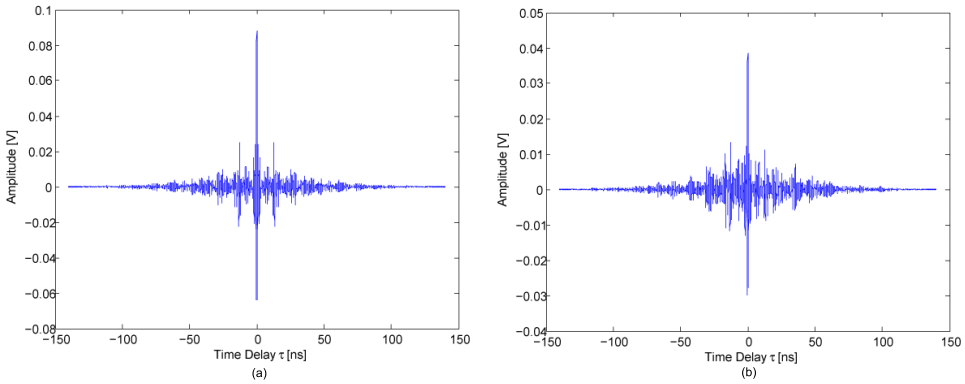

Figure 4.10 Effect of increasing the number of users in a TiR UWB-MIMO system: (a) Received signal at the intended receiver in a 1-user system, (b) Received signal at the intended receiver in a 4-user system

4.3.4 Power Allocation for TiR UWB with Transmit Diversity

The use of multiple antennas at the transmitter (transmit diversity) requires power allocation for each of the antenna elements. Several power allocation schemes have been investigated and proposed in the literature. In [24], three solutions for allocation of power are considered: (1) simple time reversal, (2) equal power allocation, and (3) optimal power allocation. The equal power allocation scheme is applied in this work since it is considered for systems where the transmitted power is constrained and should be kept constant. It also allows to adjust the power at each transmitter antenna without the knowledge of other CIRs. For each antenna, the power allocation is given by

$$A_m^{EP} = \frac{1}{\sqrt{M}\sqrt{\sum_{n=1}^{N} \|h_{mn}(t)\|^2}} \tag{4.13}$$

where A_m^{EP} is the scaling factor for the m^{th} transmit antenna (pre-coder), M is the total number of transmit antennas, N is the total number of receive antennas, $h_{mn}(t)$

is the CIR between the m^{th} transmit antenna and the n^{th} transmit antenna, and $\|\bullet\|^2$ denotes the Frobenius norm given by

$$\|\bullet\|^2 = \int_{-\infty}^{\infty} |\bullet|^2 \, d\tau \tag{4.14}$$

4.4 Simulations

The objective of this work is to investigate and evaluate the performance of a Time-Reversed UWB-MIMO wireless communication system. The theory behind TiR and UWB-MIMO has been explained in Section 4.3 and Section 4.2. It is important to note the significant role of the antennas on the performance of the system. Antenna coupling and channel spatial correlation were introduced in Chapter 3 as two coupling effects when two antennas are close to each other. In UWB-MIMO, the distance between the antenna elements, at either the transmitter or receiver, is reduced when a system with limited space is considered. For narrowband signals, the distance between the elements should be far enough for the channel paths to be independent. For UWB signals, this issue has not been well addressed yet and it is the scope of this work.

Furthermore, TiR improves the performance of UWB systems, alleviates ISI, reduces interference, and allows the design and implementation of less complex receivers. The improvements when using TiR can be degraded if coupling effects arise. The robustness of TiR is then to be tested during the simulations of this work as well as the advantages of UWB-MIMO over UWB-MISO. The UWB-channel information was measured as explained in Chapter 3. Experiments were performed in several locations and in all measurements the distance between the receive antennas was varied. The recorded signals were used to carry out simulations in an AWGN channel.

At the transmitter, A-PAM modulation and TiR pre-coder are used. A-PAM modulation was explained in Section 2.4.1, and in all simulations each symbol consists of one bit (i.e. $E_s = E_b$). For the TiR pre-coder in the first simulations, two approaches are considered: the time-reversed replica of the CIR and the time-reversed replica of the recorded signal. Since the second option improves the performance of the system, in the final simulations the time-reversed replica of the recorded signal is used as the TiR pre-coder. Also, equal power allocation is used in all simulations due to the need of delivering a constant power from each transmit antenna and a total power of 1 from all transmit antennas.

At the receiver front end, AWGN noise with zero mean and power spectral density of $N_o/2$ is added. Two receive antennas separated by distance D are considered for UWB-SIMO and UWB-MIMO systems, and SNR is measured at each antenna. No ISI is considered since the scope of this work is to explain performance degradation due to coupling effects. The signal is considered a real base-band signal and perfect synchronization is assumed. The simulations are performed for all distances considered when measuring the channel. The receiver design consists of a coherent combiner, when the system has receive diversity, a threshold detector whith an integrator, which focuses on the signal peak, and a decision block in which the threshold value is set to zero (i.e. if greater than zero the detected bit is '1' and if less than zero the detected bit is '0'). Figure 4.11 presents the simulation block diagram of the system.

Two performance metrics are considered to evaluate the performance of the system, SINR and BER. SINR can be defined as

$$SINR = \frac{P_r}{N_0 B + P_I} \tag{4.15}$$

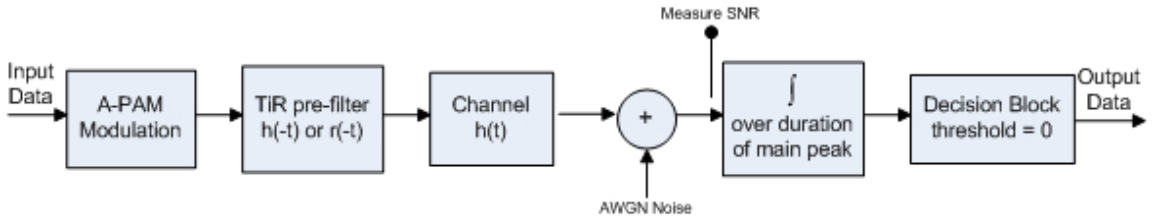

Figure 4.11 Block diagram for simulations

where P_r is the power of the intended signal, N_0B is the noise power determined by the bandwidth of the transmitted signal and the spectral properties of the noise, and P_I is the average power of the interference.

The interference signal $I(t)$ received at the intended user for a UWB-MISO system is given by the second term of Equation 4.8, for a single-user UWB-MIMO system by the second term in Equation 4.9, and for a multi-user UWB-MIMO system by the second and third terms of Equation 4.11. P_I can then be computed as

$$P_I = \frac{\int_0^{T_b} I^2(t)dt}{T_b} \tag{4.16}$$

where T_b is the duration of the received waveform.

To obtain the BER, Monte Carlo Simulation is used. MC simulation is a widely used technique to study performance in communication systems. It randomly generates values for data bits and uses probability statistics to evaluate BER in a system. Each data bit is sent through the channel and received. The received bit is compared to the actual sent bit and errors are detected. Dividing the total number of errors by the number of total sent bits will give a solution for the BER value for a particular SNR. The minimum target BER in this work is 10^{-4}, thus the number of data bits per simulation should be at least 10 times the inverse of the minimum

target BER to be estimated (10^5 in this work). BER is evaluated as a function of E_b/N_o which relates to SNR as

$$SNR = \frac{E_b}{N_o B T_b} \tag{4.17}$$

where E_b is the energy per bit, $N_o B$ is the noise power within the bandwidth $2B$, and T_b is the bit period time. E_b/N_o is sometimes called the SNR per bit [15].

To verify that simulations are correct, a correlator receiver is used. The correlator is set to the time-reversed replica of the received waveform (match filter) to obtain optimum performance. The resulted BER curve is expected to perform as the theoretical BER curve for A-PAM in an AWGN channel presented in Section 2.5.1. The obtained BER curve as a function of E_b/N_o is presented in Figure 4.12. The theoretical BER curve for A-PAM in an AWGN channel is plotted as well to compare and show the validity of the simulations in this work. For all further results, this theoretical AWGN performance is plotted as a lower bound.

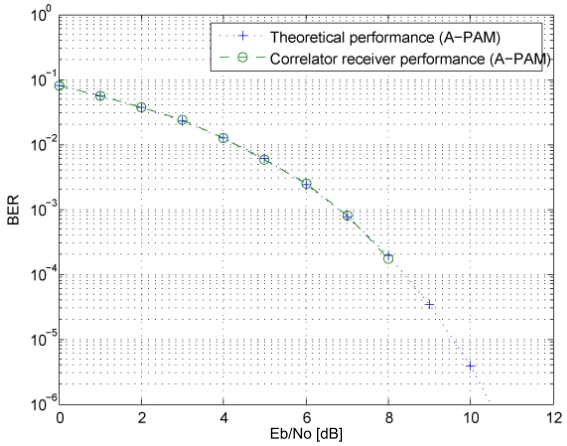

Figure 4.12 Comparison between theoretical BER curve for A-PAM and resulted BER curve when using a correlator receiver (match filter) in simulation

4.5 Summary

This chapter discussed the theory behind the simulations in this work. The concepts of MIMO and TiR were presented and explained. MIMO was first developed in acoustics and is now being extended to wireless communications. It shows to be a promising technology in both narrowband and UWB systems. Antenna arrays schemes were presented, and specifically, UWB-MIMO was discussed. The features of TiR were also shown and mathematical expressions were presented for several systems including UWB-MISO, single-user UWB-MIMO and multi-user UWB-MIMO. Finally, power allocation and an explanation of the simulations in this thesis, as well as their validity, was presented.

CHAPTER 5
RESULTS

This chapter presents the results for all simulation experiments performed in a time-reversed UWB-MIMO communication system. The motivation to use TiR and UWB-MIMO has been discussed in previous chapters, as well as their theory and background. MC simulation is employed to evaluate the performance of the system and the CIR was obtained via the CLEAN algorithm when needed. MATLAB software is used to obtain all results discussed in this chapter. An analysis of coupling effects is first presented, followed by a discussion of using a virtual array when the distance between the antenna elements is small. BER and SINR results for single-user TiR UWB-MIMO system are shown and compared to UWB-MISO. Finally, it addresses a multi-user TiR UWB-MIMO and UWB-MISO systems.

5.1 Analysis of coupling effects

In previous chapters, coupling effects were described as two major issues that arise when two antennas are located close to each other. To understand the influence of these effects on a communication system, two LOS experiments were performed in which the distance between the transmitter and receiver is small (1m). The objective is to compare two cases: the received waveform at the targeted antenna when it is the only one present in the system (case 1) , and the received waveform at the targeted antenna with the presence of another receive antenna (case 2). It is evident that the received waveform in case 1 does not have coupling effects while the waveform in case 2 is affected by coupling effects. In the measurement experiment explained in Section 3.3.2, the distance D between the targeted receive antenna and the added

receive antenna was varied from 3cm to 15cm and waveforms were recorded for each case. To get insight on the influence of the coupling effects, the cross-correlation between the received signal in case 1 and the received signal in case 2 is computed and compared to the autocorrelation of the received waveform in case 1.

Furthermore, the distance between transmit and receive antennas is small and thus the channel has low effects on the received waveform. It then follows that the received waveform without coupling effects (case 1) can be expressed as

$$y_1(t) = h_a(t) \otimes p(t) \tag{5.1}$$

where $h_a(t)$ is the antenna impulse response, and $p(t)$ is the sent pulse. With the addition of another receive antenna (case 2), the received signal can be expressed as

$$y_2(t) = h_a(t) \otimes p(t) + h_c(t) \otimes p(t) \tag{5.2}$$

where $h_c(t)$ is the coupling impulse response.

The coupling impulse response can then be obtained by subtracting Equation 5.2 from Equation 5.1 as follows

$$y_2(t) - y_1(t) = h_a(t) \otimes p(t) + h_c(t) \otimes p(t) - h_a(t) \otimes p(t) = h_c(t) \otimes p(t) \tag{5.3}$$

For the outdoor measurement, Figure 5.1 presents the received waveform for case 1 ($y_1(t)$) and its autocorrelation. The received signal for case 2 ($y_2(t)$) at different distances D, the solution to $h_c(t) \otimes p(t)$ for each case, and the comparison between the cross-correlation (of $y_2(t)$ and $y_1(t)$) and autocorrelation (of $y_1(t)$), are presented in Figure 5.3 for $D = 3cm$, in Figure 5.4 for $D = 6cm$, in Figure 5.5 for $D = 9cm$,

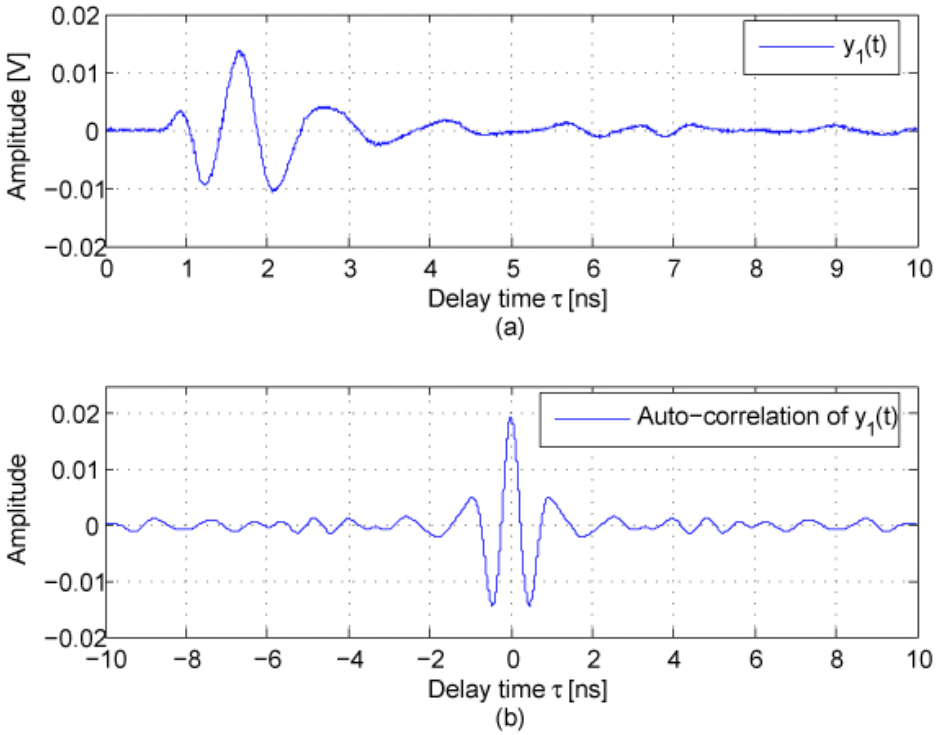

Figure 5.1 Case 1 for outdoor measurements: (a) Received waveform $y_1(t)$, (b) Autocorrelation of $y_1(t)$

in Figure 5.6 for $D = 12cm$, in Figure 5.7 for $D = 15cm$, and in Figure 5.8 for $D = 30cm$.

Figure 5.2 shows the normalized value of the cross-correlation peak for several distances D. At $D = 15cm$ the cross-correlation peak is high and less coupling effects can be observed after this point which can also be noted in Figure 5.7 and Figure 5.8. Furthermore, for $D = 3cm$ the cross-correlation peak is low and coupling effects are high as shown in Figure 5.3.

The same simulation experiment was performed on an indoor environment as explained in the measurement results in Section 3.3.2. The received waveform for $y_1(t)$ and its autocorrelation are shown in Figure 5.9. For $y_2(t)$, the received waveform, the solution to $h_c(t) \otimes p(t)$, and the comparison between the cross-correlation (of $y_2(t)$

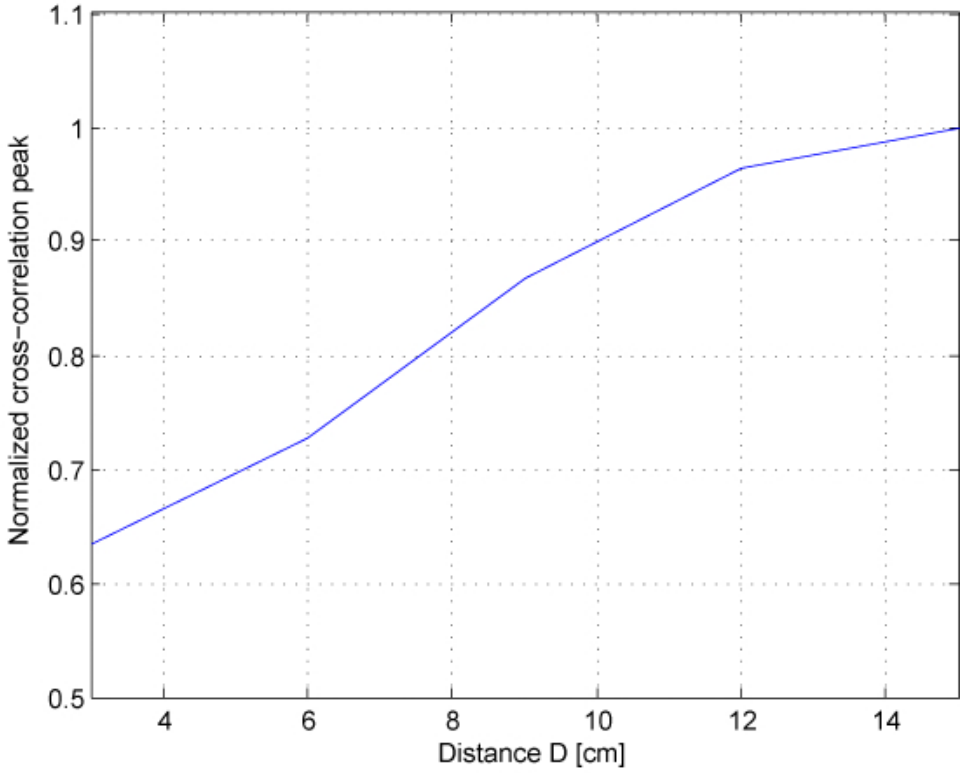

Figure 5.2 Normalized cross-correlation peak for several distances D in outdoor measurements

and $y_1(t)$) and autocorrelation (of $y_1(t)$) are presented in Figure 5.10 for $D = 3cm$, in Figure 5.11 for $D = 6cm$, in Figure 5.12 for $D = 9cm$, in Figure 5.13 for $D = 12cm$, in Figure 5.14 for $D = 15cm$, and in Figure 5.15 for $D = 30cm$. Figure 5.16 presents the normalized value of the cross-correlation peak for several distances D. After $D = 15cm$ the peak is high and coupling effects are not strong. Furthermore, the greater the distance D between the antennas, the less the impulse response of coupling effects and after $D = 30cm$ these effects can be neglected.

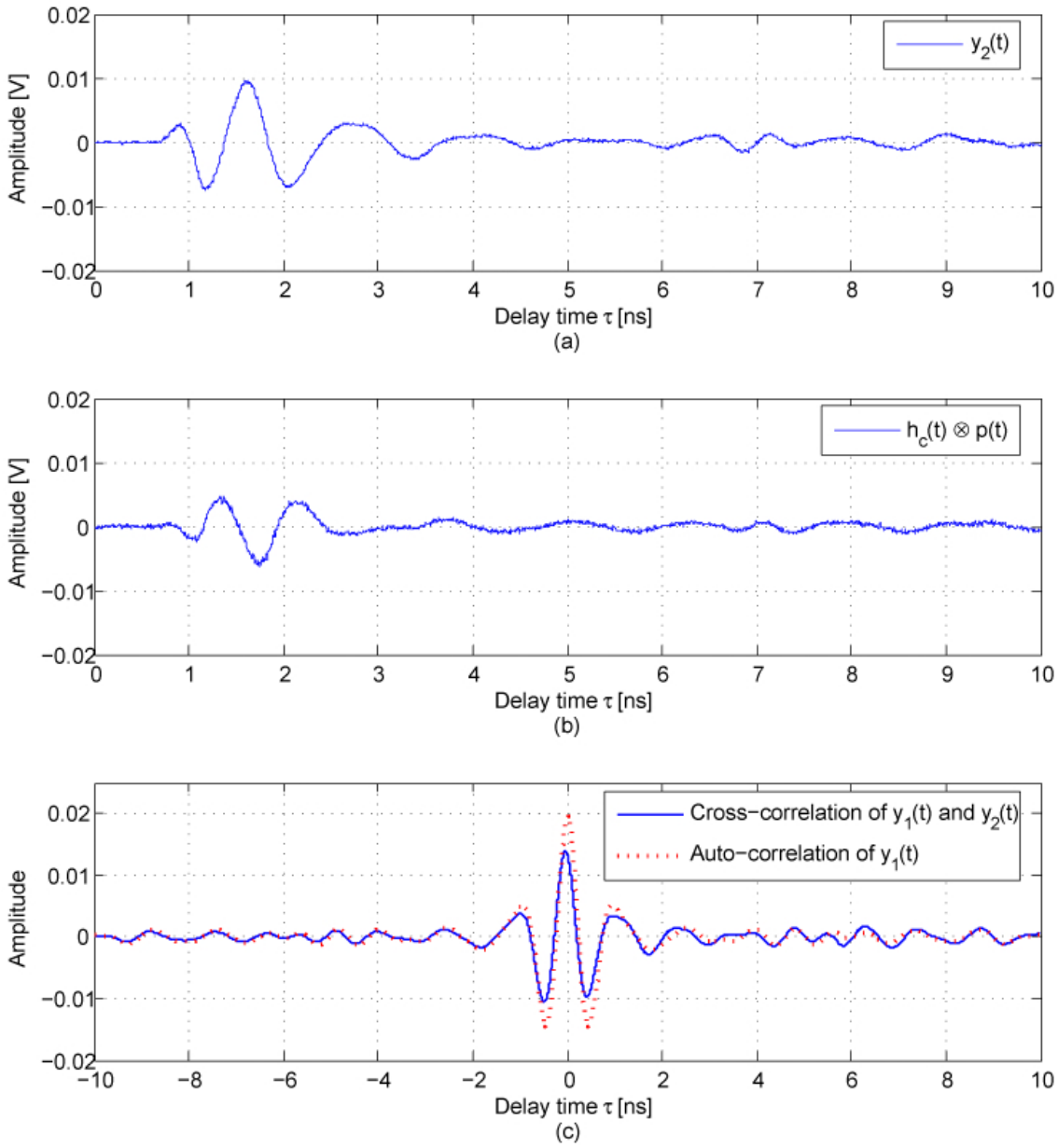

Figure 5.3 Case 2 at $D = 3cm$ for outdoor measurements: (a) Received waveform $y_1(t)$, (b) $h_c(t) \otimes p(t)$, and (c) Comparison of cross-correlation ($y_2(t)$ and $y_1(t)$) and autocorrelation ($y_1(t)$)

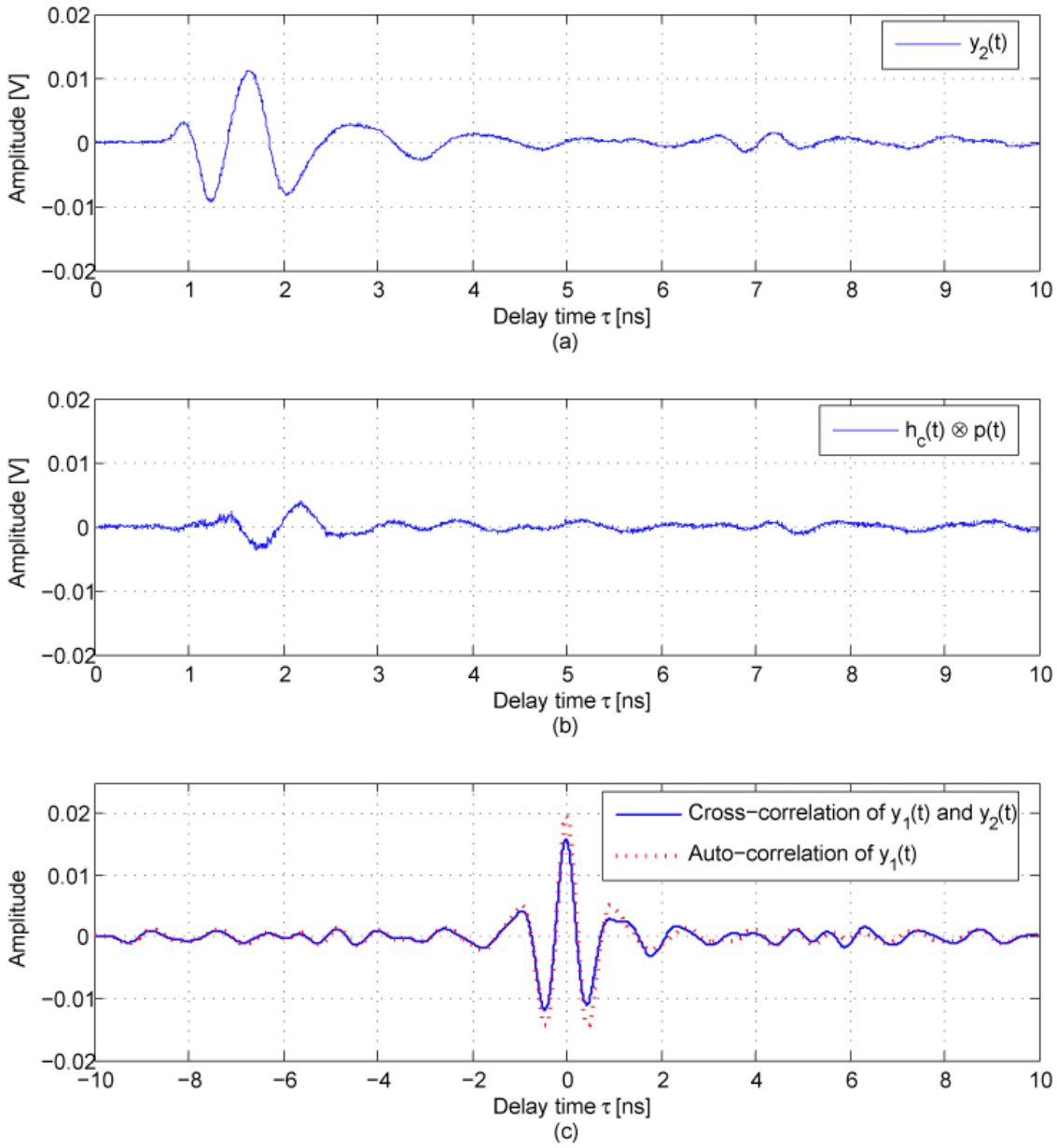

Figure 5.4 Case 2 at $D = 6cm$ for outdoor measurements: (a) Received waveform $y_1(t)$, (b) $h_c(t) \otimes p(t)$, and (c) Comparison of cross-correlation ($y_2(t)$ and $y_1(t)$) and autocorrelation ($y_1(t)$)

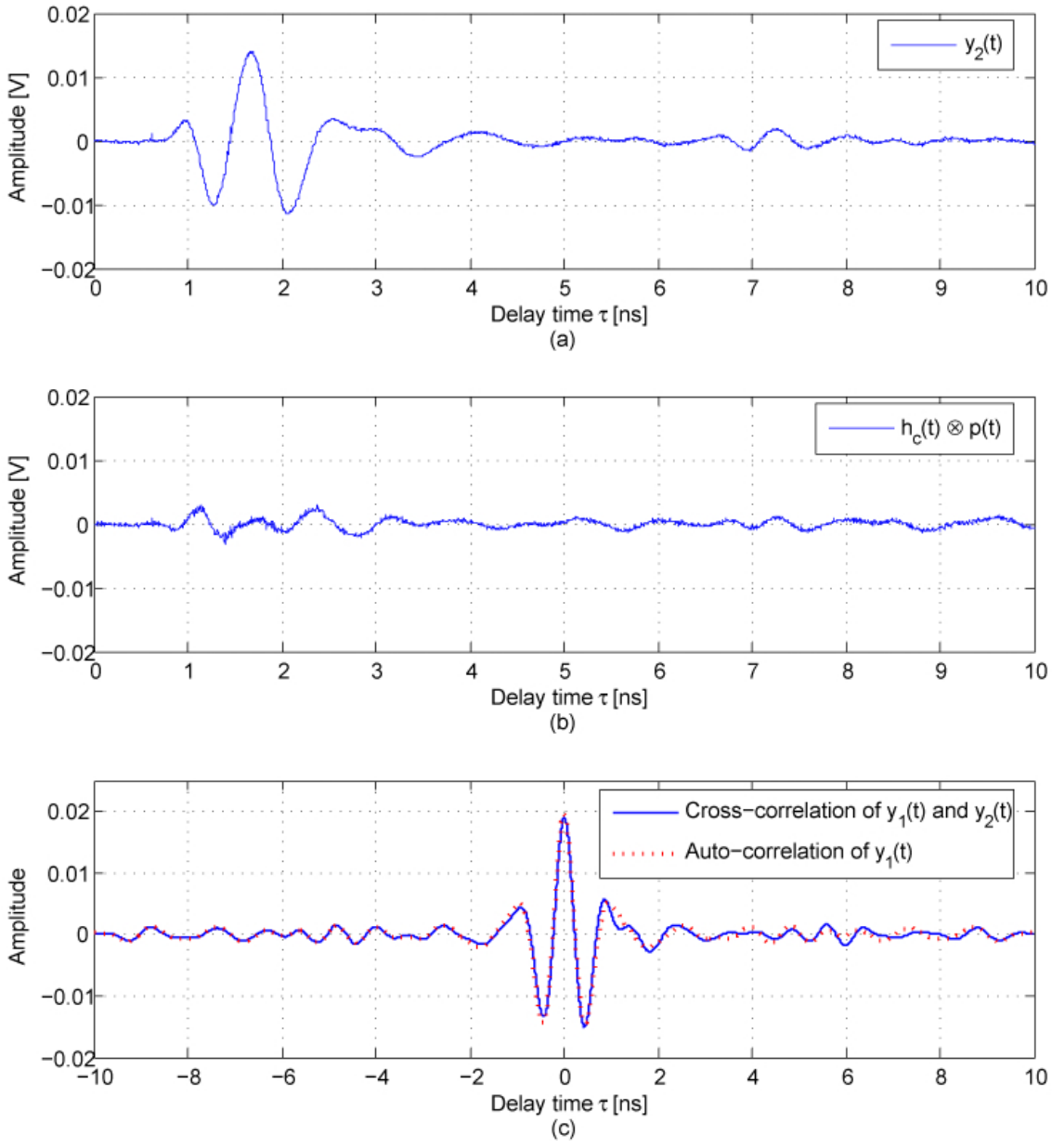

Figure 5.5 Case 2 at $D = 9cm$ for outdoor measurements: (a) Received waveform $y_1(t)$, (b) $h_c(t) \otimes p(t)$, and (c) Comparison of cross-correlation ($y_2(t)$ and $y_1(t)$) and autocorrelation ($y_1(t)$)

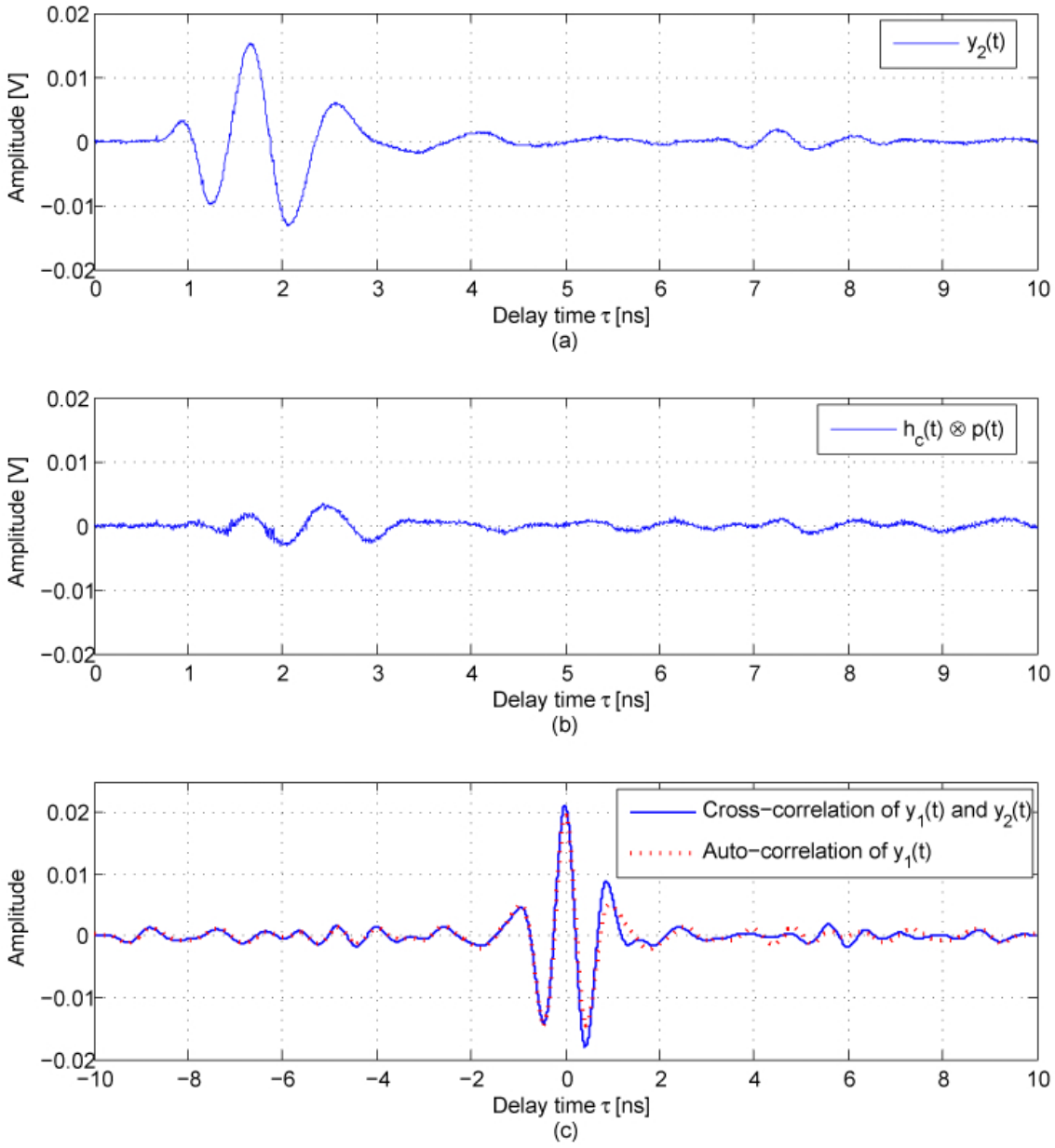

Figure 5.6 Case 2 at $D = 12cm$ for outdoor measurements: (a) Received waveform $y_1(t)$, (b) $h_c(t) \otimes p(t)$, and (c) Comparison of cross-correlation ($y_2(t)$ and $y_1(t)$) and autocorrelation ($y_1(t)$)

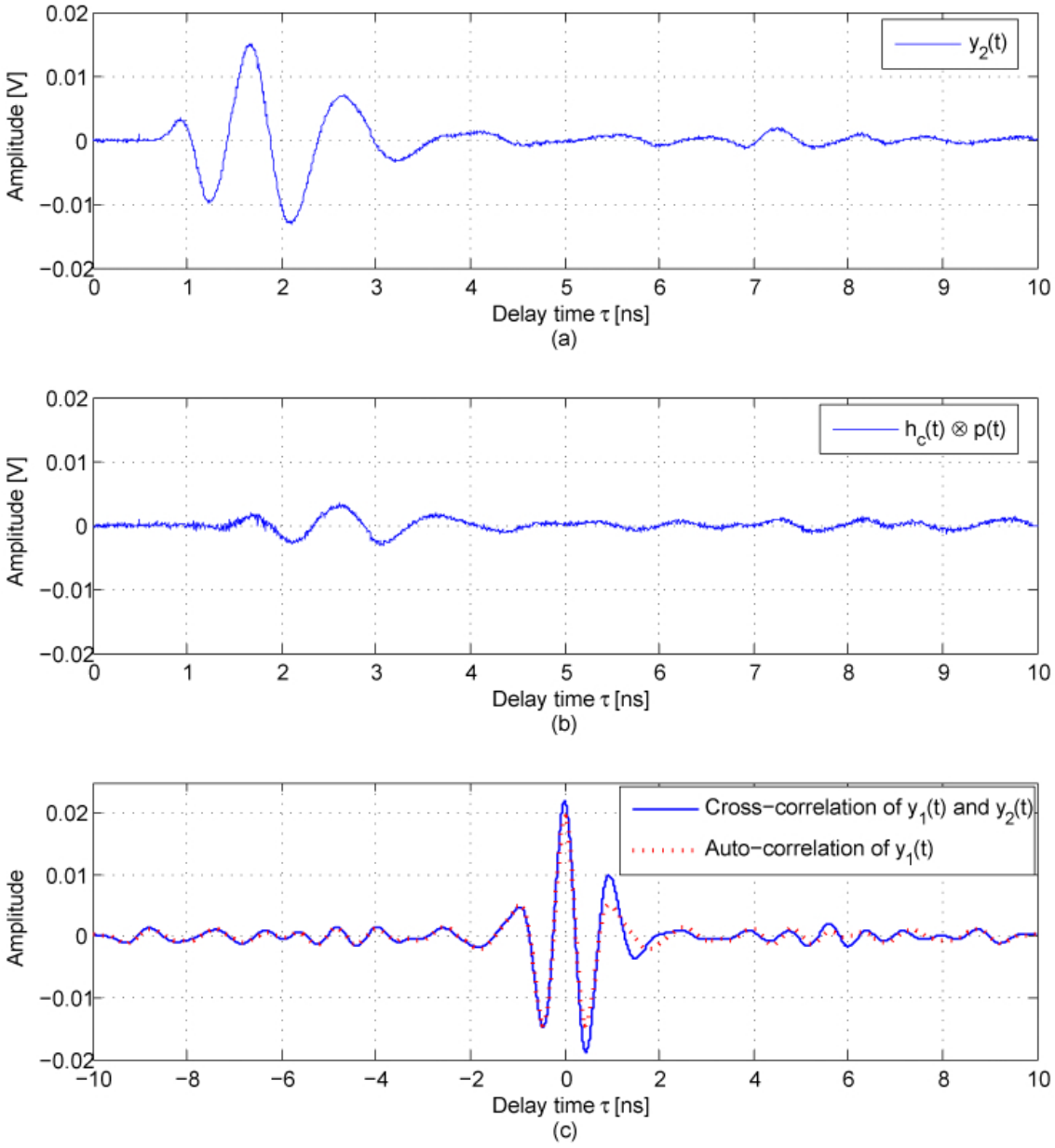

Figure 5.7 Case 2 at $D = 15cm$ for outdoor measurements: (a) Received waveform $y_1(t)$, (b) $h_c(t) \otimes p(t)$, and (c) Comparison of cross-correlation ($y_2(t)$ and $y_1(t)$) and autocorrelation ($y_1(t)$)

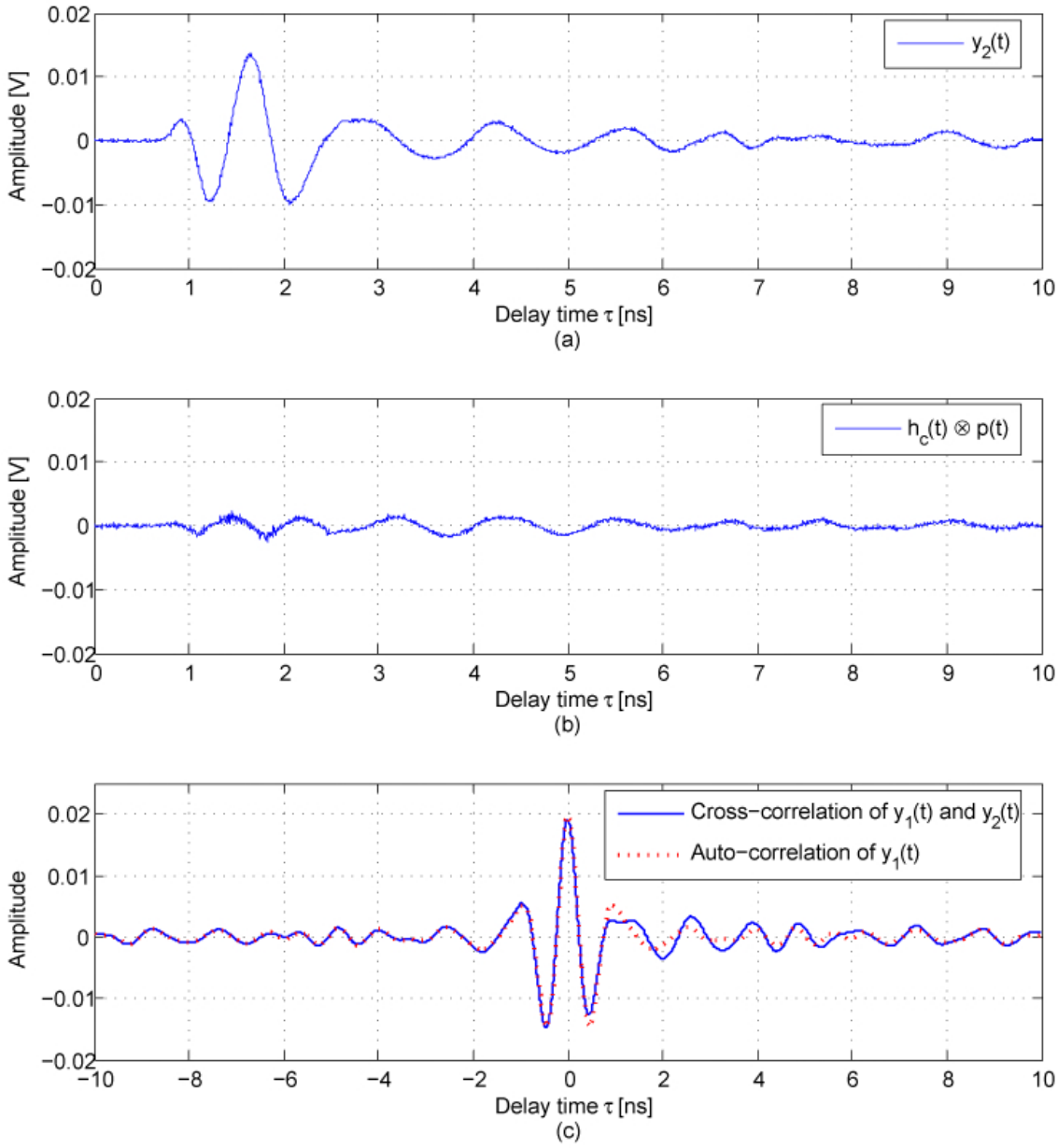

Figure 5.8 Case 2 at $D = 30cm$ for outdoor measurements: (a) Received waveform $y_1(t)$, (b) $h_c(t) \otimes p(t)$, and (c) Comparison of cross-correlation ($y_2(t)$ and $y_1(t)$) and autocorrelation ($y_1(t)$)

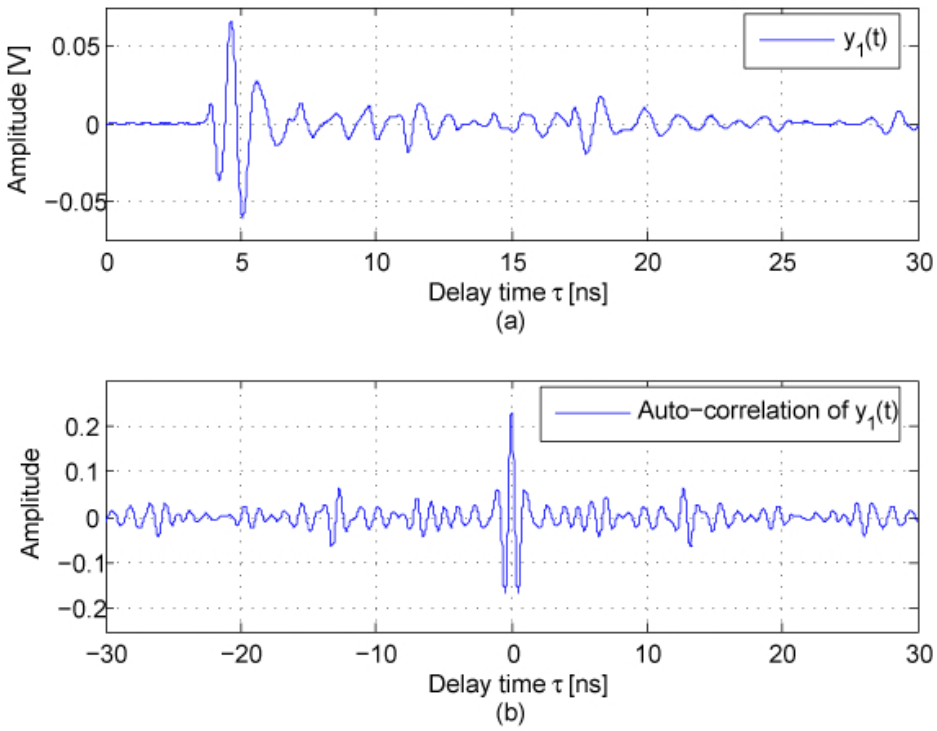

Figure 5.9 Case 1 for indoor measurements: (a) Received waveform $y_1(t)$, (b) Autocorrelation of $y_1(t)$

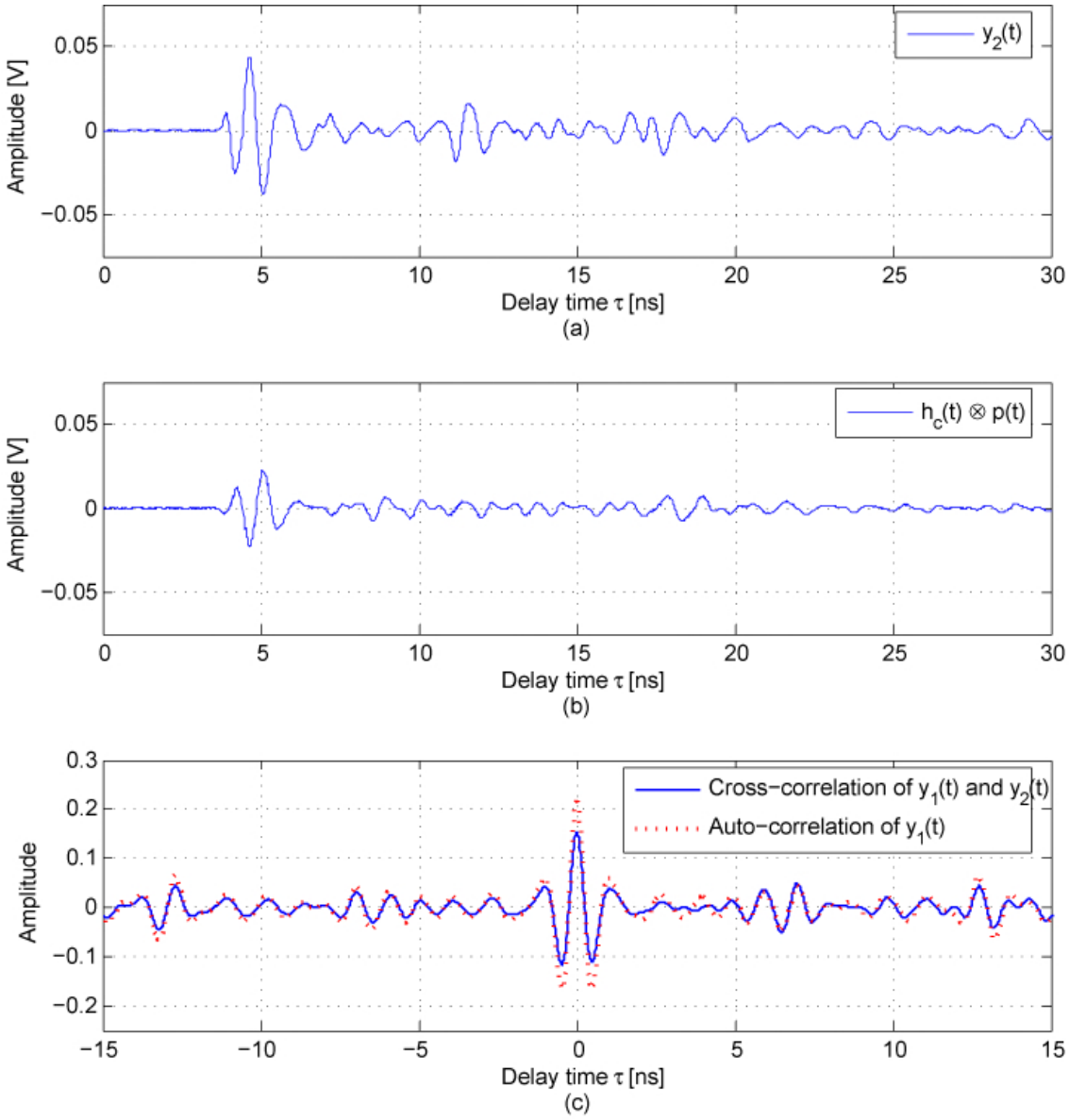

Figure 5.10 Case 2 at $D = 3cm$ for indoor measurements: (a) Received waveform $y_1(t)$, (b) $h_c(t) \otimes p(t)$, and (c) Comparison of cross-correlation ($y_2(t)$ and $y_1(t)$) and autocorrelation ($y_1(t)$)

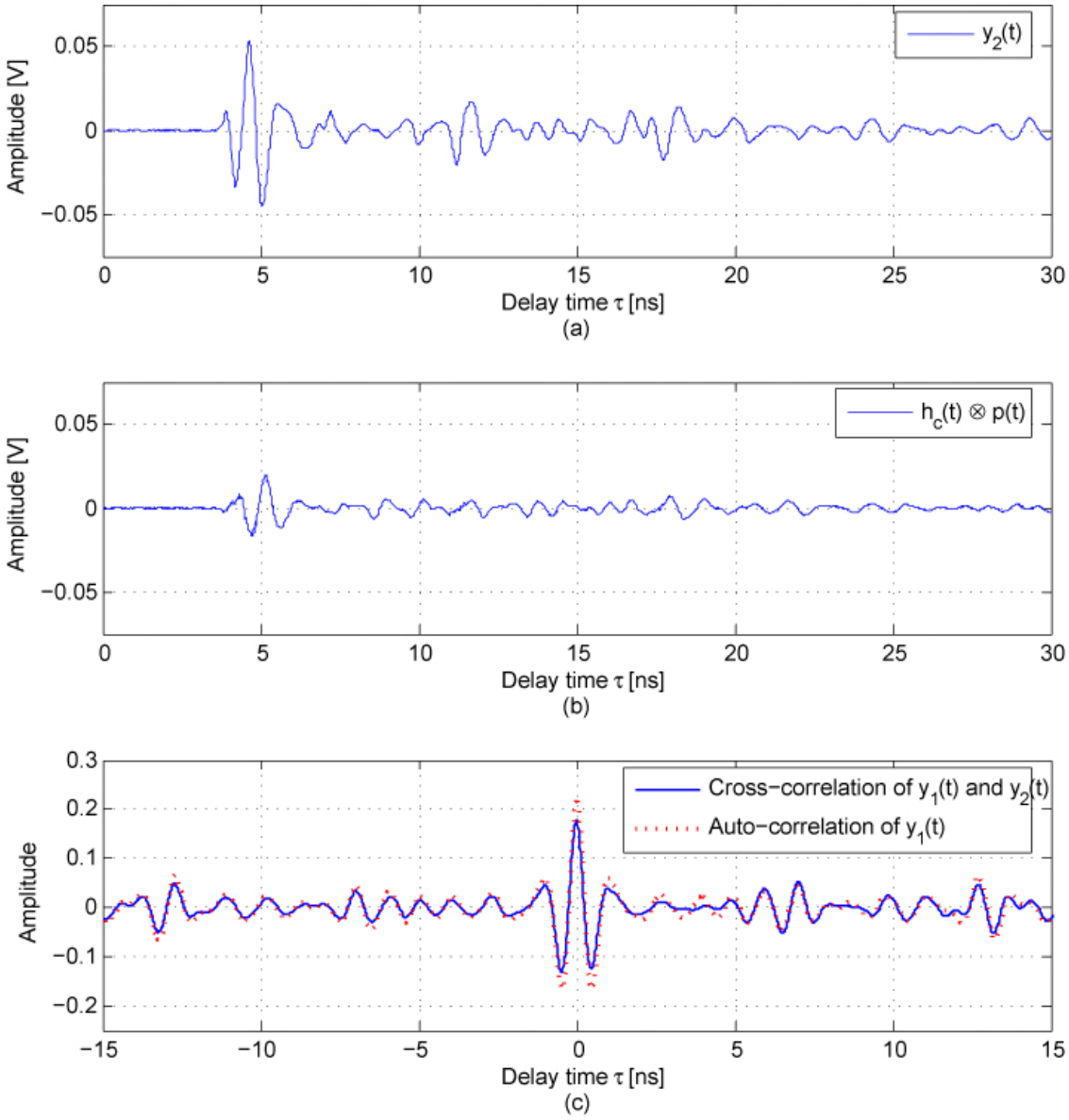

Figure 5.11 Case 2 at $D = 6cm$ for indoor measurements: (a) Received waveform $y_1(t)$, (b) $h_c(t) \otimes p(t)$, and (c) Comparison of cross-correlation ($y_2(t)$ and $y_1(t)$) and autocorrelation ($y_1(t)$)

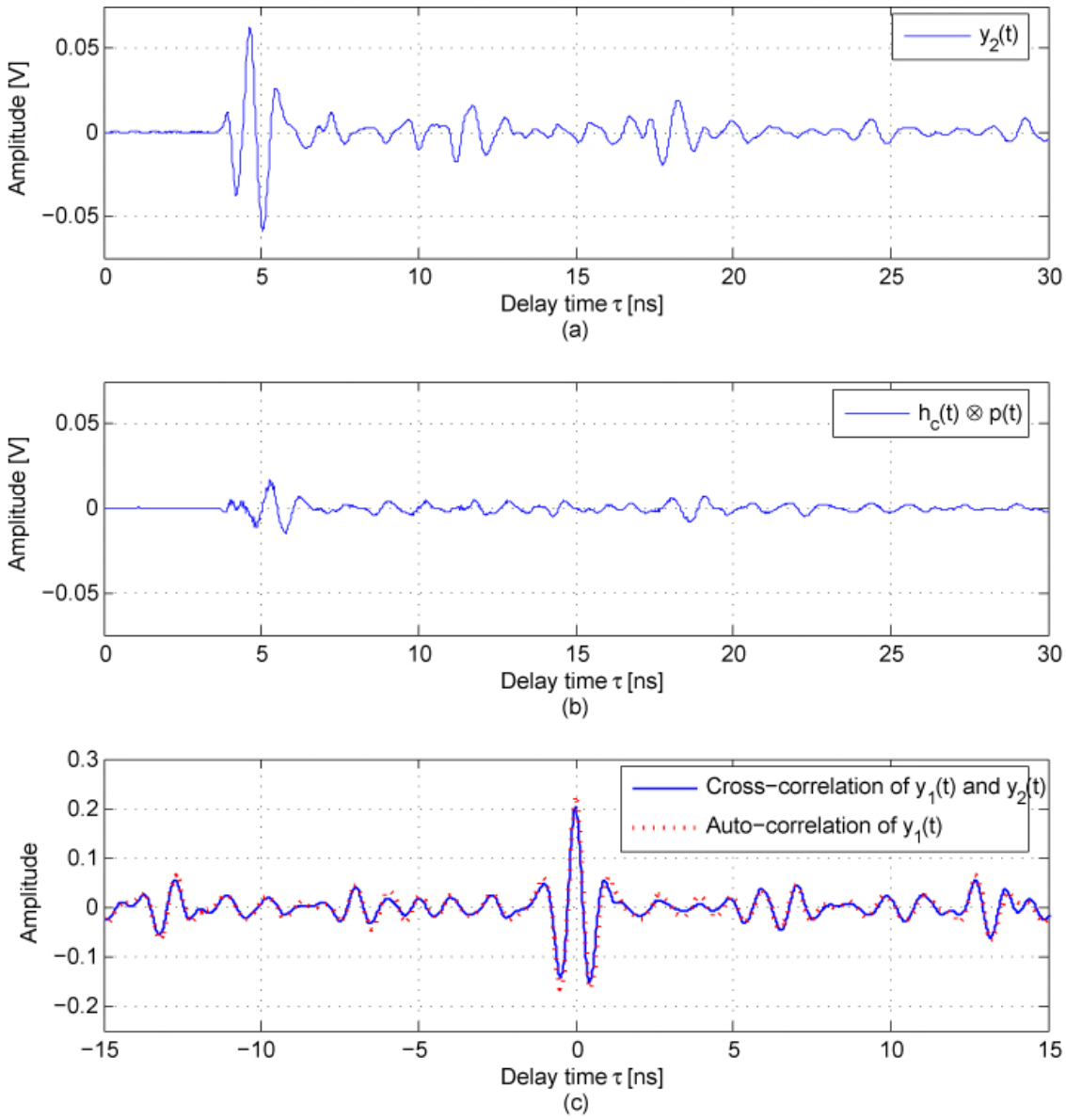

Figure 5.12 Case 2 at $D = 9cm$ for indoor measurements: (a) Received waveform $y_1(t)$, (b) $h_c(t) \otimes p(t)$, and (c) Comparison of cross-correlation ($y_2(t)$ and $y_1(t)$) and autocorrelation ($y_1(t)$)

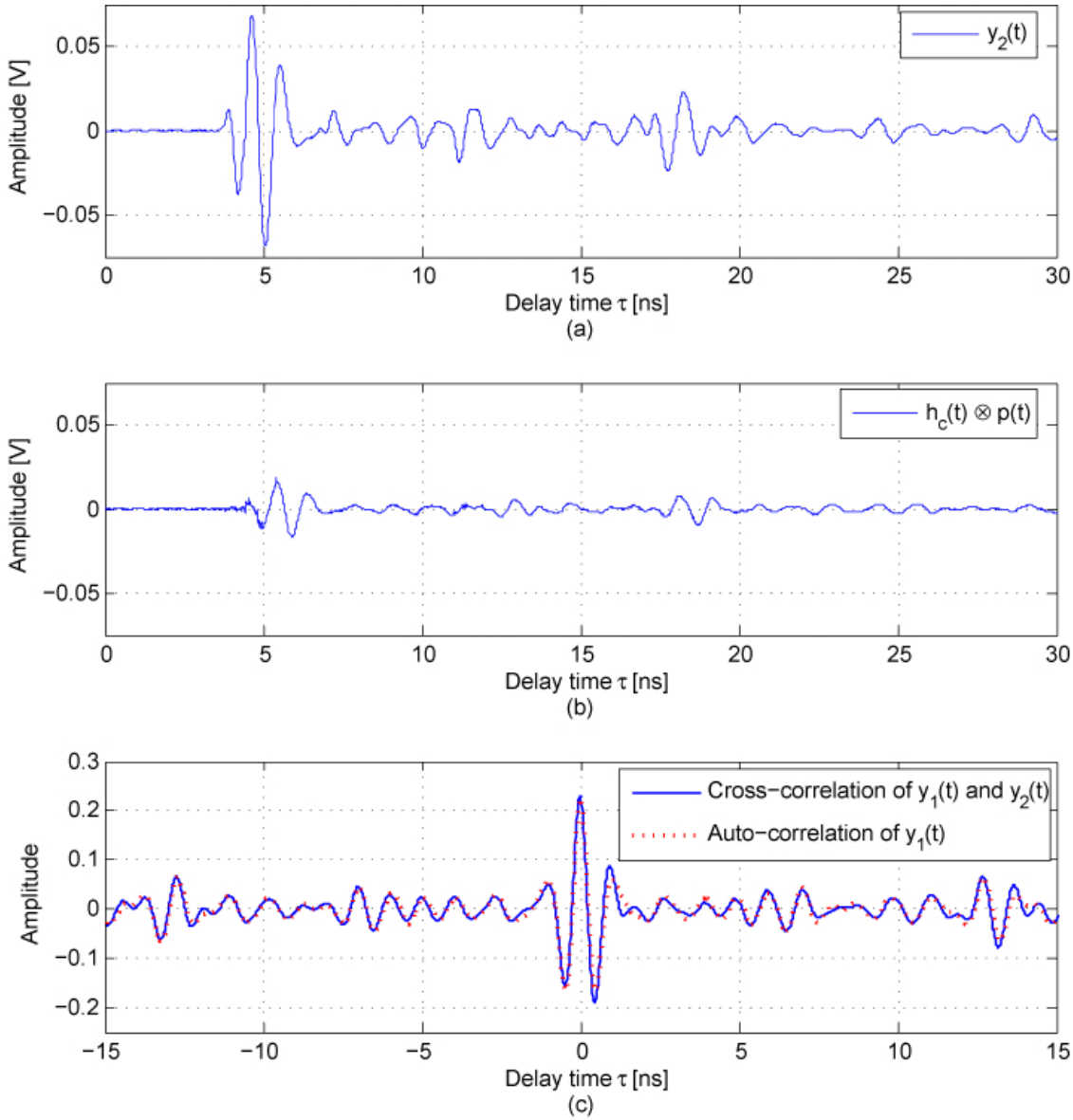

Figure 5.13 Case 2 at $D = 12cm$ for indoor measurements: (a) Received waveform $y_1(t)$, (b) $h_c(t) \otimes p(t)$, and (c) Comparison of cross-correlation ($y_2(t)$ and $y_1(t)$) and autocorrelation ($y_1(t)$)

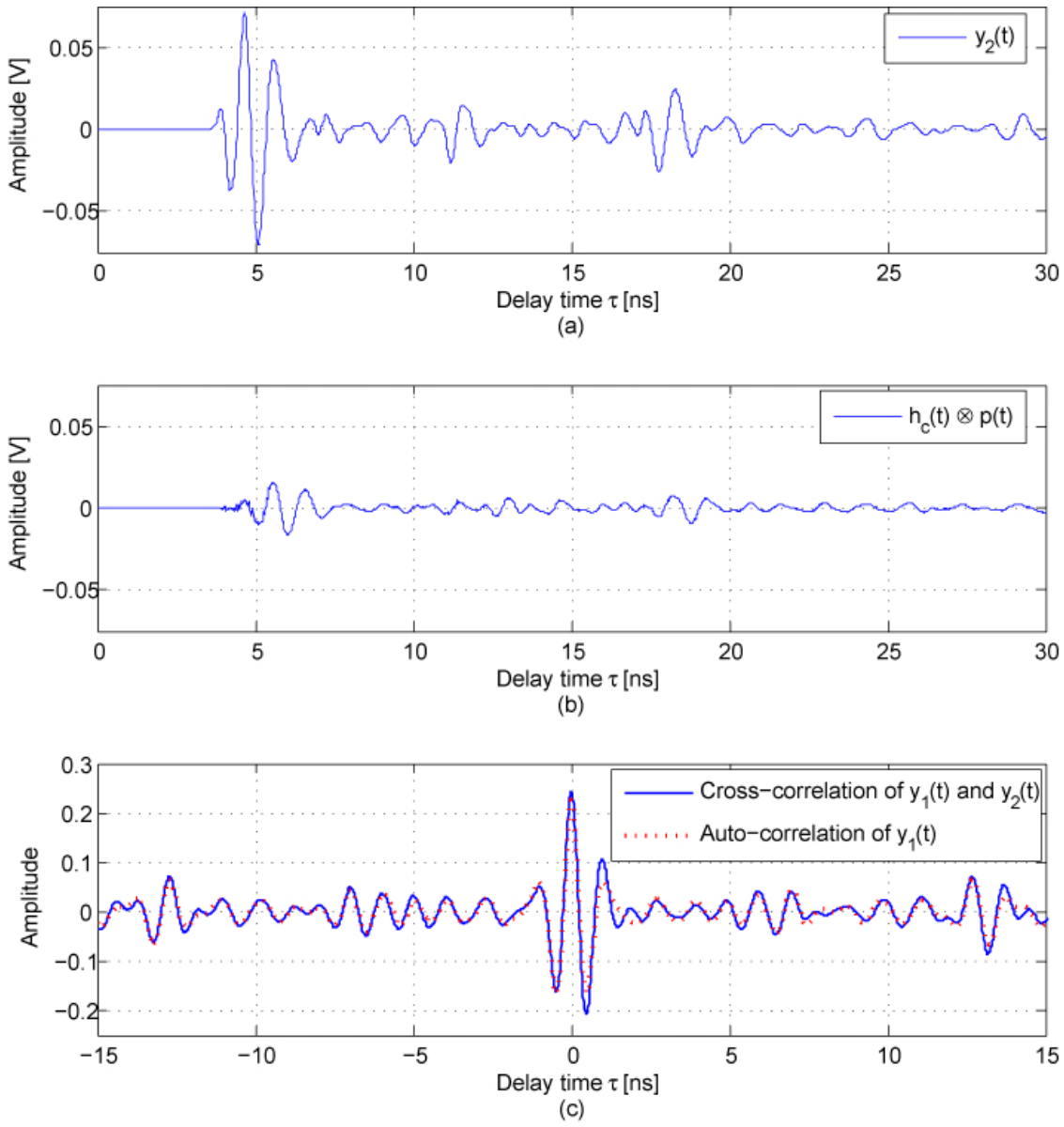

Figure 5.14 Case 2 at $D = 15cm$ for indoor measurements: (a) Received waveform $y_1(t)$, (b) $h_c(t) \otimes p(t)$, and (c) Comparison of cross-correlation ($y_2(t)$ and $y_1(t)$) and autocorrelation ($y_1(t)$)

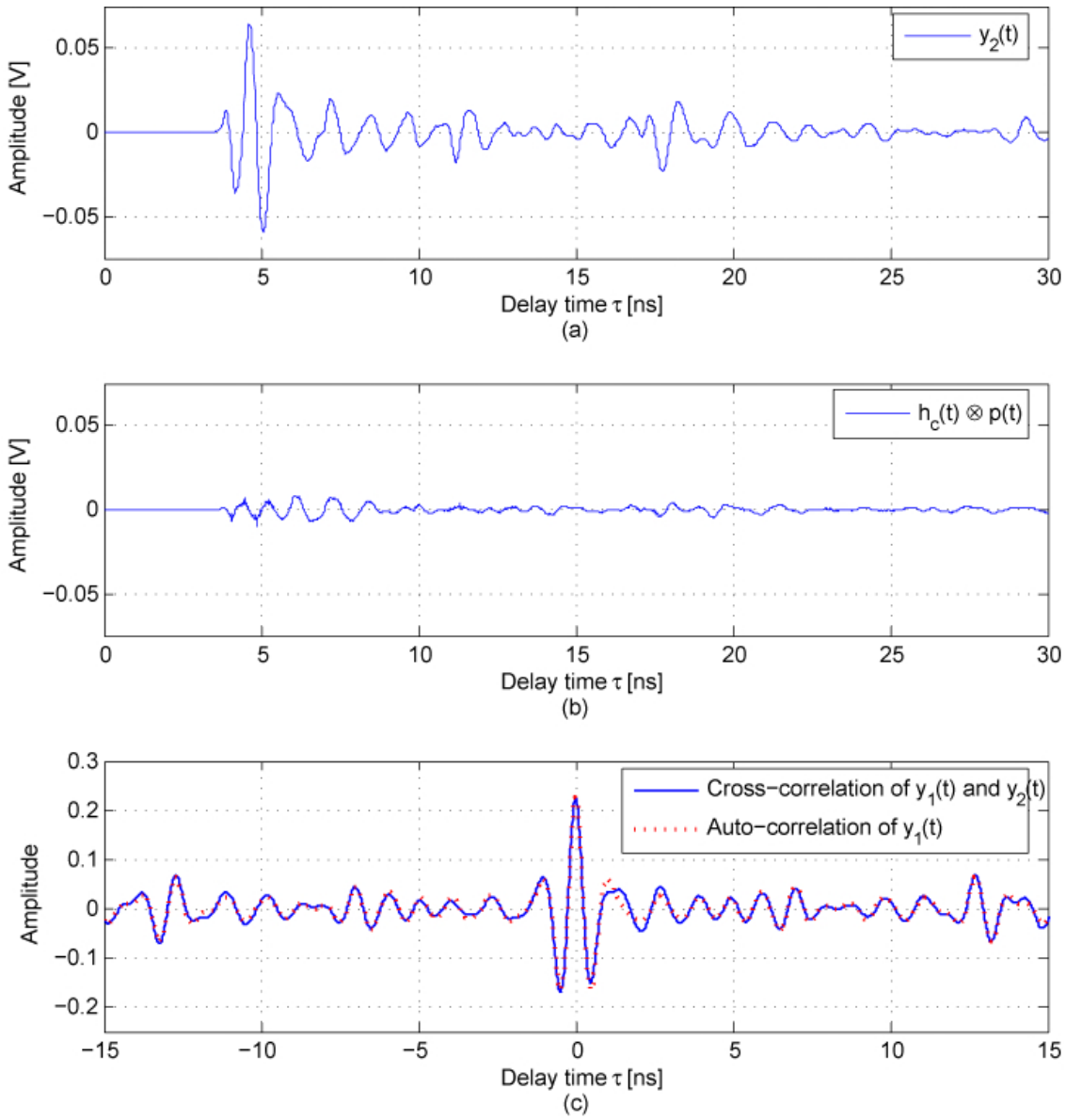

Figure 5.15 Case 2 at $D = 30cm$ for indoor measurements: (a) Received waveform $y_1(t)$, (b) $h_c(t) \otimes p(t)$, and (c) Comparison of cross-correlation ($y_2(t)$ and $y_1(t)$) and autocorrelation ($y_1(t)$)

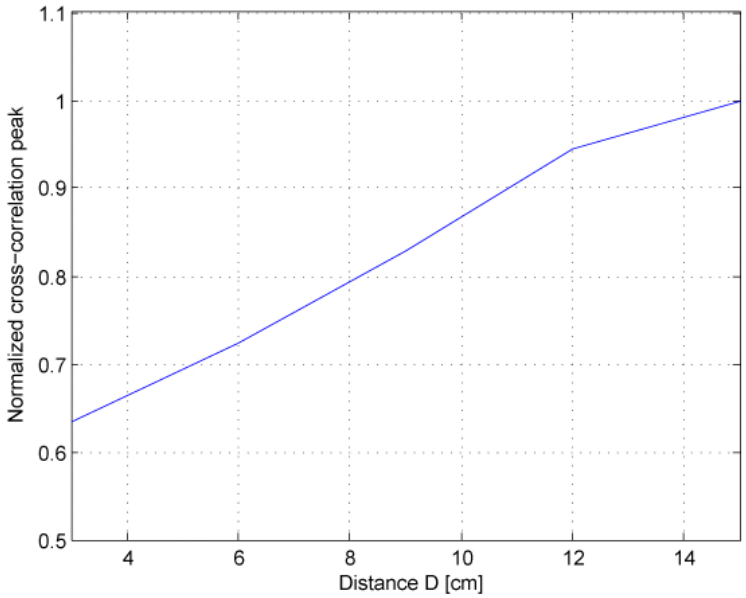

Figure 5.16 Normalized cross-correlation peak for several distances D in indoor measurements

5.2 Virtual Array and Real Array Results

Results in Section 5.1 indicate that a virtual array model when the distance between antennas is smaller than $D = 15cm$ is not realistic. In Section 3.3.3, it was shown that the received waveform for a small distance, D, between two receive antennas is greatly distorted compared to the case when only one receive antenna is present. Therefore, a simulation experiment is performed in which the performance of a UWB-SIMO communication system is evaluated for both the virtual and real array measurements. The objective of this simulation is to identify the distance D at which the virtual array does not hold true.

In this system the transmitter and receiver designs explained in Section 4.4 are considered. The time-reversed replica of the received waveform is used as the TiR

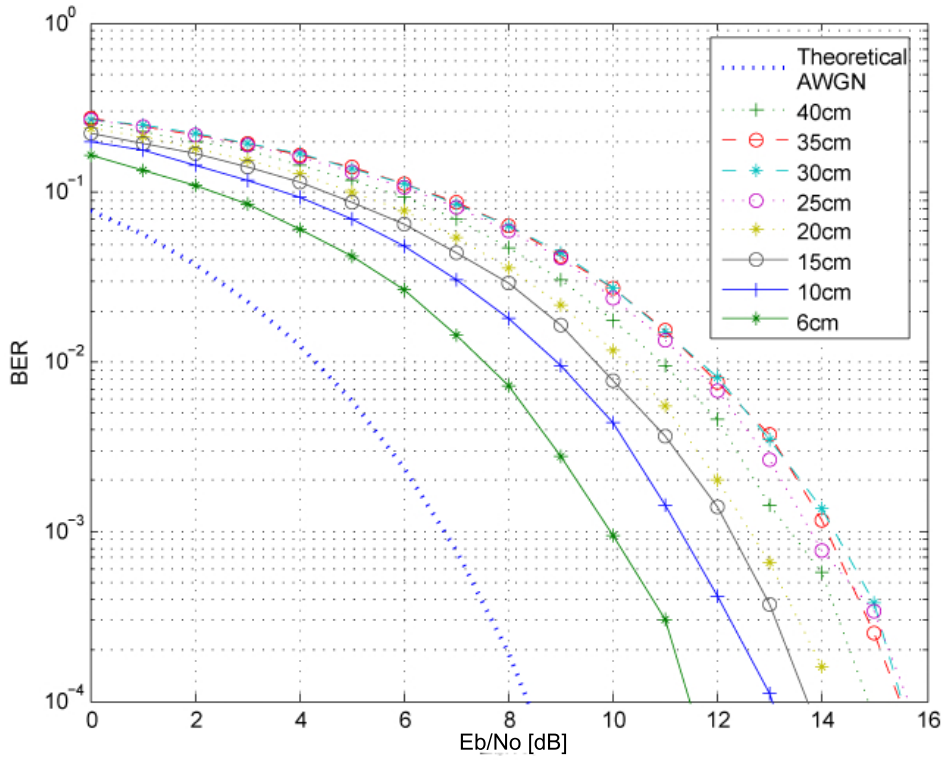

Figure 5.17 BER for the real array at several distances D

pre-coder. MC simulation is performed to obtain BER and evaluate performance of the UWB-SIMO system. Figure 5.17 presents the real array results and Figure 5.18 shows the virtual array results for several distances D. Clearly there is a difference between the BER curves, and thus, the two measurements. To gather more insight, the BER for the virtual and the real array for $D = 35cm$ is presented in Figure 5.19, for $D = 25cm$ in Figure 5.20, for $D = 15cm$ in Figure 5.21, and for $D = 10cm$ in Figure 5.22. These plots indicate that using a virtual array when $D = 10cm$ will have a performance error of more than 3dB for a BER of 10^{-3}. A performance error of 1dB to 2dB is observed when D ranges between 15cm and 25cm for a BER of 10^{-3}. Furthermore, using a virtual array gives the same performance as measuring a real array when $D = 35cm$.

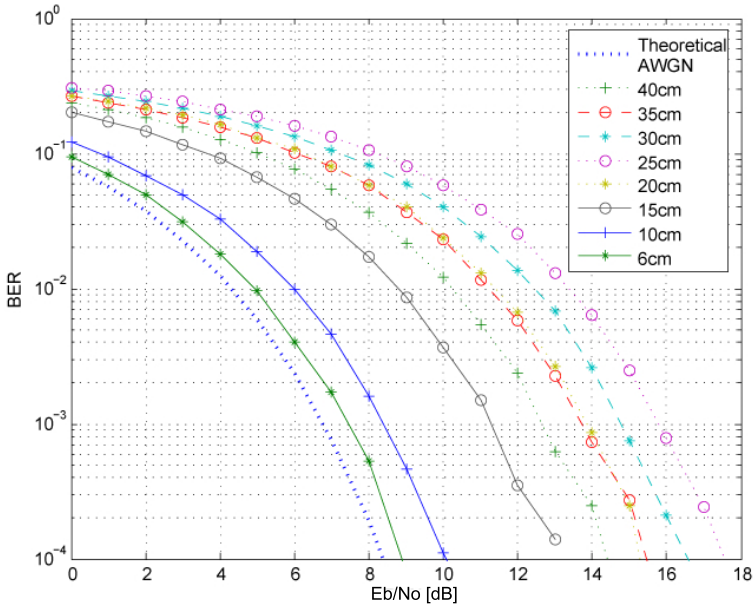

Figure 5.18 BER for the virtual array at several distances D

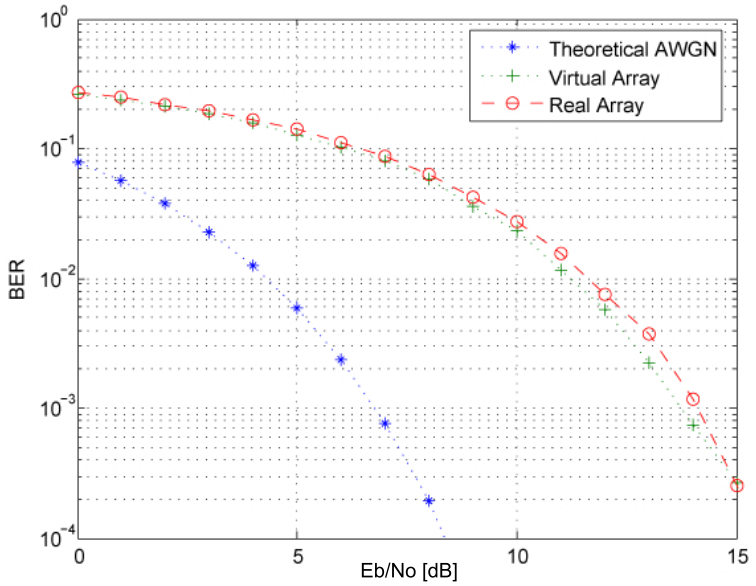

Figure 5.19 BER for the virtual and real arrays at distances $D = 35cm$

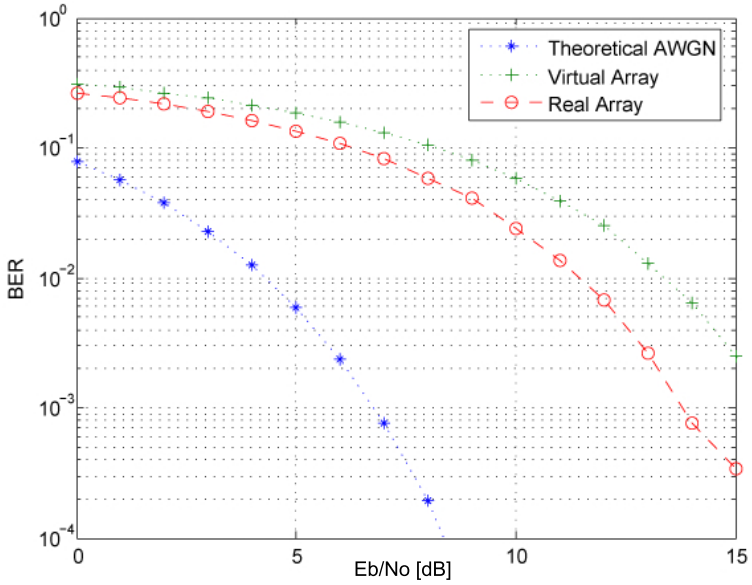

Figure 5.20 BER for the virtual and real arrays at distances $D = 25cm$

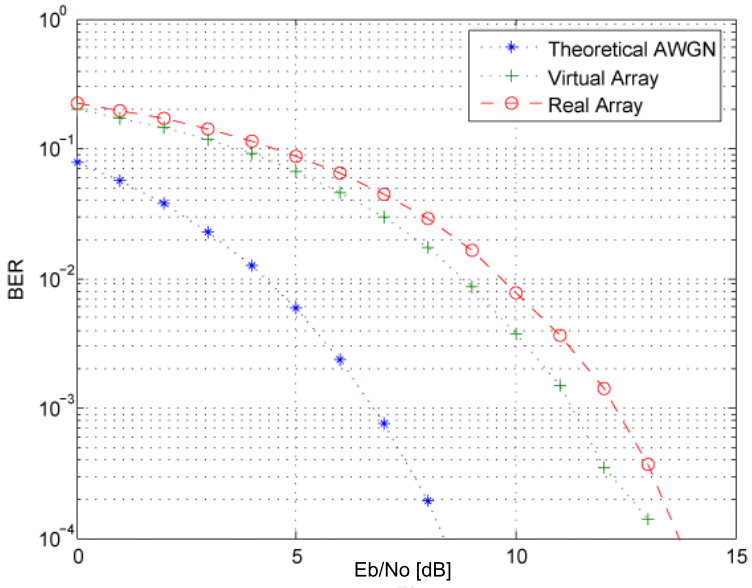

Figure 5.21 BER for the virtual and real arrays at distances $D = 15cm$

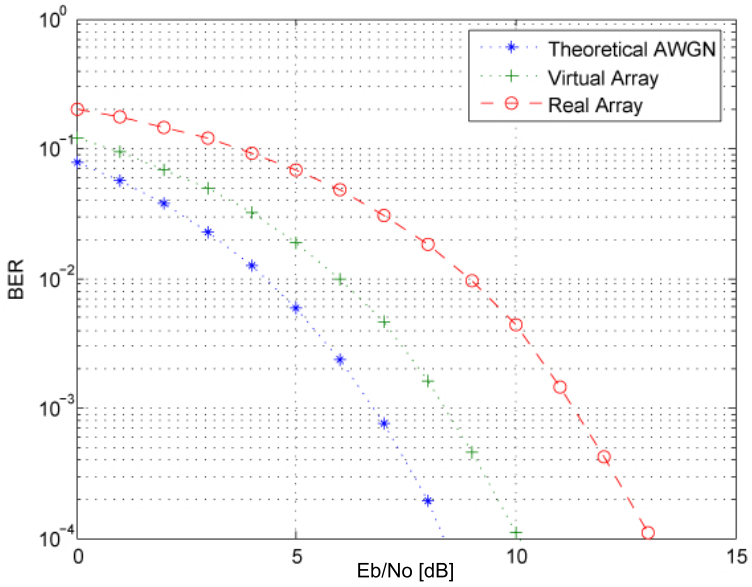

Figure 5.22 BER for the virtual and real arrays at distances $D = 10cm$

5.3 UWB-MIMO single-user

UWB-MIMO considers transmit and receive diversity. Section 3.3.4 presented two measurement experiments for a UWB single-user channel. The two sites considered for these measurements are the Wireless Networking Systems Lab and the Office environment. The recorded signals are used for the simulation of a time-reversed single-user UWB-MIMO system in which the performance is evaluated. The transmitter and receiver designs in the system were presented in Section 4.4 and the metrics used are the BER, computed using MC simulation, and the SINR. Two antennas are considered for the receiver where the distance between them D, was varied during channel measurements. The objective of these simulations is to evaluate and discuss the performance of a single-user TiR UWB-MIMO system when D decreases.

5.3.1 Results for the Wireless Networking Systems Lab

Two approaches can be used to determine the TiR pre-coder at the transmitter as explained in Section 4.3. The first approach uses the time-reversed replica of the CIR while the second approach uses the time-reversed replica of the recorded signal. In this simulation, performance of a single-user TiR UWB-MIMO system is evaluated, and the two pre-coder approaches are compared. For this site, four antennas at the transmitter and two antennas at the receiver (user) are considered. The BER as a function of E_b/N_o for several distances D is presented in Figure 5.23 for the first pre-coder approach and in Figure 5.24 for the second pre-coder approach. These results suggest that setting the TiR pre-coder to the time-reversed replica of the recorded signal increases the performance of the system for all values of D. This gives a match filter at the transmitter side that is matched to the composite receive signal.

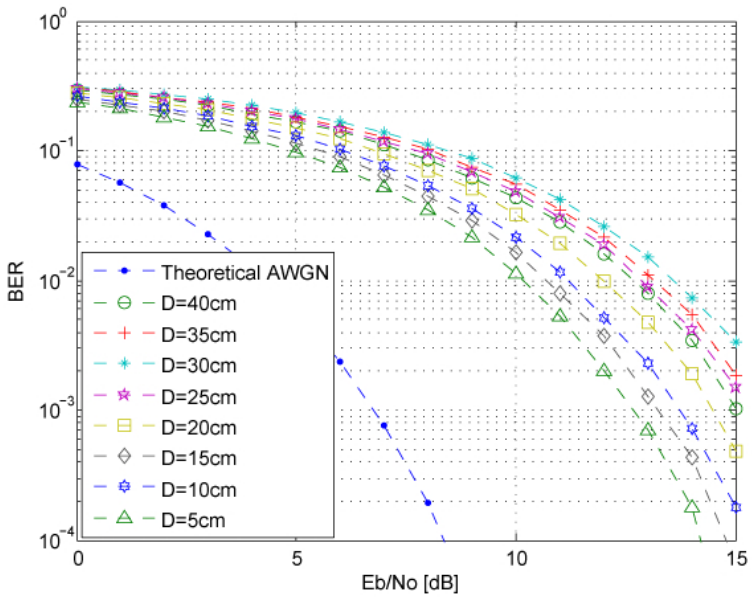

Figure 5.23 BER performance of a single-user TiR UWB-MIMO system for several D when the CIR is used on the TiR pre-coder

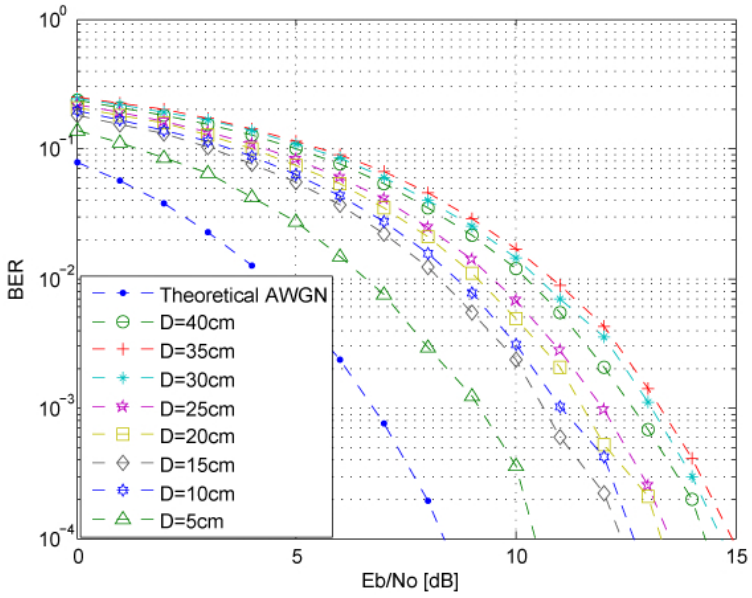

Figure 5.24 BER performance of a single-user TiR UWB-MIMO system for several D when the recorded signal is used on the TiR pre-coder

Furthermore, there is an improvement of performance when the distance D between the two receive antennas is 5cm. For a BER of 10^{-3} an improvement of 2.5dB is observed when D is decreased from 40cm to 5cm for the first pre-coder approach, while an improvement of 3.5dB is noted for the second pre-coder approach. In both cases, $D = 30cm$ and $D = 35cm$ gives the worst performance.

To get insight of the interference in each case, Figure 5.25 presents SINR as a function of SNR for several distances D when the first pre-coder approach is used, while Figure 5.26 presents the case when the second pre-coder approach is used. In both cases, an improvement of 5dB in SINR is observed when SNR is 15dB and $D =$ is varied from 5cm to 40cm. Although SINR is 5dB less for $D = 5cm$ than $D = 40cm$, the BER performance increases when using a small distance between the receive antennas which suggests the interference is constructive.

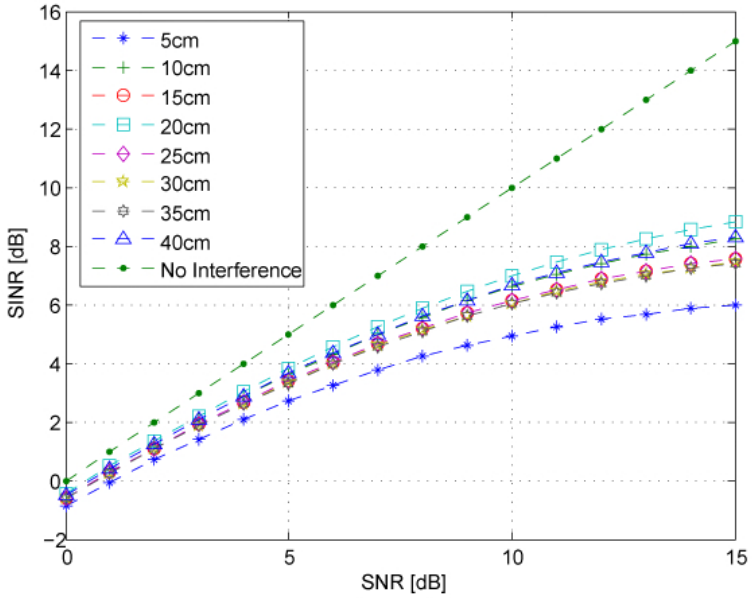

Figure 5.25 SINR as a function of SNR for a single-user TiR UWB-MIMO system when the CIR is used on the TiR pre-coder

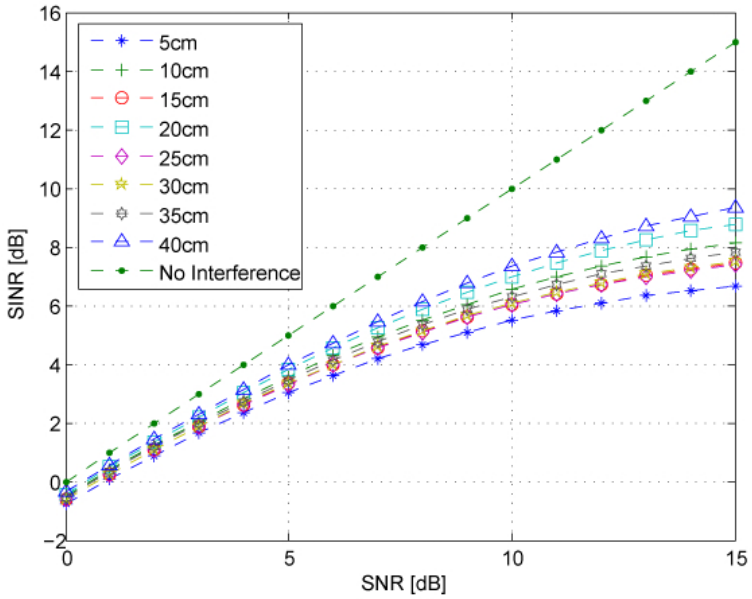

Figure 5.26 SINR as a function of SNR for a single-user TiR UWB-MIMO system when the recorded signal is used on the TiR pre-coder

5.3.2 Results for the Office Environment

In this site, measurements were performed and signals were recorded for two antennas at the transmitter and two antennas for the receiver (user). The purpose of this simulation is to find D at which the performance of the system is best, and to compare with a single-user TiR UWB-MISO system. The TiR pre-coder is set to the time-reversed replica of the recorded signal since it was shown in Section 5.3.1 that it performs better than the other approach. Power allocation was considered as explained in Section 4.3.4. Figure 5.27 presents the BER as a function of E_b/N_o for several distances D between the receive antennas. The best performance of the system is achieved at $D = 3cm$ with an improvement of 2dB compared to the case when $D = 15cm$ for a BER of 10^{-3}. Furthermore, the overall performance of UWB-MIMO is better than for UWB-MISO in all cases. For $D = 3cm$, the performance of UWB-MIMO at a BER of 10^{-3} has more than a 3dB improvement over UWB-MISO. Figure 5.28 presents SINR as a function of SNR for several D. For a SNR of 15dB, an improvement of 5dB when D is varied from 15cm to 3cm is observed. These results are consistent with the results discussed in Section 5.3.1.

5.4 Multi-user UWB-MIMO Network

The multi-user TiR UWB-MIMO network consists of several users each having two receive antennas. The distance between the receive antennas was varied when measuring the channel as explained in Section 3.3.4. The performance of the system is evaluated at the intended user when the number of users increases. The transmitter consists of four transmit antennas and power allocation is used as explained in Section 4.3.4. Transmitter and receiver designs are as considered in Section 4.4 and

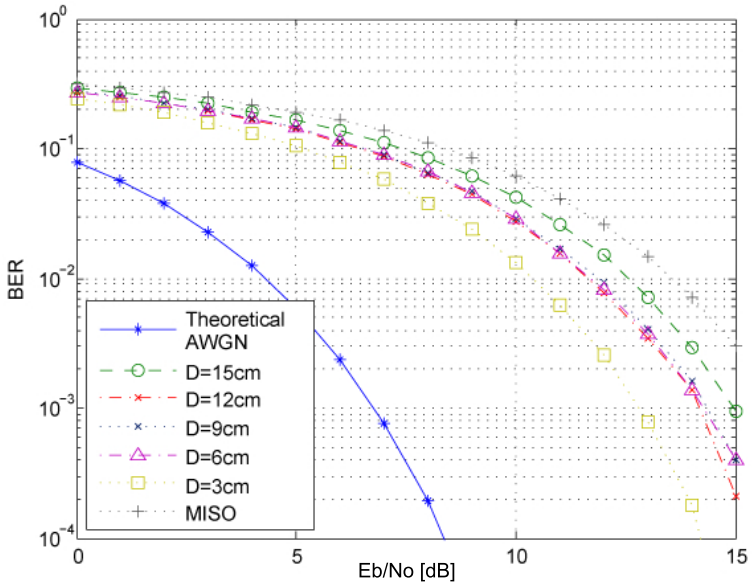

Figure 5.27 BER as a function of E_b/N_o for a single-user TiR UWB-MIMO system for several D

data is sent to all users simultaneously (i.e. a multiple access scenario). The metrics to evaluate the performance of the system are the BER and the SINR.

5.4.1 Results for Wireless Networking Systems Lab

The objective of this simulation experiment is to study multi-user interference by incrementing the number of users in a network. A multi-user TiR UWB-MIMO network is considered where each user (receiver) has two receive antennas which distance D between them, is varied as explained in the measurement results for the Wireless Networking Systems Lab in Section 3.3.4. The transmitter consists of four transmit antennas with power allocation as explained in Section 4.3.4. The number of users varies from 1 to 4 as shown in the lab layout presented in Figure 3.23, and D is varied from 5cm to 40cm in 5cm increments. The BER as a function of E_b/N_o for a TiR UWB-MIMO network with up to 4 users is presented in Figure 5.29 when

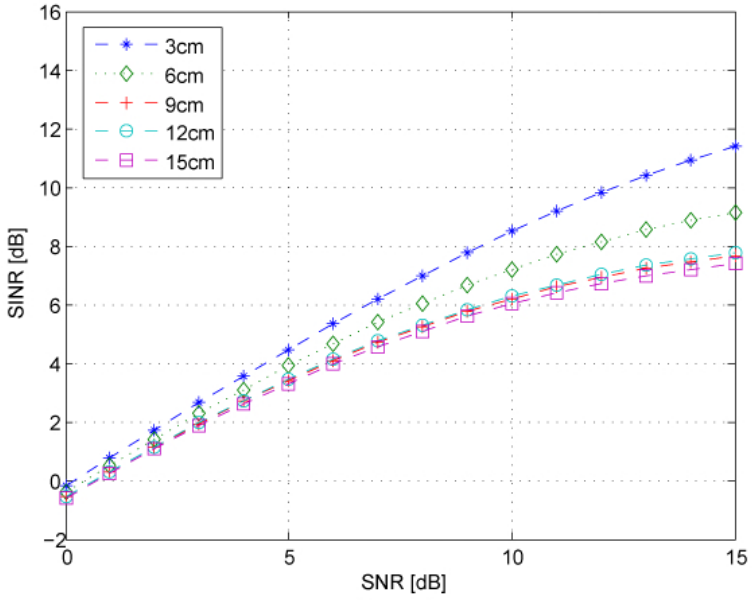

Figure 5.28 SINR as a function of SNR for a single-user TiR UWB-MIMO system for several D

$D = 5cm$, in Figure 5.30 when $D = 10cm$, in Figure 5.31 when $D = 15cm$, in Figure 5.32 when $D = 20cm$, in Figure 5.33 when $D = 25cm$, in Figure 5.34 when $D = 30cm$, in Figure 5.35 when $D = 35cm$, and in Figure 5.36 when $D = 40cm$. It can be observed that the best performance is achieved when $D = 5cm$ for all networks. For systems with up to 3 users, the BER performance is very similar, and for the 4-user network the performance is poor in all cases. $D = 25cm$ yields the worst performance for all systems with a 5dB degradation for the 4-user network compared with other networks at a BER of 10^{-2}.

For a 4-user TiR UWB-MIMO network, the BER as a function of E_b/N_o for several D is shown in Figure 5.37. It can be observed that the best performance is given when $D = 5cm$, followed by $D = 10cm$ and $D = 15cm$. The worst performance is obtained when $D = 25cm$. SINR as a function of SNR for several number of users is presented in Figure 5.38 when $D = 10cm$, in Figure 5.39 when $D = 20cm$, in

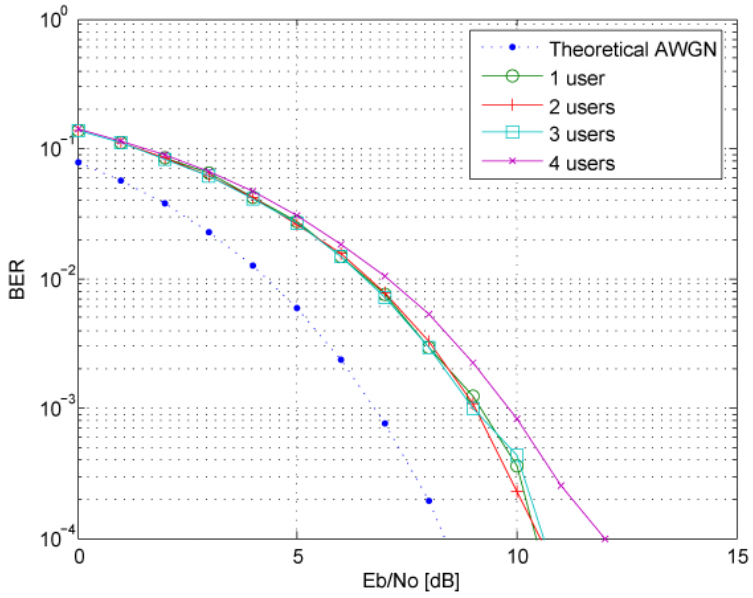

Figure 5.29 BER as a function of E_b/N_o for a TiR UWB-MIMO system at $D = 5cm$ for several number of users

Figure 5.40 when $D = 30cm$, and in Figure 5.41 when $D = 40cm$. A 1 user system achieves the best SINR as expected. A 2-user and 3-user networks perform similar with a difference of 2dB when $D = 20cm$ for a SNR of 15dB, and a difference of approximately 1dB when D is greater than 25cm at a SNR of 15dB. For all plots, the 4-user network has the lowest SINR. Figure 5.42 shows SINR as a function of SNR for several distances D in a 4-users TiR UWB-MIMO network, and Figure 5.43 for a 3-users TiR UWB-MIMO network. In the 4-user case, a 2dB difference between the best and worst SINR at a SNR of 15dB is observed and suggest that the interference is similar for all D. The same conclusion can be obtained from the 3-user network with the difference that SINR is higher at a SNR of 15dB which is expected since less users contribute interference.

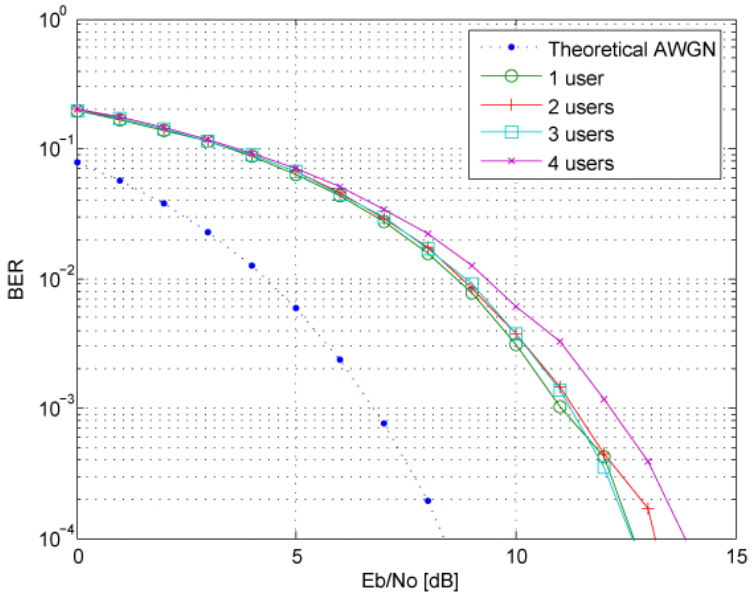

Figure 5.30 BER as a function of E_b/N_o for a TiR UWB-MIMO system at $D = 10cm$ for several number of users

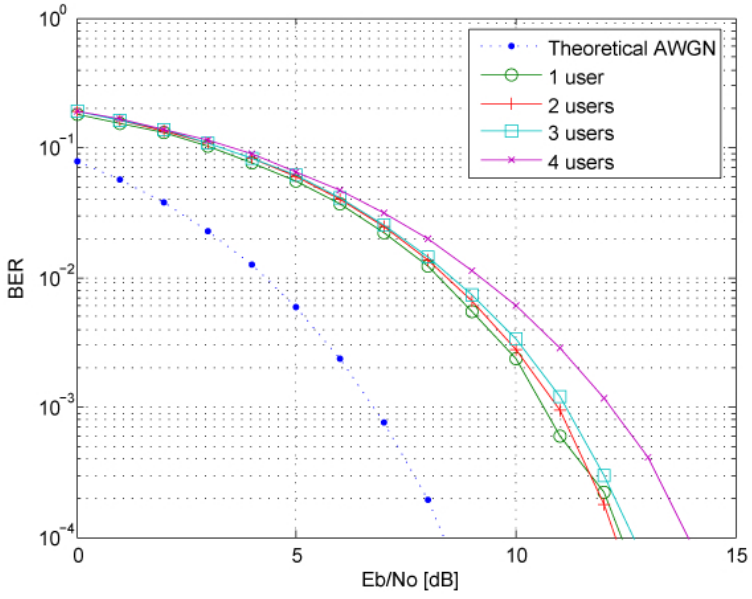

Figure 5.31 BER as a function of E_b/N_o for a TiR UWB-MIMO system at $D = 15cm$ for several number of users

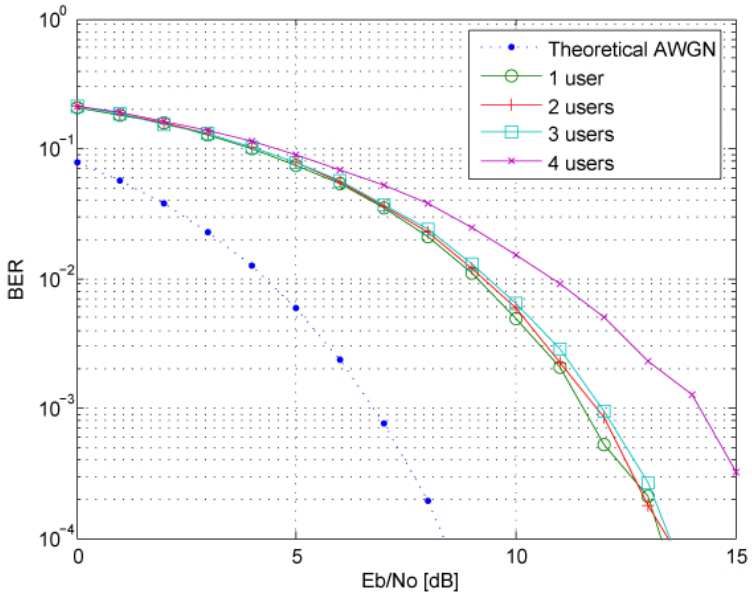

Figure 5.32 BER as a function of E_b/N_o for a TiR UWB-MIMO system at $D = 20cm$ for several number of users

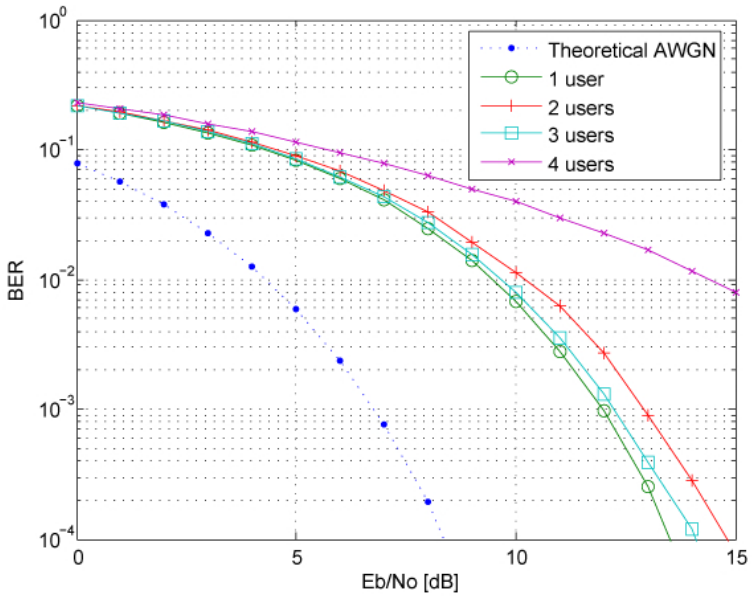

Figure 5.33 BER as a function of E_b/N_o for a TiR UWB-MIMO system at $D = 25cm$ for several number of users

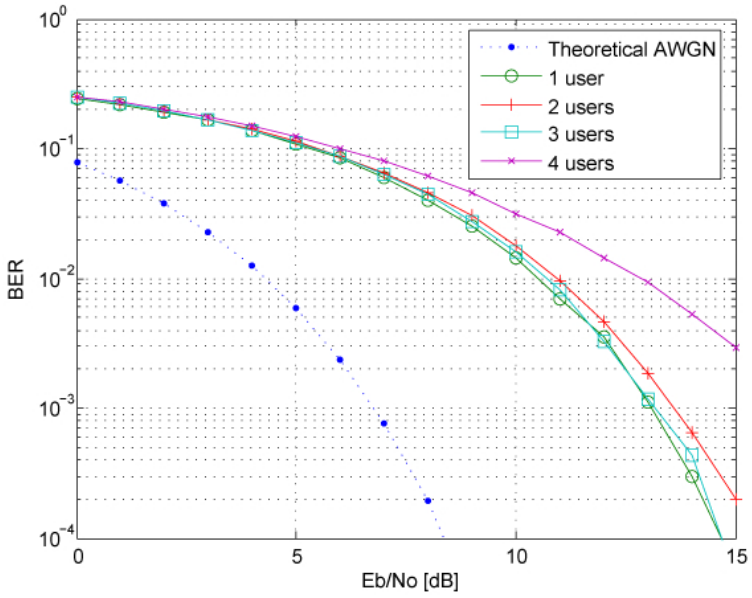

Figure 5.34 BER as a function of E_b/N_o for a TiR UWB-MIMO system at $D = 30cm$ for several number of users

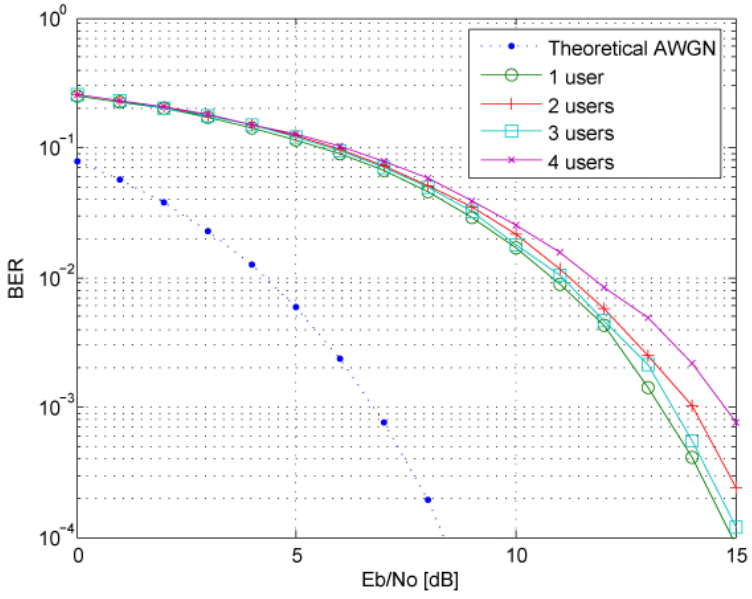

Figure 5.35 BER as a function of E_b/N_o for a TiR UWB-MIMO system at $D = 35cm$ for several number of users

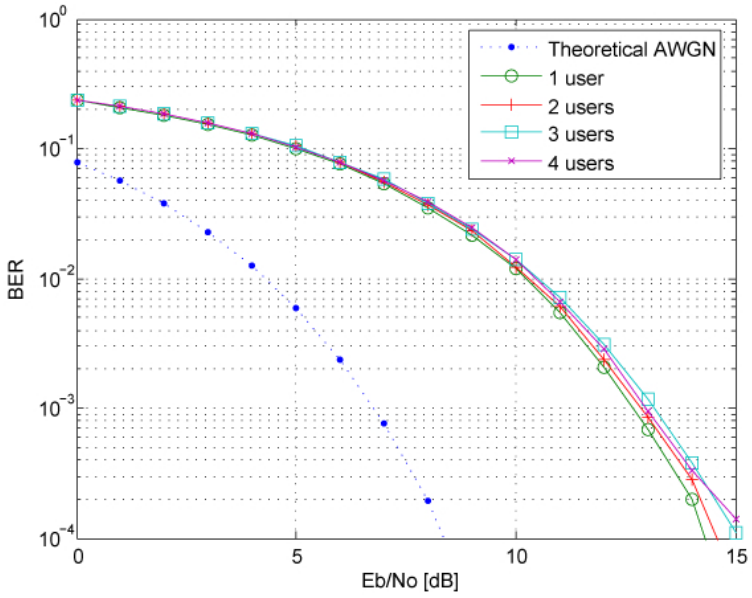

Figure 5.36 BER as a function of E_b/N_o for a TiR UWB-MIMO system at $D = 40cm$ for several number of users

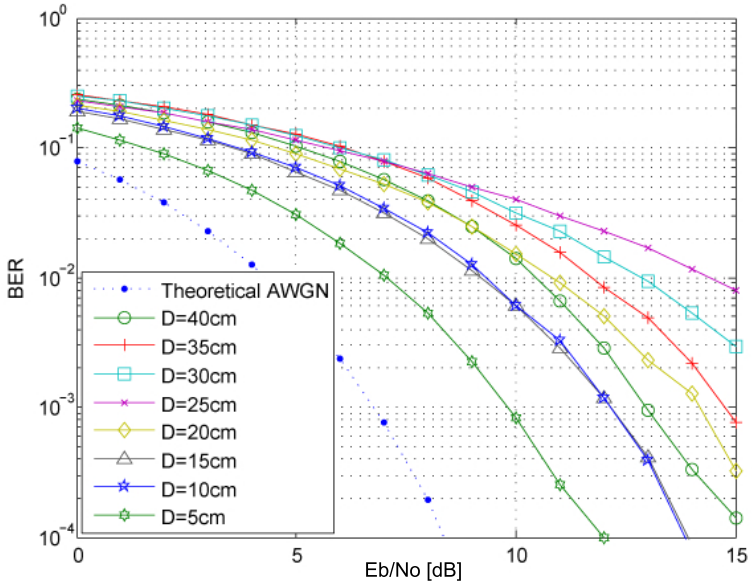

Figure 5.37 BER as a function of E_b/N_o for a TiR UWB-MIMO system with 4 users for several D

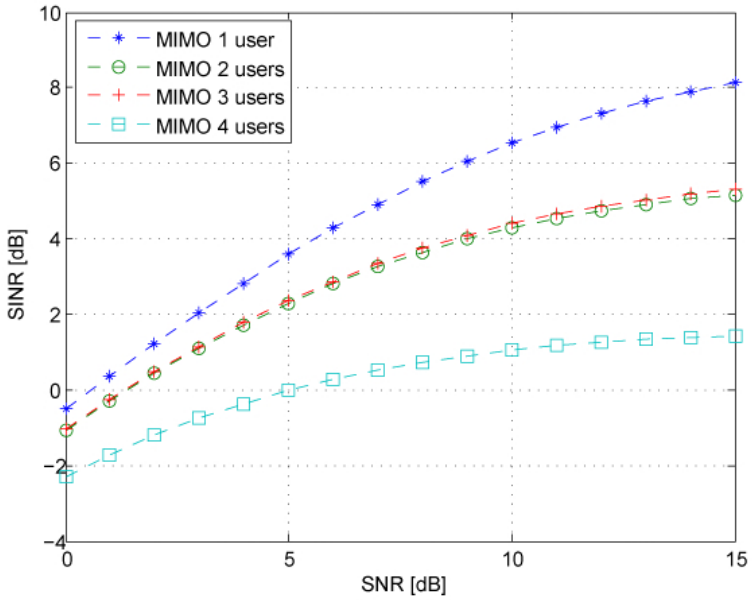

Figure 5.38 SINR as a function of SNR for a TiR UWB-MIMO system with $D = 10cm$ for several number of users

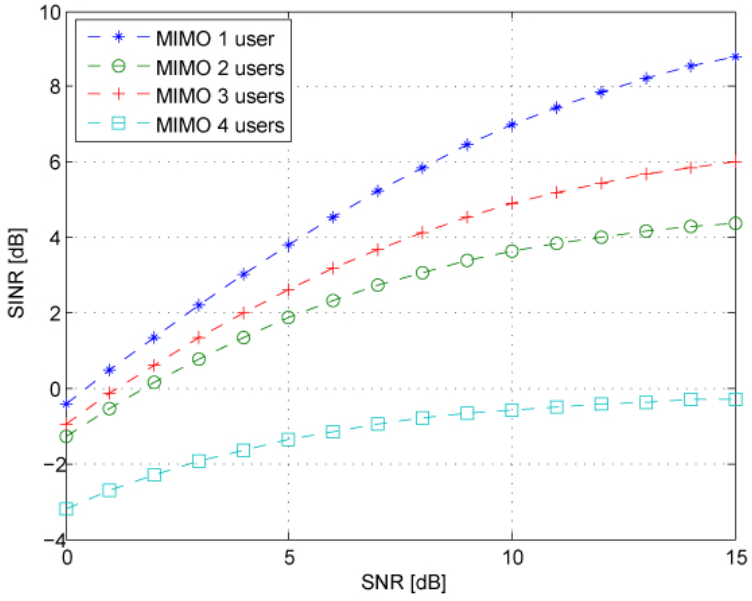

Figure 5.39 SINR as a function of SNR for a TiR UWB-MIMO system with $D = 20cm$ for several number of users

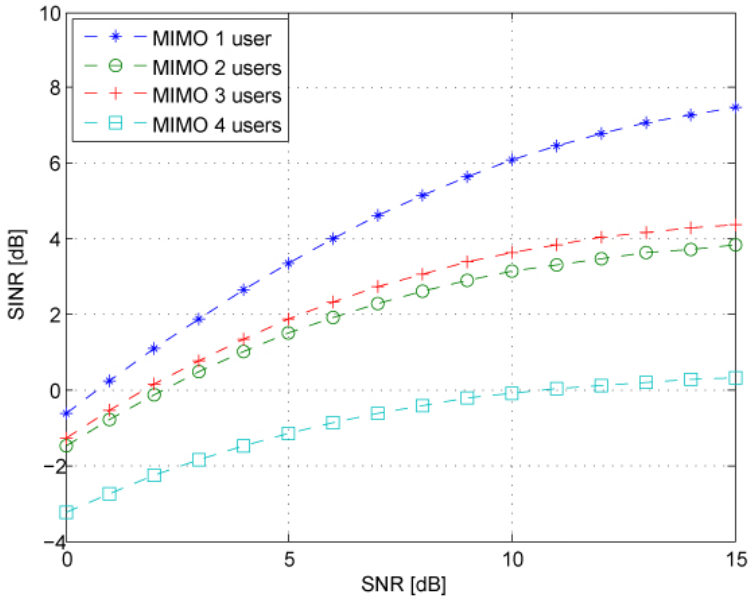

Figure 5.40 SINR as a function of SNR for a TiR UWB-MIMO system with $D = 30cm$ for several number of users

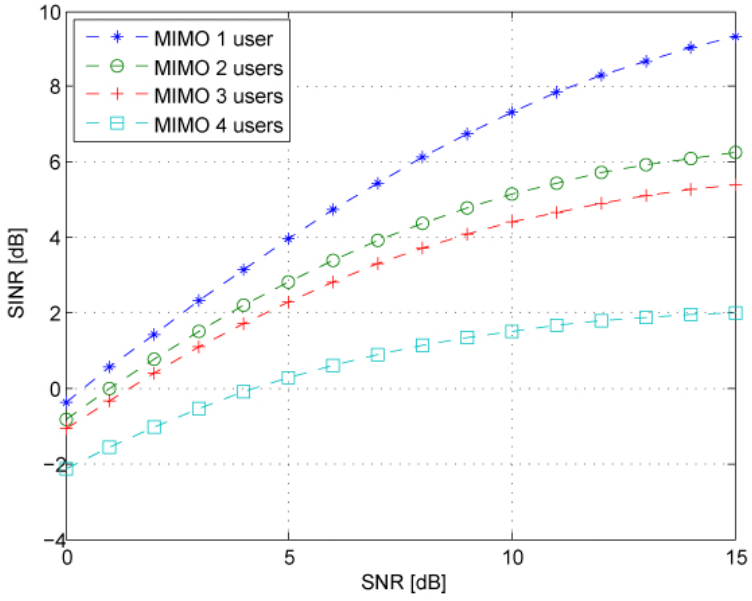

Figure 5.41 SINR as a function of SNR for a TiR UWB-MIMO system with $D = 40cm$ for several number of users

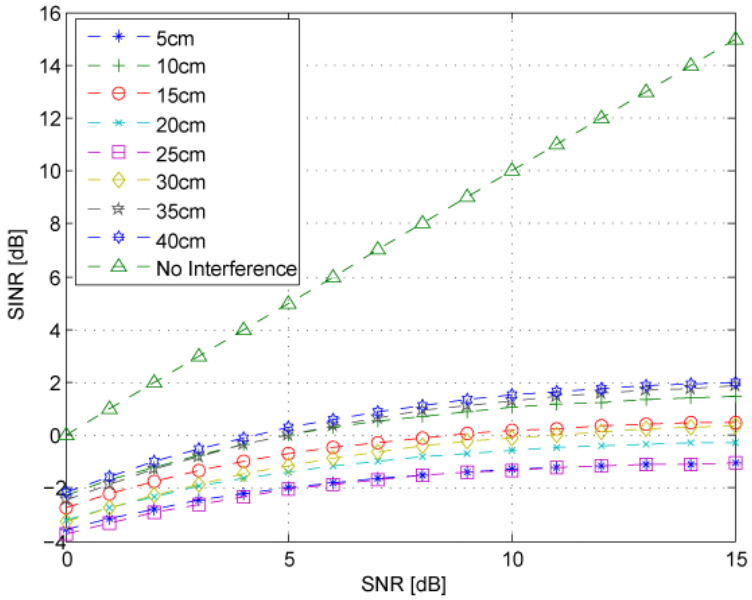

Figure 5.42 SINR as a function of SNR for a TiR UWB-MIMO system with 4 users for several D

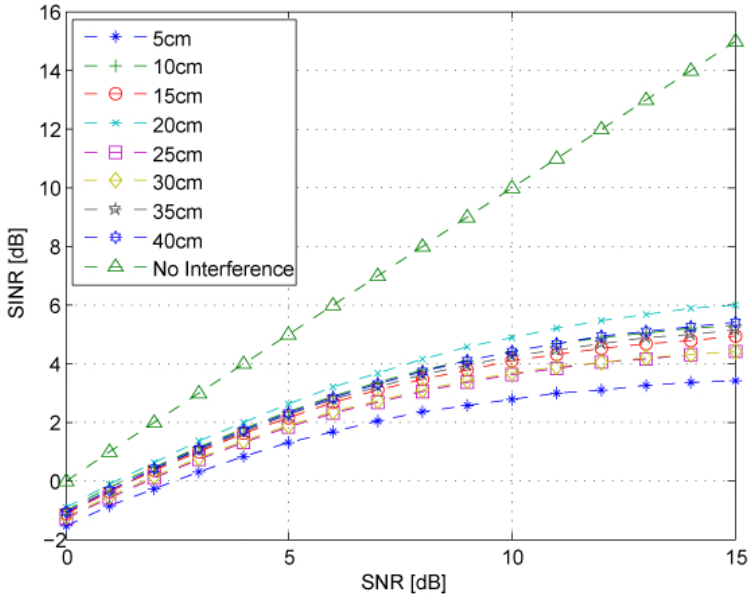

Figure 5.43 SINR as a function of SNR for a TiR UWB-MIMO system with 3 users for several D

5.4.2 Results for the Office Environment

The objective of this simulation experiment is to analyze the performance of a multi-user TiR UWB-MIMO network when the number of users increase from 1 to 25. Each user (receiver) has two receive antennas which distance between them D, is varied as explained in the measurement results for the Office environment in Section 3.3.4. The transmitter consists of two transmit antennas with power allocation as explained in Section 4.3.4. The number of users varies from 1 to 25 as presented in the office layout in Figure 3.24, and D is varied from 3cm to 15cm in 3cm increments. The BER as a function of E_b/N_o for a TiR UWB-MIMO network with up to 25 users is presented in Figure 5.44 when $D = 15cm$, in Figure 5.45 when $D = 12cm$, in Figure 5.46 when $D = 9cm$, in Figure 5.47 when $D = 6cm$, and in Figure 5.48 when $D = 3cm$. When the distance between the receive antennas is 3cm, the system has the best performance. Also, performance for more than 10 users in the system gives a degradation of approximately 5dB at a BER of 10^{-2} when $D = 3cm$. When $D = 15cm$, BER reaches a floor of 10^{-1} at an E_b/N_o of 15dB. In all cases, the system with up to 10 users yields a very similar BER performance. BER as a function of E_b/N_o for a TiR UWB-MIMO network with 5 users for several D is presented in Figure 5.49, for 10 users in Figure 5.50, for 15 users in Figure 5.51 and for 25 users in Figure 5.52. For the networks with 5 and 10 users, the best performance is achieved when $D = 6cm$ and the worst performance when $D = 15cm$ with a 2dB difference for a BER of $2x10^{-3}$. For 15 and 25 users, the worst performance is obtained when $D = 15cm$ and the best performance when $D = 6cm$ for an E_b/N_o of 15dB.

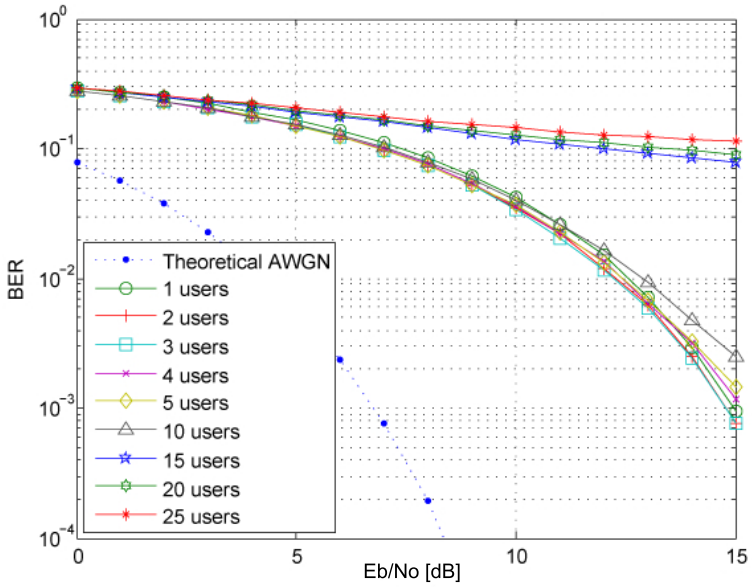

Figure 5.44 BER as a function of E_b/N_o for a TiR UWB-MIMO system at $D = 15cm$ for several number of users

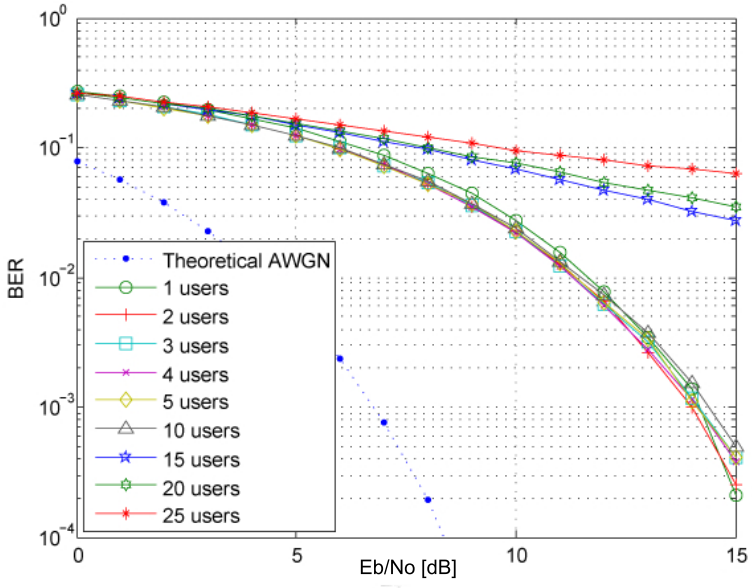

Figure 5.45 BER as a function of E_b/N_o for a TiR UWB-MIMO system at $D = 12cm$ for several number of users

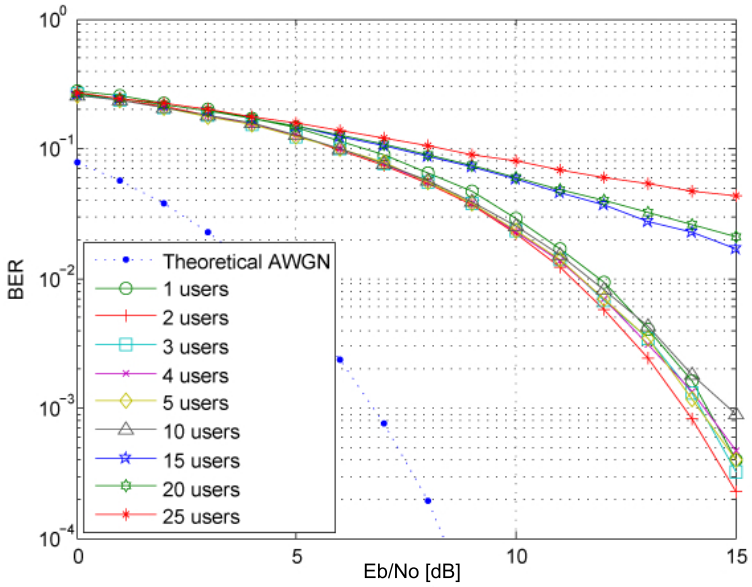

Figure 5.46 BER as a function of E_b/N_o for a TiR UWB-MIMO system at $D = 9cm$ for several number of users

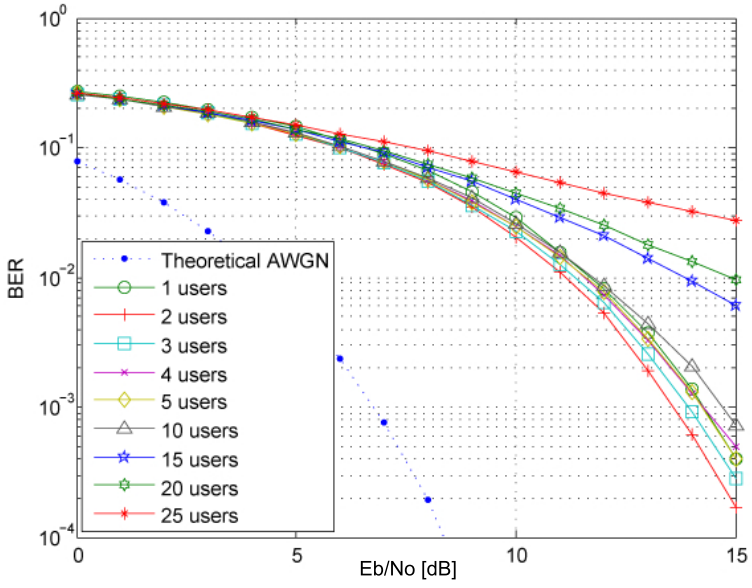

Figure 5.47 BER as a function of E_b/N_o for a TiR UWB-MIMO system at $D = 6cm$ for several number of users

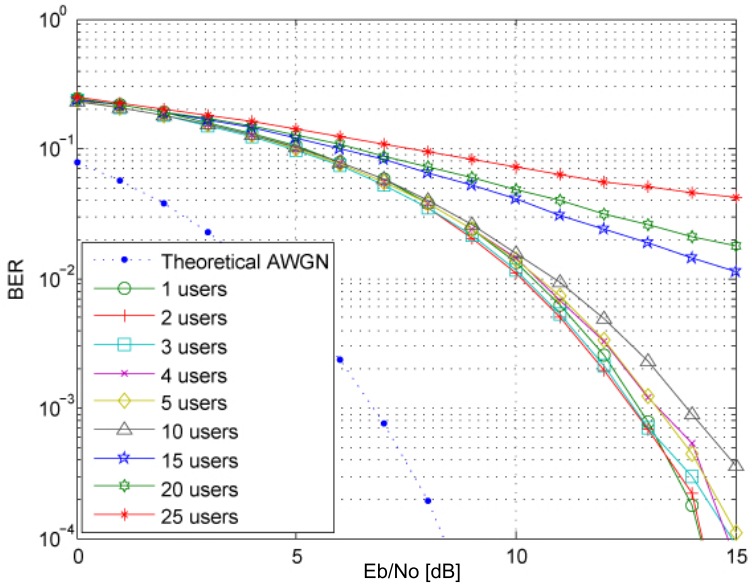

Figure 5.48 BER as a function of E_b/N_o for a TiR UWB-MIMO system at $D = 3cm$ for several number of users

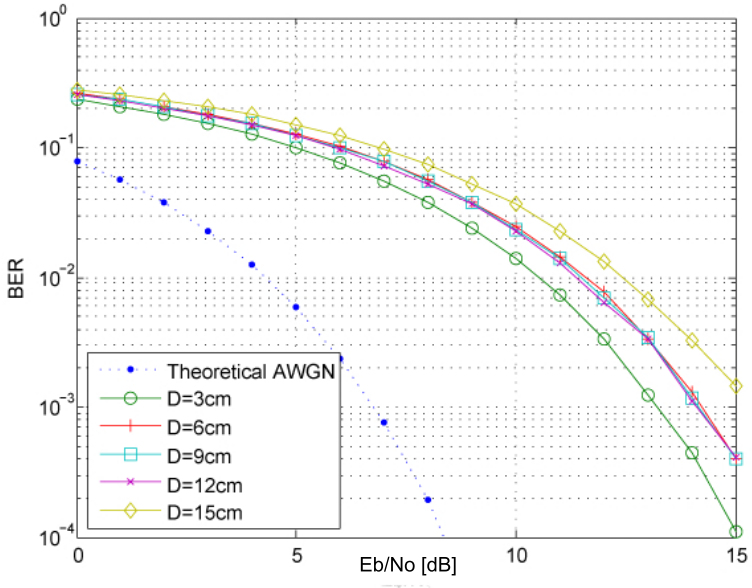

Figure 5.49 BER as a function of E_b/N_o for a TiR UWB-MIMO system with 5 users for several D

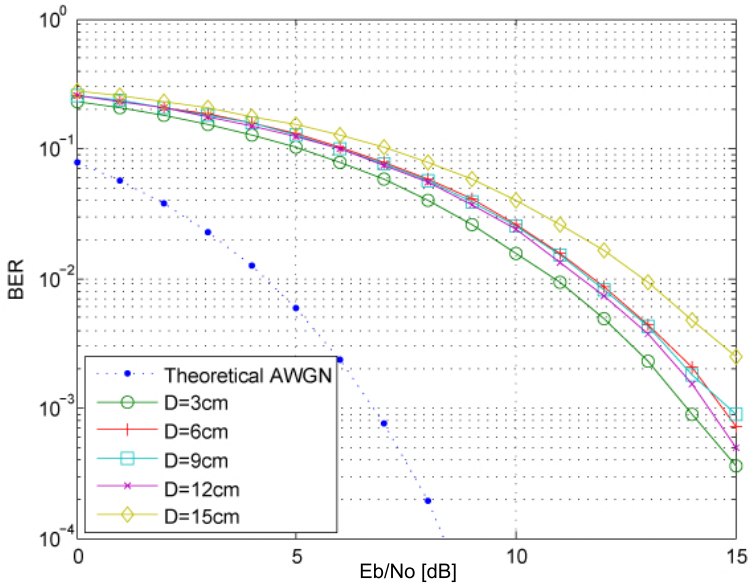

Figure 5.50 BER as a function of E_b/N_o for a TiR UWB-MIMO system with 10 users for several D

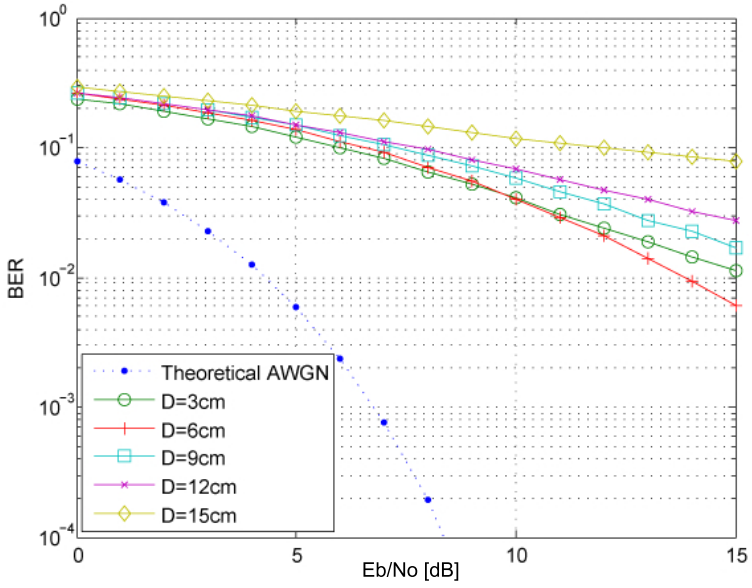

Figure 5.51 BER as a function of E_b/N_o for a TiR UWB-MIMO system with 15 users for several D

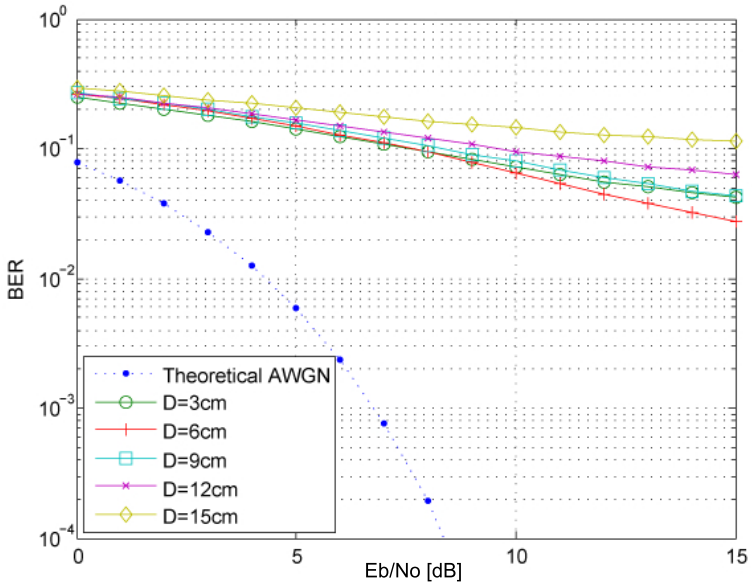

Figure 5.52 BER as a function of E_b/N_o for a TiR UWB-MIMO system with 25 users for several D

SINR is plotted as a function of SNR for the TiR UWB-MIMO network for several number of users when $D = 3cm$ in Figure 5.53, when $D = 3cm$ in Figure 5.53, when $D = 9cm$ in Figure 5.54, and when $D = 15cm$ in Figure 5.55. As expected, the SINR decreases when the number of users increase for all D. The interference is similar for all D when more than 1 user is present in the network. To gather more information, the SINR as a function of SNR for several D in a TiR UWB-MIMO network with 5 users is presented in Figure 5.56, with 15 users in Figure 5.57, and with 25 users in Figure 5.58. For all cases, at $D = 3cm$ the lowest SINR is observed and at $D = 15cm$ the highest SINR is achieved. For a 25-user network, the SINR is very low compared with 15-user and 10-user networks.

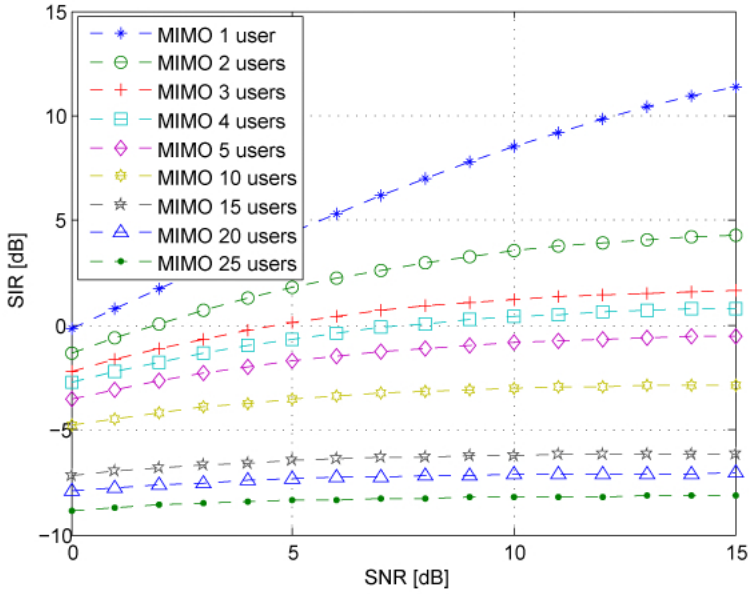

Figure 5.53 SINR as a function of SNR for a TiR UWB-MIMO system with $D = 3cm$ for several number of users

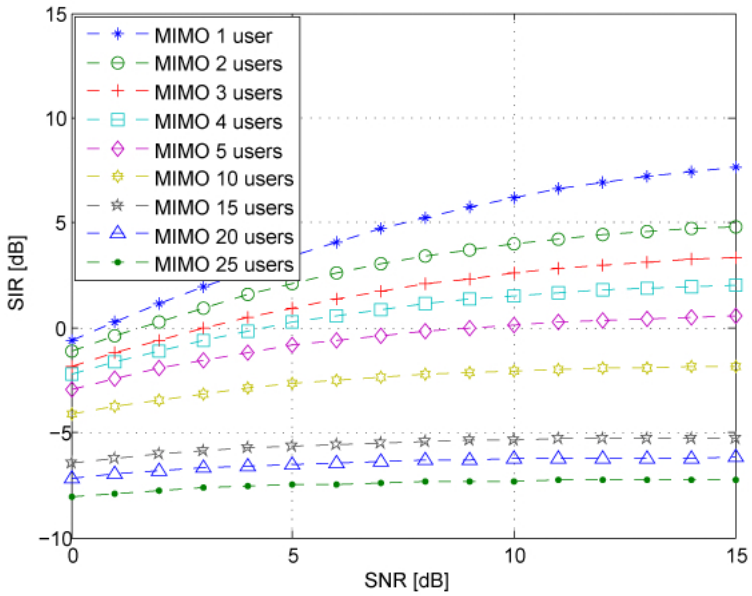

Figure 5.54 SINR as a function of SNR for a TiR UWB-MIMO system with $D = 9cm$ for several number of users

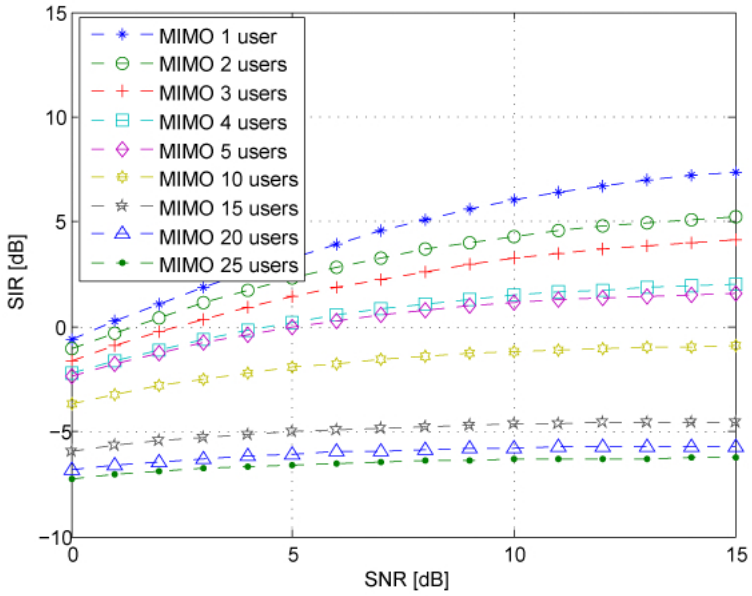

Figure 5.55 SINR as a function of SNR for a TiR UWB-MIMO system with $D = 15cm$ for several number of users

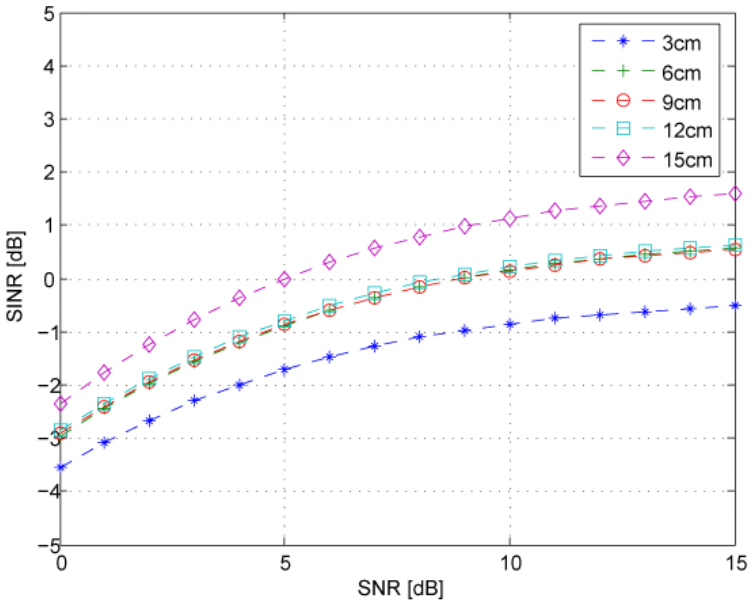

Figure 5.56 SINR as a function of SNR for a TiR UWB-MIMO system with 5 users for several D

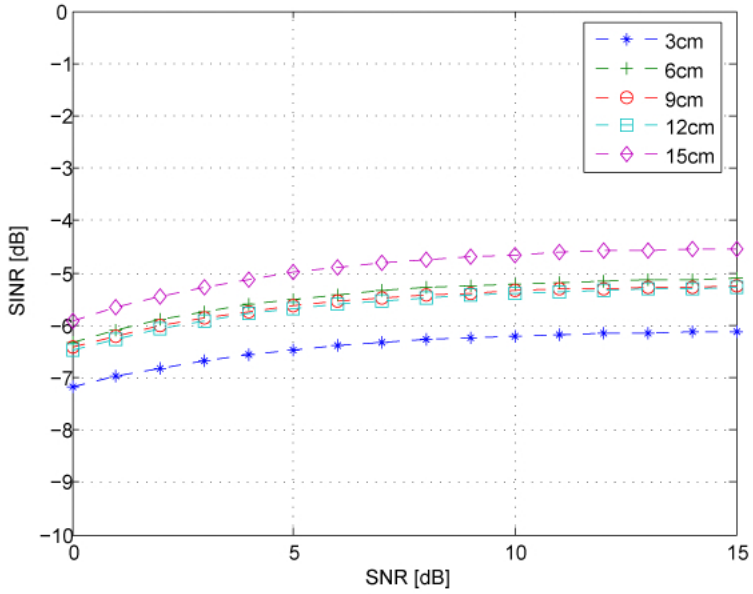

Figure 5.57 SINR as a function of SNR for a TiR UWB-MIMO system with 15 users for several D

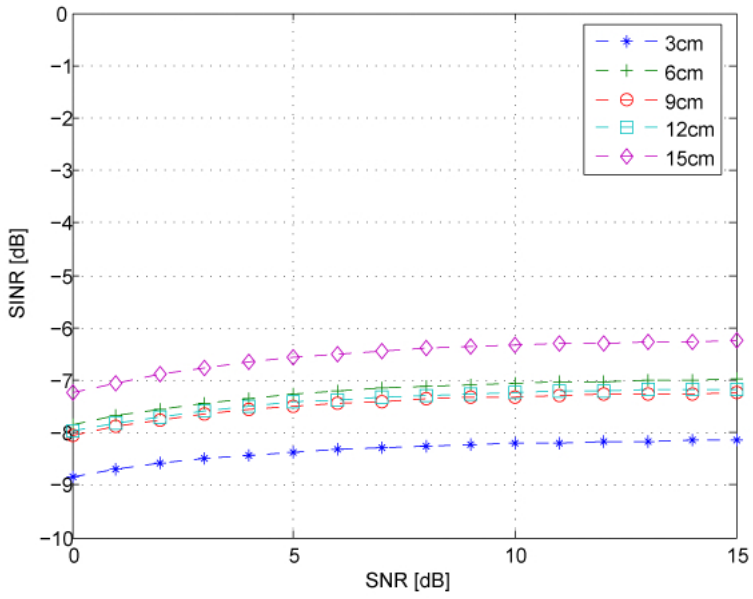

Figure 5.58 SINR as a function of SNR for a TiR UWB-MIMO system with 25 users for several D

5.4.3 Comparison with UWB-MISO Multi-user

A multi-user TiR UWB-MISO network is evaluated to compare with the results shown previously. Figure 5.59 presents the BER performance of up to 25 users in the network as a function of E_b/N_o. The overall performance of the TiR UWB-MIMO network is better than the overall performance of the TiR UWB-MISO network. For a 25-user network, the BER performance reaches a floor of 0.2 at an E_b/N_o of 7dB. Due to inter-user interference, methods like zero-forcing precoding must be used to separate the signal from this type of interference [64]. Aditionally, it is clear that receive diversity yields a better performance even when the number of users is small.

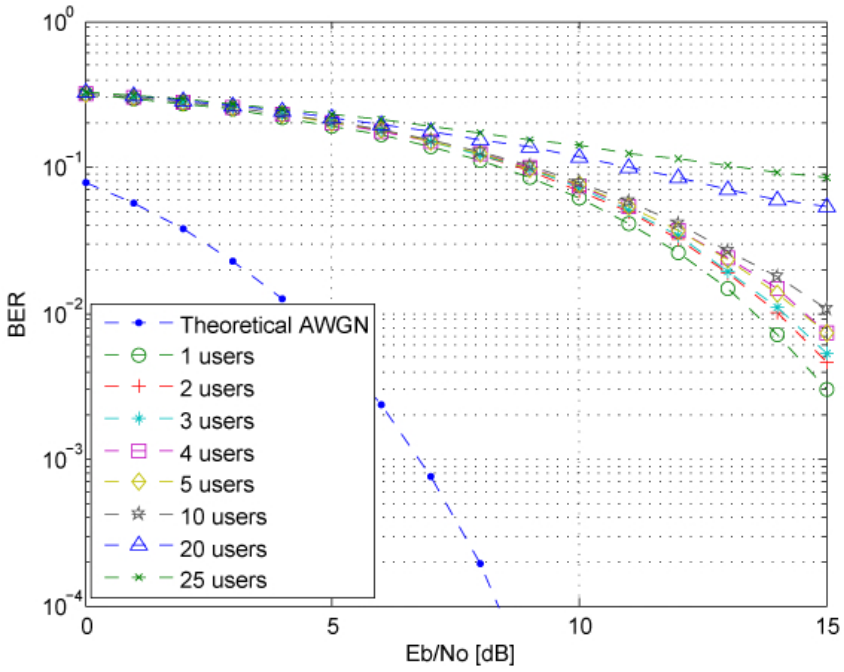

Figure 5.59 BER as a function of E_b/N_o in a TiR UWB-MISO system for several number of users

5.5 Summary

In this chapter, the results of simulation experiments were presented and discussed. It analyzed antenna mutual coupling and channel spatial correlation effects on the performance of TiR UWB systems. It presented an analysis of coupling effects on antennas that are located close to each other. Results show that at smaller distances between two receive antennas, coupling effects are present and can impact the performance of the system. The results show that measuring a virtual array when two antenna elements are located less than 30 cm apart would yield an error in the system performance and if located less than 10cm apart the virtual array does not yield an accurate measurement. A single-user TiR UWB-MIMO system was addressed where two pre-coder approaches were compared. Results show that by using the time-reversed replica of the recorded signal as the TiR pre-coder the system has an increase in performance. A multi-user TiR UWB-MIMO system was investigated and compared with a multi-user TiR UWB-MISO system. Results yield a better performance of using MIMO over MISO. Furthermore, an analysis of the how close two receive antennas should be on a TiR UWB-MIMO system was performed. Results show that although there is an increase in SINR when the distance between the antennas is small, the BER performance increases.

CHAPTER 6
CONCLUSIONS AND FUTURE WORK

This thesis investigates TiR UWB-MIMO for single-user and multi-user systems. The measurement and simulation experiments in this work analyzes spacing between the receive antennas in the system. Coupling effects are investigated when the distance between the receive antennas is small. To evaluate performance, the BER and SINR metrics are used. This chapter summarizes the main measurement and simulation results explained in Chapter 3 and 5. It also states the potential future work derived from this research.

6.1 Conclusions

This report first studied coupling effects without the influence of the channel on a UWB wireless communication system. It was observed that at small distances between two receive antennas, the waveform experiences distortion and coupling effects. The computation of the cross-correlation between the unaffected signal and the affected signal shows this at distances smaller than 15cm. Additionally, the coupling impulse response for a small distance (i.e. $D = 3cm$) between the receive antennas is noticeable and can affect the performance of the system. For distances greater than 30cm, this effect is very small, and therefore, can be neglected.

The analysis of a virtual array is also investigated in this work. A real array and a virtual array were measured and the recorded signals are compared. This comparison shows that for close spaced antennas, there are substantial differences on the obtained waveforms. The performance of a TiR UWB-SIMO system with two receive antennas is evaluated in both the real array and the virtual array. It is

shown that the BER performance is very similar for distances (between the receive antennas) greater than 30cm. For distances between 15cm and 30cm a 1dB error in BER performance is observed, and for D=10cm or less an error of more than 3dB is found. There results suggests that measuring a virtual array when distances between antennas is smaller than 30cm can yield errors and either a method of compensation must be used or a real array must be measured.

TiR UWB-MIMO is studied by evaluating performance for single-user and multi-user systems. It was presented that TiR, UWB, and MIMO technologies combined, results in a potential system which promises many advantages and applications. TiR is shown to be a robust technique to focus the signal in time and space at the intended receiver. Results show that the best pre-coder approach consists of using the time-reversed replica of the recorded signal when the receiver sends a pulse to sound the channel. The advantage of using UWB-MIMO over UWB-MISO is demonstrated with an improvement of 2dB when the distance between the receive antennas (when using MIMO) is 15cm, and an improvement of 4dB when distance is 3cm for up to 10 users. When transmitting to 10 users simultaneously in the system, it is found that the interference is high and BER performance is poor, thus, multiple access schemes must be considered. For the Wireless Networking Systems Lab, the worst performance for a 4-user TiR UWB-MIMO system is given when the distance D between the receive antennas is 25cm, and the best performance when it is 5cm. SINR drops 9dB when D=20cm and the number of users increase from 1 to 4 at a SNR of 15dB. For the Office environment, the best BER performance is given at D=3cm. SINR is low for a system with more than 10 simultaneous users and it ranges between -9dB and-7dB for a SNR of 15dB. Therefore, interference is significant to achieve a good performance. Even though the interference is more severe at smaller distances (i.e.

D=3cm), the best BER performance in all simulations were obtained at the smallest distances. This indicates that inter-channel interference is not a destructive interference and improves the overall BER of a system. Additionally, co-channel interference is destructive and results in worst BER performance of a multi-user system.

6.2 Future Work

This research presents an investigation of single-user and multi-user TiR UWB-MIMO, and an initial study of antenna spacing in UWB systems with receive diversity. Therefore, several aspects may be studied. First, omni-directional antennas are used in the measurement experiments conducted in this work, thus, other types of UWB antennas could be considered. Additionally, the indoor environments are office like and other more hostile environments can be considered.

The addition of other performance metrics could be included in this particular study, but because of time and scope, they were not analyzed. This metrics include capacity analysis, outage probability (when fading is considered), and inter-symbol interference. Additionally, other modulation techniques and receiver designs could be considered. To alleviate interference, multiple access schemes like time division multiple access (TDMA) or code division multiple access (CDMA) may be investigated. Finally, research on multi-user UWB-MIMO with other pre-coding technologies, like dirty-paper coding and zero-forcing coding, can be conducted.

Especially, a chirp UWB system [46] needs further investigation in the framework of time reversal MIMO for range extension and anti-jamming. A chirp UWB can be viewed as a combination of direct spreading (DS) and frequency hopping (FH) spread spectrum (SS).

The testbed is the final answer to many technical questions. The Wireless Networking System Laboratory at Tennessee Technological University (TTU) [1] has been working in this direction for the last several years. The first generation (1G) UWB testbed has been finished. The 1G system is based on the concept of impulse radio. The transceiver uses the energy-detection [18] [50] [17]. The second generation (2G) system uses time reversal that is the topic of this report.

[1] http://iweb.tntech.edu/rqiu/index.htm

REFERENCES

[1] A. Akogun, R. C. Qiu, and N. Guo, "Demonstrating Time-Reversal in Ultra-Wideband Communications using Time Domain Measurements," in *Fifty-first International Intrumentation Symposium, ISA'2005*, Knoxville, TN, May 2005.

[2] A. E. Akogun, "Theory and Application of Time Reversal Technique to Ultra Wideband Wireless Communications," Master's thesis, Tennessee Technological University, Cookeville, TN, 2005.

[3] S. Alamouti, "A Simple Transmit Diversity Technique for Wireless Communications," *IEEE Journal on Selected Areas in Communications*, vol. 16, no. 8, pp. 1451–1458, October 1998.

[4] G. Caire and S. Shamai, "On the Achievable Throughput of a Multi Antenna Gaussian Broadcast Channel," *IEEE Transactions on Information Theory*, vol. 49, pp. 1691–1706, July 2003.

[5] M. Calderon, "Time-Reversed MIMO for Ultra-wideband Communications: Experiments and Performance," Master's thesis, Tennessee Technological University (TTU), Cookeville, TN, December 2007.

[6] J. D. Choi and W. E. Stark, "Performance of Ultra-Wideband Communications with Suboptimal Receivers in Multipath Channels," *IEEE Journal on Selected Areas in Communications*, vol. 20, no. 9, December 2001.

[7] A. Derode, A. Tourin, J. D. Rosny, M. Tanter, S. Yon, and M. Fink, "Taking Advantage of Multiple Scattering to Communicate with Time-Reversal Antennas," *Physical Review Letters*, vol. 90, no. 1, 2003.

[8] G. Durisi and S. Benedetto, "Performance of Coherent and Non-coherent Receivers for UWB Communications," in *2004 IEEE International Conference on Communications*, vol. 6, June 2004, pp. 3429–3433.

[9] G. F. Edelmann, T. Akal, W. Hodgkiss, K. Seongil, W. A. Kuperman, and C. S. Hee, "An Initial Demonstration of Underwater Acoustic Communication Using Time Reversal," *IEEE Journal of Oceanic Engineering*, vol. 27, pp. 602–609, 2002.

[10] S. Emami, J. Hansen, A. Kim, G. Papanicolaou, A. Paulraj, D. Cheung, and C. Prettie, "Predicted Time Reversal Performance in Wireless Communications Using Channel Measurements," *Accepted for publication in IEEE Communication Letters*, 2005.

[11] M. Fink, "Time Reversal of Ultrasonic Fields Part 1: Basic Principles," *IEEE Transactions on Ultrasonics Ferro Electronics and Frequency Control*, vol. 39, pp. 555–566, September 1992.

[12] ——, "Time-Reversed Acoustics," *Scientific American*, pp. 67–73, November 1999.

[13] S. Gezici, Z. Tian, G. Giannakis, H. Kobayashi, A. M. H. Poor, and Z. Sahinoglu, "Localization via Ultra-Wideband Radios," *IEEE Signal Processing Magazine*, vol. 22, pp. 70–84, July 2005.

[14] M. Ghavami, L. Michael, and R. Kohno, *Ultrawideband Signals and Systems in Communication Engineering*. USA: Wiley, 2004.

[15] A. Goldsmith, *Wireless Communications*. USA: Cambridge University Press, 2005.

[16] N. Guo and R. C. Qiu, "Decision-Feedback-Aided Autocorrelation Demodulation Receivers for UWB Communications," *Submitted to IEEE Transactions on Vehicular Technology*, 2006.

[17] N. Guo, J. Zhang, R. Qiu, and S. Mo, "UWB MISO Time Reversal With Energy Detector Receiver Over ISI Channels," Jan. 2007.

[18] N. Guo, Q. Zhang, and R. C. Qiu, "A UWB Radio Testbed System Design and Implementation," in *IEEE 38th Southeastern Symposium on System Theory*, Cookeville, TN, 2006.

[19] S. Imada and T. Ohtsuki, "Pre-Rake Diversity Combining for UWB Systems in IEEE 802.15 UWB Multipath Channel," in *Joint UWBST and IWUWBS: 2004 International Workshop on Ultrawideband Systems joint with Conference on Ultrawideband Systems and Technologies*, May 2004, pp. 236–240.

[20] A. D. Kim, P. Kysitsi, P. Blomgren, and G. Papanicolaou, "Low Probability of Intercept and Intersymbol Interference in Multiple-input/Single-output Time Reversal Communication Systems," *Submitted to IEEE Journal of Oceanic Engineering*, November 2004.

[21] B. Kull and S. Zeisberg, "UWB Receiver Performance Comparison," in *Joint UWBST and IWUWBS: 2004 International Workshop on Ultrawideband Systems joint with Conference on Ultrawideband Systems and Technologies*, May

2004, pp. 21–25.

[22] W. A. Kuperman, W. S. H. W. S., C. S. Hee, T. Akal, C. Ferla, and D. R. Jackson, "Phase Conjugation in the Ocean: Experimental Demonstration of an Acoustic Time-Reversal Mirror," *Journal of Acoustic Society of America*, vol. 103, pp. 25–40, 1998.

[23] P. Kyritsi, D. C. Cox, R. A. Valenzuela, and P. W. Wolniansky, "Correlation Analysis Based on MIMO Channel Measurements in an Indoor Environment," *IEEE Journal on Selected Areas in Communications*, vol. 21, no. 5, pp. 713–720, June 2003.

[24] P. Kyritsi, G. Papanicolaou, P. Eggers, and A. Oprea, "MISO Time Reversal and Delay Spread Compression for FWA Channels at 5GHz," *IEEE Antennas and Wireless Propagation Letters*, vol. 3, no. 6, pp. 96–99, 2004.

[25] G. Lerosey, J. de Rosny, A. Tourin, A. Derode, G. Montaldo, and M. Fink, "Time Reversal of Electromagnetic Waves," *Phyrical Review Letters*, vol. 92, no. 19, May 2004.

[26] Q. Li and L. A. Rush, "Hybrid RAKE/ Multiuser Receivers for UWB," in *Proceedings of Radio and Wireless Conference, RAWCON'03*, Santa Clara, CA, August 2003, pp. 203–206.

[27] H. Liu, R. Qiu, and Z. Tian, "Error Performance of Pulse-Based Ultra-Wideband MIMO Systems Over Indoor Wireless Channels," *IEEE Transactions on Wireless Communications*, vol. 4, no. 6, pp. 2939–2944, Nov 2005.

[28] H. Liu, Y. Song, and R. Qiu, "The Impact of Fading Correlation on the Error Performance of MIMO Systems Over Rayleigh Fading Channels," *IEEE Transactions on Wireless Communications*, vol. 4, no. 5, pp. 2014–2019, September 2005.

[29] D. Love and R. W. Heath, "Equal Gain Transmission in Multiple-Input Multiple-Output Wireless Systems," *IEEE Transactions on Communications*, vol. 51, pp. 1102–1110, July 2003.

[30] D. R. McKinstry, "Ultra-Wideband Small Scale Channel Modeling and its Application to Receiver Design," Master's thesis, Virginia Polytechnic Institute and State University, Virginia, 2003.

[31] A. Molisch, M. Steinbauer, M. Toeltsch, E. Bonek, and R. Thoma, "Capacity of MIMO Systems Based on Measured Wireless Channels," *IEEE Journal on Selected Areas in Communications*, vol. 20, pp. 561–569, April 2002.

[32] G. Montaldo, M. Tanter, and M. Fink, "Real Time Inverse Filter Focusing through Iterative Time Reversal," *Journal of Acoustical Society of America*, vol. 115, pp. 768–775, February 2004.

[33] R. Nabar, O. Oyman, H. Bolcskei, and A. J. Paulraj, "Capacity Scaling Laws in MIMO Wireless Networks," in *Proceedings on Communications, Control and Computing*, October 2003, pp. 378–389.

[34] F. Nekoogar, *Ultra-Wideband Communications: Fundamentals and Applications*. NJ: Prentice Hall, 2006.

[35] H. T. Nguyen, J. B. Andersen, and G. F. Pedersen, "The Potential Use of Time Reversal Technique in Multiple Element Antenna Systems," *IEEE Communication Letters*, vol. 9, no. 1, pp. 40–42, January 2005.

[36] H. T. Nguyen, J. B. Andersen, G. F. Pedersen, P. Kyritsi, and P. Eggers, "Time Reversal in Wireless Communications: A Measurement-Based Investigation," *IEEE Transactions on Wireless Communications*, vol. 5, no. 8, pp. 2242–2252, August 2006.

[37] C. Oestges, J. Hansen, S. Emami, A. Kim, G. Papanicolaou, and A. Paulraj, "Time Reversal Techniques for Broadband Wireless Communication Systems," in *European Microwave Conference*, Amsterdam, October 2004, pp. 49–66.

[38] I. Oppermann, M. Hamalainen, and J. Iinatti, *UWB Theory and Applications*. USA: Wiley, 2004.

[39] R. Qiu, "A Generalized Time Domain Multipath Channel and its Applications in Ultra-Wideband (UWB) Wireless Optimal Receiver Design: Wave-based System Analysis," *IEEE Transactions on Wireless Communications*, pp. 2312–2324, 2004.

[40] R. C. Qiu, "A Theoretic Study of the Ultra-Wideband Wireless Propagation Channel Based on the Scattering Centers," in *Proceedings of the IEEE VTC'98*, Ottawa, Canada, May 1998.

[41] ——, "A Study of the Ultra-Wideband Wireless Propagation Channel and Optimum UWB Receiver Design," *IEEE Journal on Selected Areas in Communications*, vol. 20, December 2002.

[42] R. C. Qiu and et al, "Ultra-wideband Communications Systems and Testbed," in *Final Report to Army Research Office, Grant no. W911NF-05-01-0111, 240 pages, TTU*, Cookeville, TN, July 31, 2007.

[43] R. C. Qiu, H. Liu, and X. Shen, "Ultra-Wideband for Multiple Access Communications," *IEEE Communications Magazine*, pp. 2–9, 2005.

[44] R. C. Qiu and I. Lu, "Wideband Wireless multipath Channel Modeling with Path Frequency Dependence," in *IEEE Conference on Communications (ICC'96)*, Dallas, TX, June 1996.

[45] R. C. Qiu and I. T. Lu, "A Novel High-Resolution Algorithm for Ray Resolving and Wireless Channel Modeling," in *IEEE Princeton/Central Jersey Sarnoff Symposium*, NJ, April 1995.

[46] R. C. Qiu, B. M. Sadler, and Z. Hu, "Time Reversed Transmission with Chirp Signaling for UWB Communications and Its Application in Confined Metal Environments," in *International Conference on Ultra-wideband, ICUWB'07*, Singapore, September 2007.

[47] R. C. Qiu, C. Zhou, N. Guo, and J. Q. Zhang, "Time Reversal with MISO for Ultra-Wideband Communications: Experimental Results," *IEEE Antenna and Wireless Propagation Letters*, vol. 5, pp. 269–273, 2006.

[48] R. C. Qiu, C. M. Zhou, Q. Zhang, and N. Guo, "Channel Reciprocity and Time-Reversed Propagation for Ultra-Wideband Communications," in *IEEE Conf. Antenna Prop., APS'07*, Hawaii, May 2007.

[49] R. C. Qiu, C. Zhou, and Q. Liu, "Physics-Based Pulse Distortion for Ultra-Wideband Signals," *IEEE Transactions on Vehicular Technology*, vol. 54, no. 5, pp. 1546–1555, September 2005.

[50] R. Qiu, "A Theory of Time-Reversed Impulse Multiple-Input Multiple-Output (MIMO) for Ultra-Wideband (UWB) Communications," in *Proceedings of the IEEE International Conference on Ultra-Wideband, ICUWB'06*, MA, September 2006.

[51] R. C. Qiu, "Time/Frequency Dispersion of Digital Transmission Media: Wideband Wireless Channel, Chiral Optical Fiber, and Superconductig Mimic," Ph.D. dissertation, Polytechnic University, Brooklyn, New York, January 1996.

[52] J. H. Reed, *An introduction to Ultra Wideband Communication Systems.* NJ: Prentice Hall, 2005.

[53] S. M. Riad, "The Deconvolution Problem, and Overview," in *Proceedings of the IEEE*, vol. 74, January 1986, pp. 82–85.

[54] S. Roy and J. F. C. S. S. andD. G. Leeper, "Ultrawideband Radio Design: The Promise of High-Speed, Short-Range Wireless Connectivity," *Proceedings of the IEEE*, vol. 92, February 2004.

[55] A. A. Saleh and R. A. Valenzuela, "A Statistical Model for Indoor Multipath Propagation," *IEEE Journal on Selected Areas in Communications*, vol. 5, no. 2, pp. 128–137, February 1987.

[56] H. Shen, W. Zhang, X. An, and K. S. Kwak, "DS-PAM UWB System Using Non-linear Chirp Waveform," *ETRI Journal*, vol. 29, pp. 322–328, June 2007.

[57] K. Siwiak and D. McKeown, *Ultra-wideband radio technology.* USA: Wiley, 2004.

[58] T. Strohmer, M. Emami, J. Hansen, G. Papanicolaou, and A. Paulraj, "Application of Time-Reversal with MMSE Equalizer to UWB Communications," in *IEEE Global Telecommunications Conference, GLOBECOM'04*, vol. 5, Dallas, TX, Nov–Dec 2004, pp. 3123–3127.

[59] S. Tan, B. Kannan, and A. Nallanathan, "Performance of UWB Multiple Access Impulse Radio Systems in Multipath Environment with Antenna Array," in *Conference on Global Telecommunications*, vol. 4, San Francisco, CA, December 2003, pp. 2182–2186.

[60] G. L. Turin, F. D. Clapp, T. L. Johnston, S. B. Fine, and D. Lavry, "A Statistical Model of Urban Multipath Propagation," *IEEE Transactions on Vehicular Technology*, vol. 21, pp. 1–9, February 1972.

[61] R. G. Vaughan and N. L. Scott, "Super-Resolution of Pulsed Multipath Channels for Delay Spread Characterization," *IEEE Transactions on Communications*, vol. 47, no. 3, March 1999.

[62] M. Weisenhorn and W. Hirt, "Performance of Binary Antipodal Signaling over the Indoor UWB MIMO Channel," in *International Conference on Communications*, vol. 4, May 2003, pp. 2872–2878.

[63] M. Z. Win and R. S. Scholtz, "On the Robustness of Ultra-Wide Bandwidth Signals in Dense Multipath Environments," *IEEE Communications Letters*, vol. 2, February 1998.

[64] C. Windpassinger, R. F. Fischer, T. Vencel, and J. Huber, "Precoding in Multiantenna and Multiuser Communications," *IEEE Transactions on Wireless Communications*, vol. 3, pp. 1305–1316, 2004.

[65] M. Yavuz and F. Teixeira, "Frequency Dispersion Compensation in Time Reversal Techniques for UWB Electromagnetic Waves," *IEEE Geoscience and Remote Sensing Letters*, vol. 2, pp. 233–237, April 2005.

[66] M. Zatman and B. Tracey, "Underwater Acoustic MIMO Channel Capacity," in *Conference Record of the 36th Asilomar Conference on Signals, Systems and Computers*, vol. 2, November 2002, pp. 1364–1368.

[67] C. Zhou and R. C. Qiu, "Spatial Focusing of Time-Reversed UWB Electromagnetic Waves in a Hallway Environment," in *Proceeding of the Thirty-Eight Southeastern Symposium on System Theory*, Knoxville, TN, March 2004.

[68] C. M. Zhou, B. M. Sadler, and R. C. Qiu, "Performance Study on Time Reversed Impulse MIMO for UWB Communications Based on Realistic Channels," in *IEEE Conf. Military Comm., MILCOM'07*, Orlando, FL, October 2007.